

1 **PA-4.3.4 Numerical Solution**

2 *Equation (83) is numerically solved by the NUTS program (WIPP PA 1997a) on the same*  
 3 *computational grid (Figure PA-8) used by BRAGFLO in the solution of Equation (25). In the*  
 4 *solution procedure, Equation (83a) is numerically solved with  $S_l = 0$  for each time step, with*  
 5 *the instantaneous updating of concentrations indicated in Equation (84) and the appropriate*  
 6 *modification to  $C_{sl}$  in Equation (83b) taking place after the time step. The solution is carried*  
 7 *out for the five radionuclides indicated in Equation (94).*

8 *The initial value and boundary value conditions used with Equation (83) are given in Table*  
 9 *PA-13. At time  $t = 0$  (i.e., year 2033), the total inventory of each radionuclide is assumed to be*  
 10 *in brine; the solubility constraints associated with Equation (84) then immediately adjust the*  
 11 *values for  $C_{bl}(x, y, t)$  and  $C_{sl}(x, y, t)$  for consistency with the constraints imposed by*  
 12  *$S_T [Br(t), Ox(l), Mi, El(l)]$  and available radionuclide inventory.*

13 **Table PA-13. Initial and Boundary Conditions for  $C_{bl}(x, y, t)$  and  $C_{sl}(x, y, t)$**

<i>Initial Conditions for <math>C_{bl}(x, y, t)</math> and <math>C_{sl}(x, y, t)</math></i>
<p><math>C_{bl}(x, y, t) = A_l(0)/V_b(0)</math> if <math>x, y</math> is a point in the repository (i.e., areas Waste Panel, South RoR and North RoR, in Figure PA-8), where <math>A_l(0)</math> is the amount (kg) of radionuclide <math>l</math> present at time <math>t = 0</math> (Table PA-12) and <math>V_b(0)</math> is the amount (<math>m^3</math>) of brine in repository at time <math>t = 0</math> (from solution of Equation (25) with BRAGFLO) for all <math>x, y</math>.</p> <p><math>= 0</math> otherwise.</p> <p><math>C_{sl}(x, y, t) = 0</math> if <math>x, y</math> is a point in the repository.</p>
<i>Boundary Conditions for <math>C_{bl}(x, y, t)</math></i>
<p><math>f_l(\mathcal{B}, t) = \int_{\mathcal{B}} \mathbf{v}_b(x, y, t) C_{bl}(x, y, t) \alpha(x, y) \cdot \mathbf{n}(x, y) ds</math>, where <math>\mathcal{B}</math> is any subset of the outer boundary of the computational grid in Figure PA-8, <math>f_l(\mathcal{B}, t)</math> is the flux (kg/s) at time <math>t</math> of radionuclide <math>l</math> across <math>\mathcal{B}</math>, <math>\mathbf{v}_b(x, y, t)</math> is the Darcy velocity (<math>(m^3/m^2)/s</math>) of brine at <math>(x, y)</math> on <math>\mathcal{B}</math> and is obtained from the solution of Equation (25) by BRAGFLO, <math>\mathbf{n}(x, y)</math> denotes an outward-pointing unit normal vector, and <math>\int_{\mathcal{B}} ds</math> denotes a line integral along <math>\mathcal{B}</math>.</p>

14 *The nR partial differential equations in Equation (83a) are discretized in two dimensions and*  
 15 *then developed into a linear system of algebraic equations for numerical implementation. The*  
 16 *following conventions are used in the representation of each discretized equation:*

- 17 • *the subscript  $b$  is dropped from  $C_{bl}$ , with the result that the unknown function is*  
 18 *represented by  $C_l$ ,*

- 1 • a superscript  $n$  denotes time ( $t_n$ ), with the assumption that the solution  $C_l$  is known at
- 2 time  $t_n$  and is to be advanced (i.e., computed) at time  $t_{n+1}$ ,
- 3 • the grid indices are  $i$  in the  $x$ -direction,  $j$  in the  $y$ -direction, and are identical with the
- 4 BRAGFLO grid indices; fractional indices refer to quantities evaluated at grid block
- 5 interfaces, and
- 6 • each time step by NUTS is equal to 20 BRAGFLO time steps, which results because
- 7 BRAGFLO reported (i.e., stored) results (i.e.,  $\mathbf{v}_b$ ,  $\phi$ ,  $S_b$ ) every 20 time steps.

8 The following finite difference discretization is used for the  $l^{\text{th}}$  equation in each grid block  $i, j$ :

$$\begin{aligned}
 & q_{b,i+1/2,j}^{n+1} C_{l,i+1/2,j}^{n+1} - q_{b,i-1/2,j}^{n+1} C_{l,i-1/2,j}^{n+1} + q_{b,i,j+1/2}^{n+1} C_{l,i,j+1/2}^{n+1} - q_{b,i,j-1/2}^{n+1} C_{l,i,j-1/2}^{n+1} = \\
 & \frac{V_{R,i,j}}{\Delta t} \left[ \left\{ \phi_{i,j} S_{b,i,j} C_{l,i,j} \right\}^{n+1} - \left\{ \phi_{i,j} S_{b,i,j} C_{l,i,j} \right\}^n \right] \\
 & + V_{R,i,j} \left\{ \phi_{i,j} S_{b,i,j} C_{l,i,j} \right\}^{n+1} \lambda_l - V_{R,i,j} \left( \phi_{i,j} S_{b,i,j} \right)^{n+1} \sum_{p \in P(l)} C_{p,i,j}^{n+1} \lambda_p
 \end{aligned} \tag{95}$$

10 where  $q_b$  is the grid block interfacial brine flow rate ( $m^3/s$ ) and  $V_R$  is the grid block volume

11 ( $m^3$ ). The quantity  $q_b$  is based on  $\mathbf{v}_b$  and  $\alpha$  in Equation (83a), and the quantity  $V_R$  is based

12 on grid block dimensions (Figure PA-8) and  $\alpha$ .

13 The interfacial values of concentration in Equation (95) are discretized using the one-point

14 upstream weighting method (Aziz and Settari 1979), which results in

$$\begin{aligned}
 & q_{b,i+1/2,j}^{n+1} \left( \omega_{i+1} C_{l,i,j}^{n+1} + (1 - \omega_{i+1}) C_{l,i+1,j}^{n+1} \right) - q_{b,i-1/2,j}^{n+1} \left( \omega_i C_{l,i-1,j}^{n+1} + (1 - \omega_i) C_{l,i,j}^{n+1} \right) \\
 & + q_{b,i,j+1/2}^{n+1} \left( \omega_{j+1} C_{l,i,j}^{n+1} + (1 - \omega_{j+1}) C_{l,i,j+1}^{n+1} \right) - q_{b,i,j-1/2}^{n+1} \left( \omega_j C_{b,i,j-1}^{n+1} + (1 - \omega_j) C_{l,i,j}^{n+1} \right) = \\
 & \frac{V_{R,i,j}}{\Delta t} \left[ \left\{ \phi_{i,j} S_{b,i,j} C_{l,i,j} \right\}^{n+1} - \left\{ \phi_{i,j} S_{b,i,j} C_{l,i,j} \right\}^n \right] + V_{R,i,j} \left\{ \phi_{i,j} S_{b,i,j} C_{l,i,j} \right\}^{n+1} \lambda_l \\
 & - V_{R,i,j} \left( \phi_{i,j} S_{b,i,j} \right)^{n+1} \sum_{p \in P(l)} C_{p,i,j}^{n+1} \lambda_p
 \end{aligned} \tag{96}$$

16 where  $\omega$  derives from the upstream weighting for flow between adjacent grid blocks and is

17 defined by

$$\omega_i = \begin{cases} 1 & \text{if flow is from grid block } i-1, j \text{ to grid block } i, j \\ 0 & \text{otherwise} \end{cases}$$

$$\omega_j = \begin{cases} 1 & \text{if flow is from grid block } i, j-1 \text{ to grid block } i, j \\ 0 & \text{otherwise.} \end{cases}$$

By collecting similar terms, Equation (96) can be represented by the linear equation

$$AC_{l,i,j-1}^{n+1} + BC_{l,i-1,j}^{n+1} + DC_{l,i,j}^{n+1} + EC_{l,i+1,j}^{n+1} + FC_{l,i,j+1}^{n+1} = R_{l,i,j}, \quad (97)$$

where

$$A = -\omega_j q_{b,i,j-1/2}^{n+1} \quad B = -\omega_j q_{b,i-1/2,j}^{n+1}$$

$$E = (1 - \omega_{i+1}) q_{b,i+1/2,j}^{n+1} \quad F = (1 - \omega_{j+1}) q_{b,i,j+1/2}^{n+1}$$

$$D = -\left(1 - \omega_j\right) q_{b,i,j-1/2}^{n+1} - \left(1 - \omega_i\right) q_{b,i-1/2,j}^{n+1} + \omega_{j+1} q_{b,i,j+1/2}^{n+1} + \omega_{i+1} q_{b,i+1/2,j}^{n+1}$$

$$- \left( \frac{V_{R,i,j}}{\Delta t} - V_{R,i,j} \lambda_l \right) \left\{ \phi_{i,j} S_{b,i,j} \right\}^{n+1}$$

$$R_{l,i,j} = -\frac{V_{R,i,j}}{\Delta t} \left\{ \phi_{i,j} S_{b,i,j} C_{l,i,j} \right\}^n - V_{R,i,j} \left( \phi_{i,j} S_{b,i,j} \right)^{n+1} \sum_{p \in P(l)} C_{p,i,j}^{n+1} \lambda_p.$$

Given the form of Equation (97), the solution of Equation (83a) has now been reduced to the solution of  $nR \times nG$  linear algebraic equations in  $nR \times nG$  unknowns, where  $nR$  is the number of equations for each grid block (i.e., the number of radionuclides) and  $nG$  is the number of grid blocks into which the spatial domain is discretized (Figure PA-8).

The system of partial differential equations in Equation (83a) is strongly coupled because of the contribution from parental decay to the equation governing the immediate daughter. Consequently, a sequential method is used to solve the system in which radionuclide concentrations are solved for by starting at the top of a decay chain and working down from parent to daughter. This implies that when solving Equation (97) for the  $l^{\text{th}}$  isotope concentration, all parent concentrations occurring in the right hand side term  $R$  are known. The resulting system of equations is then linear in the concentrations of the  $l^{\text{th}}$  isotope. As a result, solution of Equation (83a) is reduced from the solution of one algebraic equation at each time step with  $nR \times nG$  unknowns to the solution of  $nR$  algebraic equations each with  $nG$  unknowns at each time step, which can result in a significant computational savings.

The matrix resulting from one-point upstream weighting has the following structural form for a  $3 \times 3$  system of grid blocks and a similar structure for a larger number of grid blocks:

	1	2	3	4	5	6	7	8	9
1	X	X	0	X					
2	X	X	X	0	X				
3	0	X	X	0	0	X			
4	X	0	0	X	X	0	X		
5		X	0	X	X	X	0	X	
6			X	0	X	X	0	0	X
7				X	0	0	X	X	0
8					X	0	X	X	X
9						X	0	X	X

1 where *X* designates possible nonzero matrix entries, and 0 designates zero entries. Entries  
 2 outside of the banded structure are zero. Because of this structure, a banded direct  
 3 elimination solver (Aziz and Settari 1979, Section 8.2.1) is used to solve the linear system for  
 4 each radionuclide. The bandwidth is minimized by indexing equations first in the coordinate  
 5 direction having the minimum number of grid blocks. The coefficient matrix is stored in this  
 6 banded structure and all infill coefficients calculated during the elimination procedure are  
 7 contained within the band structure. Therefore, for the matrix system in two dimensions, a  
 8 pentadiagonal matrix of dimension  $IBW \times nG$  is inverted instead of a full  $nG \times nG$  matrix,  
 9 where *IBW* is the band width.

10 The numerical implementation of Equation (83b) enters the solution process through an  
 11 updating of the radionuclide concentrations in Equation (96) between each time step as  
 12 indicated in Equation (84). The numerical solution of Equation (83) also generates the  
 13 concentrations required for the numerical evaluation of the integral that defines  $C_1(t, \mathcal{B})$  in  
 14 Equation (88).

15 **PA-4.3.5 Additional Information**

16 Additional information on NUTS and its use in WIPP PA can be found in the NUTS users  
 17 manual (WIPP PA 1997a) and in the analysis package for Salado transport calculations for  
 18 the CRA-2004 PA (Lowry 2003). Furthermore, additional information on dissolved and  
 19 colloidal actinides is given in Attachment SOTERM.

20 **PA-4.4 Radionuclide Transport in the Salado: PANEL**

21 This section describes the model used to compute transport of radionuclides in the Salado for  
 22 E1E2 scenario. The model for transport in E0, E1, and E2 scenarios is described in Section  
 23 PA-4.3.

1 **PA-4.4.1 Mathematical Description**

2 *A relatively simple mixed-cell model is used for radionuclide transport in the vicinity of the*  
 3 *repository when connecting flow between two drilling intrusions into the same waste panel is*  
 4 *assumed to take place (i.e., an E1E2 intrusion). With this model, the amount of radionuclide l*  
 5 *contained in a waste panel is represented by*

6 
$$\frac{dA_l}{dt} = -r_b C_{bl} - \lambda_l A_l + \sum_{p \in P(l)} \lambda_p A_p, \quad (98)$$

7 *where*

8  $A_l(t)$  = amount (mol) of radionuclide l in waste panel at time t,

9  $C_{bl}(t)$  = concentration (mol/m<sup>3</sup>) of radionuclide l in brine in waste panel at time t  
 10 (Equation (99)),

11  $r_b(t)$  = rate (m<sup>3</sup>/s) at which brine flows out of the repository at time t (supplied by  
 12 BRAGFLO from solution of Equation (81), and  $\lambda_l$  and  $P(l)$  are defined in  
 13 conjunction with Equation (84).

14 *The brine concentration  $C_{bl}$  in Equation (98) is defined by*

15 
$$C_{bl}(t) = S_T [Br(t), Ox(l), Mi, El(l)] MF_l(t) \quad (99a)$$

$$\text{if } S_T [Br(t), Ox(l), Mi, El(l)] \leq \sum_{k \in El(l)} A_k(t) / V_b(t)$$

16 
$$= A_l(t) / V_b(t) \text{ if } \sum_{k \in El(l)} A_k(t) / V_b(t) < S_T [Br(l), Ox(l), Mi, El(l)], \quad (99b)$$

17 *where*

18  $MF_l(t)$  = mole fraction of radionuclide l in waste panel at time t

19 
$$= \frac{A_l(t)}{\sum_{k \in El(l)} A_k(t)} \quad (100)$$

20  $V_b(t)$  = volume (m<sup>3</sup>) of brine in waste panel at time t (supplied by BRAGFLO from  
 21 solution of Equation (25)), and  $S_T [Br(l), Ox(l), Mi, El(l)]$  and  $E(l)$  are  
 22 by Equation (89).

1 *For use in Equation (99),  $S_T [Br(l), Ox(l), Mi, El(l)]$  must be expressed in units of mol/l.*  
 2 *In words,  $C_{bl}(t)$  is defined to be the maximum concentration ( $S_T$  in Equation (89)) if there is*  
 3 *sufficient radionuclide inventory in the waste panel to generate this concentration (Equation*  
 4 *(99a)); otherwise,  $C_{bl}(t)$  is defined by the concentration that results when all the relevant*  
 5 *element in the waste panel is placed in solution (Equation (99b)).*

6 *Given  $r_b$  and  $C_{bb}$ , evaluation of the integral*

$$7 \quad \mathbf{v}_i(x, y) = [u_i(x, y), v_i(x, y)] = SFC [K_i(x, y) \nabla h_i(x, y)]^T \quad (101)$$

8 *provides the cumulative release  $R_l(t)$  of radionuclide  $l$  from the waste panel through time  $t$ .*

#### 9 *PA-4.4.2 Numerical Solution*

10 *Equation (98) is numerically evaluated by the PANEL model (WIPP PA 1998b).*

11 *A discretization based on 50-year or smaller time steps is used by PANEL. Specifically,*  
 12 *Equation (98) is evaluated with the approximation*

$$13 \quad A_l(t_{n+1}) = A_l(t_n) - \left[ \int_{t_n}^{t_{n+1}} r_b(\tau) d\tau \right] C_{bl}(t_n) - A_l(t_n) \exp(-\lambda_l \Delta t) + G_l(t_n, t_{n+1}), \quad (102)$$

14 *where*

15  $G_l(t_n, t_{n+1}) =$  *gain in radionuclide  $l$  due to the decay of precursor radionuclides between  $t_n$*   
 16 *and  $t_{n+1}$  (see Equation (103)),*

$$17 \quad \Delta t = t_{n+1} - t_n = 50 \text{ yr.}$$

18 *As the solution progresses, values for  $C_{bl}(t_n)$  are updated in consistency with Equation (99)*  
 19 *and the products  $r_b(t_n)C_{bl}(t_n)$  are accumulated to provide an approximation to  $R_l$  in*  
 20 *Equation (101).*

21 *The term  $G_l(t_n, t_{n+1})$  in Equation (102) is evaluated with the Bateman equations (Bateman*  
 22 *1910), with PANEL programmed to handle up to four succeeding generations of a given*  
 23 *radionuclide (i.e., decay chains of length 5). As a single example, if radionuclide  $l$  is the third*  
 24 *radionuclide in a decay chain (i.e.,  $l = 3$ ) and the two preceding radionuclides in the decay*  
 25 *chain are designated by  $l = 1$  and  $l = 2$ , then*

$$\begin{aligned}
 G_3(t_n, t_{n+1}) = & \lambda_2 A_2(t_n) \left[ \exp(-\lambda_2 \Delta t) - \exp(-\lambda_3 \Delta t) \right] / (\lambda_3 - \lambda_2) \\
 & + \lambda_1 \lambda_2 A_2(t_n) \left\{ \left[ \exp(-\lambda_1 \Delta t) \right] / \left[ (\lambda_2 \lambda_1) (\lambda_3 \lambda_1) \right] \right. \\
 & \quad \left. + \left[ \exp(-\lambda_2 \Delta t) \right] / \left[ (\lambda_3 - \lambda_2) (\lambda_1 - \lambda_2) \right] \right. \\
 & \quad \left. + \left[ \exp(-\lambda_3 \Delta t) \right] / \left[ (\lambda_1 - \lambda_3) (\lambda_2 - \lambda_3) \right] \right\}
 \end{aligned}
 \tag{103}$$

1  
2 *in Equation (102).*

### 3 *PA-4.4.3 Implementation in Performance Assessment*

4 *The preceding model was used in two ways in the CRA-2004 PA. First, Equation (101) was*  
 5 *used to estimate releases to the Culebra associated with EIE2 intrusions (scenario S6; see*  
 6 *Section PA-6.7). Second, with  $r_b$  set to a very small number and  $V_b$  set to a fixed value,*  
 7 *Equation (98) and Equation (99) were used to estimate radionuclide concentrations in brine*  
 8 *for use in the estimation of direct brine releases (see Section PA-6.8.5).*

9 *For EIE2 intrusions, the initial amount  $A_l$  of radionuclide  $l$  is the inventory of the isotope*  
 10 *decayed to at the time of the E1 intrusion. Isotopes considered in the PANEL calculations for*  
 11 *release to the Culebra are listed in Appendix TRU WASTE (Table TRU WASTE-9). PANEL*  
 12 *calculates the inventory of each radionuclide throughout the regulatory period. The initial*  
 13 *concentration  $C_{bl}$  of radionuclide  $l$  is computed by Equation (98) and Equation (99). For use*  
 14 *as part of the direct brine release calculations, the initial amount  $A_l$  of radionuclide  $l$  is the*  
 15 *inventory of the isotope at the time of repository closure; isotopes considered in the PANEL*  
 16 *calculations for direct brine releases are listed in Appendix TRU WASTE (Table TRU*  
 17 *WASTE-9).*

### 18 *PA-4.4.4 Additional Information*

19 *Additional information on PANEL and its use in the CRA-2004 PA calculations can be found*  
 20 *in the PANEL user's manual (WIPP PA 2003d) and the analysis package for PANEL*  
 21 *calculations (Garner 2003).*

### 22 *PA-4.5 Cuttings and Cavings to Surface: CUTTINGS\_S*

23 *Cuttings are waste solids contained in the cylindrical volume created by the cutting action of*  
 24 *the drill bit passing through the waste. Cavings are additional waste solids eroded from the*  
 25 *borehole by the upward-flowing drilling fluid within the borehole. The releases associated*  
 26 *with these processes are computed within the CUTTINGS\_S code (WIPP PA 2003e). The*  
 27 *mathematical representations used for the first two processes, cuttings and cavings, are*  
 28 *described in this section.*

#### 29 *PA-4.5.1 Cuttings*

30 *The uncompacted volume of cuttings removed and transported to the surface in the drilling*  
 31 *mud,  $V_{cub}$  is given by*

$$V_{cut} = AH_i = \pi D^2 H_i / 4, \quad (104)$$

where  $H_i$  is the initial (i.e., uncompacted) repository height (m),  $A$  is the drill bit area ( $m^2$ ), and  $D$  is the drill-bit diameter (m). In the CRA-2004 PA,  $D = 12.25 \text{ in.} = 0.31115 \text{ m}$  and  $H_i = 3.96 \text{ m}$  (Attachment PAR, Table PAR-13). For drilling intrusions through RH-TRU waste,  $H_i = 0.509 \text{ m}$  is used (Attachment PAR, Table PAR-45).

#### PA-4.5.2 Cavings

The cavings component of the direct surface release is caused by the shearing action of the drilling fluid (mud) on the waste as the mud flows up the borehole annulus. As for the cuttings release, the cavings release is assumed to be independent of the conditions that exist in the repository at the time of a drilling intrusion.

The final diameter of the borehole will depend on the diameter of the drillbit and on the extent to which the actual borehole diameter exceeds the drill-bit diameter. Although a number of factors affect erosion within a borehole (Broc 1982), the most important factor is believed to be the fluid shear stress on the borehole wall (i.e., the shearing force per unit area, ( $\text{kg m/s}^2/\text{m}^2$ )) resulting from circulating drilling fluids (Darley 1969; Walker and Holman 1971). As a result, the CRA-2004 PA estimates cavings removal with a model based on the effect of shear stress on the borehole diameter. In particular, the borehole diameter is assumed to grow until the shear stress on the borehole wall is equal to the shear strength of the waste (i.e., the limiting shear stress below which the erosion of the waste ceases).

The final eroded diameter  $D_f$  (m) of the borehole through the waste determines the volume  $V$  ( $m^3$ ) of uncompacted waste that will be removed to the surface by circulating drilling fluid. Specifically,

$$V = V_{cut} + V_{cav} = \pi D_f^2 H_i / 4, \quad (105)$$

where  $V_{cav}$  is the volume ( $m^3$ ) of waste removed as cavings.

Most borehole erosion is believed to occur in the vicinity of the drill collar (Figure PA-14) because of decreased flow area and consequent increased mud velocity (Rechard et al. 1990, Letters 1a and 1b, App. A). An important determinant of the extent of this erosion is whether the flow of the drilling fluid in the vicinity of the collar is laminar or turbulent. The CRA-2004 PA uses Reynolds numbers to distinguish between the occurrence of laminar flow and turbulent flow. The Reynolds number is the ratio between inertial and viscous (i.e., shear) forces in a fluid and can be expressed as (Fox and McDonald 1985):

$$R_e = \frac{\rho_f \|v\| D_e}{\eta}, \quad (106)$$

1 where  $R_e$  is the Reynolds number (dimensionless),  $\rho_f$  is the fluid density ( $\text{kg m}^{-3}$ ),  $D_e$  is the  
 2 equivalent diameter (m),  $\mathbf{v}$  is the fluid velocity ( $\text{m s}^{-1}$ ), and  $\eta$  is the fluid viscosity ( $\text{kg m}^{-1} \text{s}^{-1}$ ).

3 Typically,  $\rho$ ,  $\mathbf{v}$  and  $\eta$  are averages over a control volume with an equivalent diameter of  $D_e$   
 4 In the CRA-2004 PA,  $\rho_f = 1.21 \times 10^3 \text{ kg m}^{-3}$  (Attachment PAR, Table PAR-13),  
 5  $\|\mathbf{v}\| = 0.7089 \text{ m s}^{-1}$  (based on 40 gallons/min per inch of drill diameter) (Berglund 1992), and  
 6  $D_e = 2(R - R_j)$ , as shown in Figure PA-14. The diameter of the drill collar (i.e.,  $2R_i$  in Figure  
 7 PA-14) is  $8.0 \text{ in} = 0.2032 \text{ m}$  (Dunagan 2003b). The determination of  $\eta$  is discussed below.  
 8 Reynolds numbers less than 2100 are assumed to be associated with laminar flow, while  
 9 Reynolds numbers greater than 2100 are assumed to be associated with turbulent flow  
 10 (Walker 1976).

11 Drilling fluids are modeled as non-Newtonian, which means that the viscosity  $\eta$  is a function  
 12 of the shear rate within the fluid (i.e., the rate at which the fluid velocity changes normal to  
 13 the flow direction,  $((\text{m/s})/\text{m})$ . The CRA-2004 PA uses a model proposed by Oldroyd (1958) to  
 14 estimate the viscosity of drilling fluids. As discussed by Broc (1982), the Oldroyd model leads  
 15 to the following expression for the Reynolds number associated with the helical flow of a  
 16 drilling fluid within an annulus:

17 
$$R_e = \frac{0.8165 \rho_f \|\mathbf{v}\| D_e}{\eta_\infty}, \tag{107}$$

18 where  $\rho_f$ ,  $\|\mathbf{v}\|$  and  $D_e$  are defined as in Equation (106), and  $\eta_\infty$  is the asymptotic value for the  
 19 derivative of the shear stress ( $\tau$ ,  $\text{kg m}^{-1} \text{s}^{-2}$ ) with respect to the shear rate ( $\Gamma$ ,  $\text{s}^{-1}$ ) obtained as  
 20 the shear rate increases (i.e.,  $\eta_\infty = d\tau/d\Gamma$  as  $\Gamma \rightarrow \infty$ ). The CRA-2004 PA uses Equation  
 21 (107) to obtain the Reynolds numbers that are used to determine whether drilling fluids in the  
 22 area of the drill collar are undergoing laminar or turbulent flow.

23 The Oldroyd model assumes that the shear stress  $\tau$  is related to the shear rate  $\Gamma$  by the  
 24 relationship

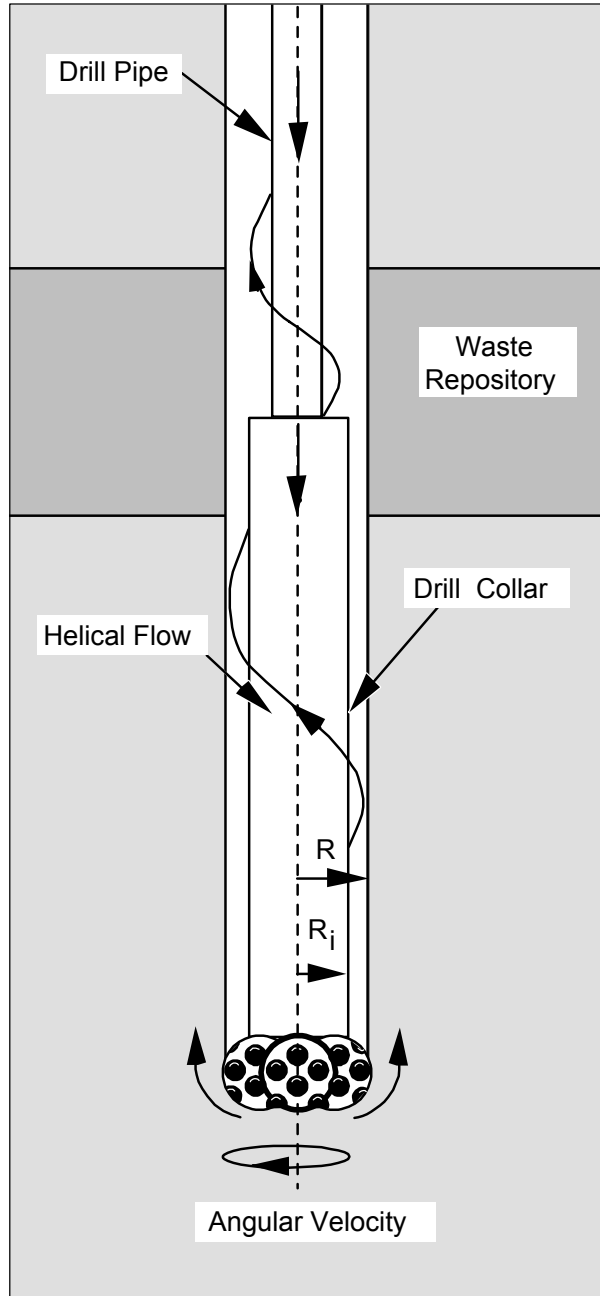
25 
$$\tau = \eta_0 \left( \frac{1 + \sigma_2 \Gamma^2}{1 + \sigma_1 \Gamma^2} \right) \Gamma, \tag{108}$$

26 where  $\eta_0$  is the asymptotic value of the viscosity ( $\text{kg m}^{-1} \text{s}^{-1}$ ) that results as the shear rate  $\Gamma$   
 27 approaches zero, and  $\sigma_1$ ,  $\sigma_2$  are constants ( $\text{s}^2$ ). The expression leads to

28 
$$\eta_\infty = \eta_0 \left( \frac{\sigma_2}{\sigma_1} \right). \tag{109}$$

29

1



2

3

*Figure PA-14. Detail of Rotary Drill String Adjacent to Drill Bit.*

4

1 *The CRA-2004 PA uses values of  $\eta_0 = 1.834 \times 10^{-2} \text{ kg m}^{-1} \text{ s}^{-1}$ ,  $\sigma_1 = 1.082 \times 10^{-6} \text{ s}^2$  and  $\sigma_2 =$   
 2  $5.410 \times 10^{-7} \text{ s}^2$  (Berglund 1996), and a resultant value of  $\eta_\infty = 9.17 \times 10^{-3} \text{ kg m}^{-1} \text{ s}^{-1}$ . The  
 3 quantity  $\eta_\infty$  is comparable to the plastic viscosity of the fluid (Broc 1982).*

4 *As previously indicated, different models are used to determine the eroded diameter  $D_f$  of a  
 5 borehole depending on whether flow in the vicinity of the drill collar is laminar or turbulent.  
 6 The model for borehole erosion in the presence of laminar flow is described next, and is then  
 7 followed by a description of the model for borehole erosion in the presence of turbulent flow.*

8 ***PA-4.5.2.1 Laminar Flow Model***

9 *As shown by Savins and Wallick (1966), the shear stresses associated with the laminar helical  
 10 flow of a non-Newtonian fluid can be expressed as*

11 
$$\tau(R, r) = \left\{ \left[ \frac{C}{r^2} \right]^2 + \left[ \frac{RJ}{2} \left( \frac{r^2 - \lambda^2}{r} \right) \right]^2 \right\}^{1/2} \quad (110)$$

12 *for  $R_i/R \leq r \leq 1$ , where  $R_i$  and  $R$  are the inner and outer radii within which the flow occurs as  
 13 indicated in Figure PA-14;  $\tau(R, \rho)$  is the shear stress ( $\text{kg m}^{-1} \text{ s}^{-2}$ ) at a radial distance  $\Delta R$   
 14 beyond the inner boundary (i.e., at  $r = (R_i + \Delta R)/R$ ); and the quantities  $C$ ,  $J$ , and  $\lambda$  are  
 15 functions of  $R$  that satisfy conditions indicated below. The shear stress at the outer boundary  
 16 (i.e.,  $R$ ) is given by*

17 
$$\tau(R, 1) = \left\{ C^2 + \left[ \frac{RJ}{2} (1 - \lambda^2) \right]^2 \right\}^{1/2} \quad (111)$$

18 *As previously indicated, the borehole radius  $R$  is assumed to increase as a result of erosional  
 19 processes until a value of  $R$  is reached at which  $\tau(R, 1)$  is equal to the shear strength of the  
 20 waste. In the CRA-2004 PA, the shear strength of the waste is treated as an uncertain  
 21 parameter (see WTAUFAIL in Table PA-17). Computationally, determination of the eroded  
 22 borehole diameter  $R$  associated with a particular value for waste shear strength requires  
 23 repeated evaluation of  $\tau(R, 1)$ , as indicated in Equation (111), until a value of  $R$  is  
 24 determined for which  $\tau(R, 1)$  equals that shear strength.*

25 *The quantities  $C$ ,  $J$ , and  $\lambda$  must satisfy the following three conditions (Savins and Wallick  
 26 1966) for the expression in Equation (111) to be valid:*

27 
$$0 = \int_{R_i/R}^1 \left( \frac{\rho^2 - \lambda^2}{\rho \eta} \right) d\rho \quad (112a)$$

1 
$$\theta = C \int_{R_i/R}^1 \left( \frac{1}{\rho^3 \eta} \right) d\rho - \Delta\Omega \quad (112b)$$

2 *and*

3 
$$\theta = \frac{4Q}{\pi R^3} + 2RJ \int_{R_i/R}^1 \left( \frac{(R_i/R)^2 - \rho^2}{\rho \eta} \right) \left( \frac{\rho^2 - \lambda^2}{\rho \eta} \right) d\rho, \quad (112c)$$

4 *where  $\eta$  is the drilling fluid viscosity ( $\text{kg m}^{-1} \text{s}^{-1}$ ) and is a function of  $R$  and  $\rho$ ,  $\Delta\Omega$  is the drill*  
 5 *string angular velocity ( $\text{rad s}^{-1}$ ), and  $Q$  is the drilling fluid flow rate ( $\text{m}^3 \text{s}^{-1}$ ).*

6 *The viscosity  $\eta$  in Equation (112) is introduced into the analysis through the assumption that*  
 7 *the drilling fluid follows the Oldroyd model for shear stress in Equation (108). In particular,*  
 8 *because*

9 
$$\tau = \eta\Gamma \quad (113)$$

10 *as a result of the definition of the viscosity  $\eta$  and*

11 
$$\Gamma^2 = \frac{(\eta - \eta_0)}{(\eta_0 \sigma_2 - \eta \sigma_1)} \quad (114)$$

12 *from Equation (108), the expression in Equation (110) can be reformulated as*

13 
$$\frac{\eta^2 (\eta - \eta_0)^2}{(\eta_0 \sigma_2 - \eta \sigma_1)^2} = \left[ \frac{C}{\rho^2} \right]^2 + \left[ \frac{RJ}{2} \left( \frac{\rho^2 - \lambda^2}{\rho} \right) \right]^2. \quad (115)$$

14 *As discussed by Savins and Wallick (1966) and also by Berglund (1992), the expressions in*  
 15 *Equation (112) and Equation (114) can be numerically evaluated to obtain  $C$ ,  $J$ , and  $\lambda$  for use*  
 16 *in Equation (110) and Equation (111). In the CRA-2004 PA, the drill string angular velocity*  
 17  *$\Delta\Omega$  is treated as an uncertain parameter (see DOMECA in Table PA-17), and*

18 
$$Q = \|\mathbf{v}\| (\pi R^2 - \pi R_i^2), \quad (116)$$

19 *where  $\|\mathbf{v}\| = 0.7089 \text{ m s}^{-1}$  as used in Equation (106), and  $\eta_0$ ,  $\sigma_1$ , and  $\sigma_2$  are defined by*  
 20 *Equation (109).*

21 **PA-4.5.2.2 Turbulent Flow Model**

22 *The model for borehole erosion in the presence of turbulent flow is now described. Unlike the*  
 23 *theoretically derived relationship for erosion in the presence of laminar flow, the model for*  
 24 *borehole erosion in the presence of turbulent flow is empirically based. In particular,*

1 *pressure loss for axial flow in an annulus under turbulent flow conditions can be*  
 2 *approximated by (Broc 1982)*

$$3 \quad \Delta P = \frac{2 f L \rho_f \|v\|^2}{0.8165 D_e} \quad (117)$$

4 *where  $\Delta P$  is the pressure change (Pa),  $L$  is distance (m) over which pressure change  $\Delta P$*   
 5 *occurs,  $f$  is the Fanning friction factor (dimensionless), and  $\rho_f$ ,  $\|v\|$  and  $D_e$  are defined in*  
 6 *Equation (106).*

7 *For pipe flow,  $f$  is empirically related to the Reynolds number  $R_e$  and a roughness term  $\varepsilon$  by*  
 8 *(Whittaker 1985)*

$$9 \quad \frac{1}{\sqrt{f}} = -4 \log_{10} \left( \frac{\varepsilon}{3.72 D} + \frac{1.255}{R_e \sqrt{f}} \right), \quad (118)$$

10 *where  $D$  is the inside diameter (m) of the pipe and  $\varepsilon$  is the average depth (m) of pipe wall*  
 11 *irregularities. In the absence of a similar equation for flow in an annulus, Equation (118) is*  
 12 *used in the CRA-2004 PA to define  $f$  for use in Equation (117), with  $D$  replaced by the*  
 13 *effective diameter  $D_e = 2(R - R_i)$  and  $\varepsilon$  equal to the average depth of irregularities in the*  
 14 *waste-borehole interface. In the present analysis,  $\varepsilon = 0.025$  m (Attachment PAR, Table PAR-*  
 15 *34), which exceeds the value often chosen for use in calculations involving very rough*  
 16 *concrete or riveted steel piping (Streeter 1958). Further, the Reynolds number  $R_e$  is defined in*  
 17 *Equation (107).*

18 *The pressure change  $\Delta P$  in Equation (117) and the corresponding shear stress  $\tau$  at the walls*  
 19 *of the annulus are approximately related by*

$$20 \quad \Delta P \left[ \pi (R^2 - R_i^2) \right] = \tau \left[ 2\pi L (R + R_i) \right] \quad (119)$$

21 *where  $\pi (R^2 - R_i^2)$  is the cross-sectional area of the annulus (see Figure PA-14) and*  
 22  *$2\pi L (R + R_i)$  is the total (i.e., interior and exterior) surface area of the annulus.*  
 23 *Rearrangement of Equation (117) and use of the relationship in Equation (113) yields*

$$24 \quad \tau = \frac{f \rho_f \|v\|^2}{2(0.8165)}, \quad (120)$$

25 *which was used in the 1991 and 1992 WIPP PAs to define the shear stress at the surface of a*  
 26 *borehole of radius  $R$ . As a reminder,  $R$  enters into Equation (112a) through the use of*  
 27  *$D = 2(R - R_i)$  in the definition of  $f$  in Equation (118). As in the case for laminar flow, the*

1 *borehole radius  $R$  is assumed to increase until a value of  $\tau$  (actually,  $\tau(R)$ ) is reached that*  
 2 *equals the sample value for the shear strength of the waste (i.e., the uncertain parameter*  
 3 *WTAUFAIL in Table PA-17). Computationally, the eroded borehole diameter is determined*  
 4 *by solving Equation (120) for  $R$  under the assumption that  $\tau$  equals the assumed shear*  
 5 *strength of the waste.*

6 *In the CRA-2004 PA, a slight modification to the definition of  $\tau$  in Equation (120) was made*  
 7 *to account for drill string rotation when fluid flow in the vicinity of the drill collars is*  
 8 *turbulent (Abdul Khader and Rao 1974; Bilgen et al. 1973). Specifically, an axial flow*  
 9 *velocity correction factor (i.e., a rotation factor),  $F_r$ , was introduced into the definition of  $\tau$ .*  
 10 *The correction factor  $F_r$  is defined by*

$$F_r = \frac{\|\mathbf{v}_{2100}\|}{\|\mathbf{v}\|}, \quad (121)$$

12 *where  $\|\mathbf{v}_{2100}\|$  is the norm of the flow velocity required for the eroded diameters to be the*  
 13 *same for turbulent and laminar flow at a Reynolds number of  $R_e = 2100$  and is obtained by*  
 14 *solving*

$$\tau_{fail} = \frac{f \rho_f \|\mathbf{v}_{2100}\|^2}{2(0.8165)} \quad (122)$$

16 *for  $\|\mathbf{v}_{2100}\|$  with  $D$  in the definition of  $f$  in Equation (118) assigned the final diameter value*  
 17 *that results for laminar flow at a Reynolds number of  $R_e = 2100$  (i.e., the  $D$  in*  
 18  *$D_e = 2(R - R_i) = D - 2R_i$  obtained from Equation (107) with  $R_e = 2100$ ). The modified*  
 19 *definition of  $\tau$  is*

$$\tau = \frac{f \rho_f (F_r \|\mathbf{v}\|)^2}{2(0.8165)}, \quad (123)$$

21 *and results in turbulent and laminar flow having the same eroded diameter at a Reynolds*  
 22 *number of 2100, which is the Reynolds number at which a transition between turbulent and*  
 23 *laminar flow is assumed to take place.*

#### 24 *PA-4.5.2.3 Calculation of $R_f$*

25 *The following algorithm was used to determine the final eroded radius  $R_f$  of a borehole and*  
 26 *incorporates the possible occurrence of a transition from turbulent to laminar fluid flow*  
 27 *within a borehole.*

28 *Step 1. Use Equation (107) to determine an initial Reynolds number  $R_e$ , with  $R$  set to*  
 29 *the drill-bit radius,  $R_0 = 12.25$  in (Attachment PAR, Table PAR-13).*

1 *Step 2. If  $R_e < 2100$ , the flow is laminar and the procedure in Section PA-4.5.2.1 is*  
 2 *used to determine  $R_f$ . Because any increase in the borehole diameter will cause the*  
 3 *Reynolds number to decrease, the flow will remain laminar and there is no need to*  
 4 *consider the possibility of turbulent flow as the borehole diameter increases, with the*  
 5 *result that  $R_f$  determined in this step is the final eroded radius of the borehole.*

6 *Step 3. If  $R_e \geq 2100$ , then the flow is turbulent and the procedure discussed in Section*  
 7 *PA-4.5.2.2 is used to determine  $R_f$ . Once  $R_f$  is determined, the associated Reynolds*  
 8 *number  $R_e$  is calculated with Equation (107) and  $R = R_f$ . If  $R_e > 2100$ , then a*  
 9 *transition from turbulent to laminar flow cannot take place, and the final eroded*  
 10 *radius is  $R_f$  determined in this step.*

11 *Step 4. If the Reynolds number  $R_e$  determined in Step 3 satisfies the inequality*  
 12  *$R_e \leq 2100$ , then a transition from turbulent to laminar flow is assumed to have taken*  
 13 *place. In this case, the calculation of  $R_f$  is redone for laminar flow, with the outer*  
 14 *borehole radius  $R$  initially defined to be the radius at which the transition from*  
 15 *turbulent to laminar flow occurs (i.e., the radius associated with  $R_e = 2100$ ). In*  
 16 *particular, the initial value for  $R$  is given by*

$$17 \quad R = R_i + \frac{2100\eta_\infty}{2(0.8165)\|\mathbf{v}\|\rho}, \quad (124)$$

18 *which is obtained from Equation (107) by solving for  $R$  with  $R_e = 2100$ . A new value*  
 19 *for  $R_f$  is then calculated with the procedure discussed in Section PA-4.5.2.1 for*  
 20 *laminar flow, with this value of  $R_f$  replacing the value from Step 3 as the final eroded*  
 21 *diameter of the borehole.*

22 *Step 5. Once  $R_f$  is known, the amount of waste removed to the surface is determined by*  
 23 *Equation (105) with  $D_f = 2R_f$ .*

#### 24 *PA-4.5.3 Additional Information*

25 *Additional information on CUTTINGS\_S and its use in the CRA-2004 PA to determine*  
 26 *cuttings and cavings releases can be found in the CUTTINGS\_S user's manual (WIPP PA*  
 27 *2003e) and in the analysis package for cuttings and cavings releases (Dunagan 2003a).*

#### 28 *PA-4.6 Spallings to Surface: DRSPALL and CUTTINGS\_S*

29 *Spallings are waste solids introduced into a borehole by the movement of waste-generated gas*  
 30 *towards the lower-pressure borehole. In engineering literature, the term "spalling" is used to*  
 31 *describe the phenomenon of dynamic fracture of a solid material such as rock or metal*  
 32 *(Antoun et al. 2003). In WIPP PA, the model for spallings describes a series of processes*  
 33 *including tensile failure of solid waste, fluidization of failed material, entrainment into the*  
 34 *wellbore flow, and transport up the wellbore to the land surface. Spallings releases could*

1 *occur when pressure differences between the repository and the wellbore are sufficient to*  
2 *cause solid stresses in the waste exceeding the waste material strength and gas velocities*  
3 *sufficient to mobilize failed waste material.*

4 *The spallings model is described in the following sections. Presented first are the primary*  
5 *modeling assumptions used to build the conceptual model. Next, the mathematical model and*  
6 *its numerical implementation in the FORTRAN code DRSPALL (for Direct Release Spall) are*  
7 *described. Finally, implementation of the spallings model in WIPP PA by means of the code*  
8 *CUTTINGS\_S.*

#### 9 *PA-4.6.1 Summary of Assumptions*

10 *Assumptions underlying the spallings model include the future state of the waste,*  
11 *specifications of drilling equipment, and the driller's actions at the time of intrusion.*  
12 *Consistent with the other PA models, the spallings model assumes massive degradation of the*  
13 *emplaced waste through mechanical compaction, corrosion, and biodegradation. Waste is*  
14 *modeled as a homogeneous, isotropic, weakly-consolidated material with uniform particle size*  
15 *and shape. The rationale for selection of the spallings model material properties is addressed*  
16 *in detail in reports by Hansen et al. (1997, 2003).*

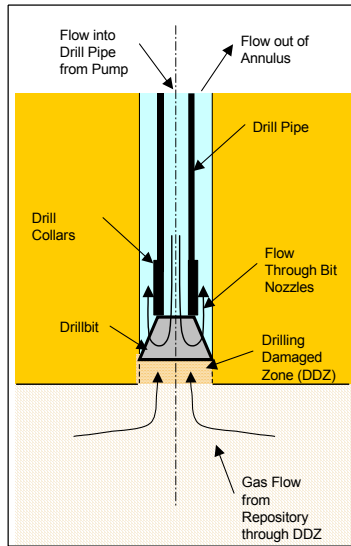
17 *Drilling equipment specifications, such as bit diameter and drilling mud density, are based on*  
18 *surveys of drillers in the Delaware Basin (Hansen et al. 2003). Assumptions about the*  
19 *driller's actions during the intrusion are conservative. Typically, the drilling mud density is*  
20 *controlled to maintain a slightly "overbalanced" condition so that the mud pressure is always*  
21 *slightly higher than the fluid pressures in the formation. If the borehole suddenly passes*  
22 *through a high-pressure zone, the well can quickly become "underbalanced," with a resulting*  
23 *fluid pressure gradient driving formation fluids into the wellbore. This situation is known as a*  
24 *"kick," and is of great concern to drillers because a violent kick can lead to a blowout of mud,*  
25 *gas, and oil from the wellbore, leading to equipment damage and worker injury. Standard*  
26 *drilling practice is to watch diligently for kicks. The first indicator of a kick is typically an*  
27 *increase in mud return rate leading to an increase in mud pit volume (Frigaard and*  
28 *Humphries 1997). Down-hole monitors detect whether the kick is air, H<sub>2</sub>S, or brine. If the*  
29 *kick fluid is air, the standard procedure is to stop drilling and continue pumping mud in order*  
30 *to circulate the air pocket out. If the mud return rate continues to grow after drilling has*  
31 *stopped and the driller believes that the kick is sufficiently large to cause damage, the well may*  
32 *be shut in by closing the blowout preventer. Once shut in, the well pressure may be bled off*  
33 *slowly and mud weight eventually increased and circulated to offset the higher formation*  
34 *pressure before drilling continues. The spallings model simulates an underbalanced system in*  
35 *which a gas kick is assured, and the kick proceeds with no intervention from the drill*  
36 *operation. Therefore, drilling and pumping continue during the entire blowout event.*

#### 37 *PA-4.6.2 Conceptual Model*

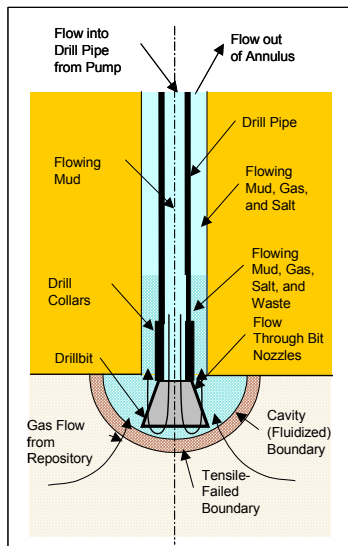
38 *The spallings model calculates transient repository and wellbore fluid flow before, during, and*  
39 *after the drilling intrusion. To simplify the calculations, both the wellbore and the repository*  
40 *are modeled by one-dimensional geometries. The wellbore assumes a compressible Newtonian*  
41 *fluid consisting of a mixture of mud, gas, salt and waste solids; viscosity of the mixture varies*

1 *with the fraction of waste solids in the flow. In the repository, flow is viscous, isothermal,*  
 2 *compressible single-phase (gas) flow in a porous medium.*

3 *The wellbore and repository flows are coupled by a cylinder of porous media before*  
 4 *penetration, and by a cavity representing the bottom of the borehole after penetration.*  
 5 *Schematic diagrams of the flow geometry prior to and after penetration are shown in Figure*  
 6 *PA-15 and Figure PA-16, respectively. The drill bit moves downward as a function of time,*  
 7 *removing salt or waste material. After penetration, waste solids freed by drilling, tensile*  
 8 *failure, and associated fluidization may enter the wellbore flow stream at the cavity forming*  
 9 *the repository-wellbore boundary.*



10  
 11 *Figure PA-15. Schematic Diagram of the Flow Geometry Prior to Repository Penetration.*



12  
 13 *Figure PA-16. Schematic Diagram of the Flow Geometry After Repository Penetration.*

1 ***PA-4.6.2.1 Wellbore Flow Model***

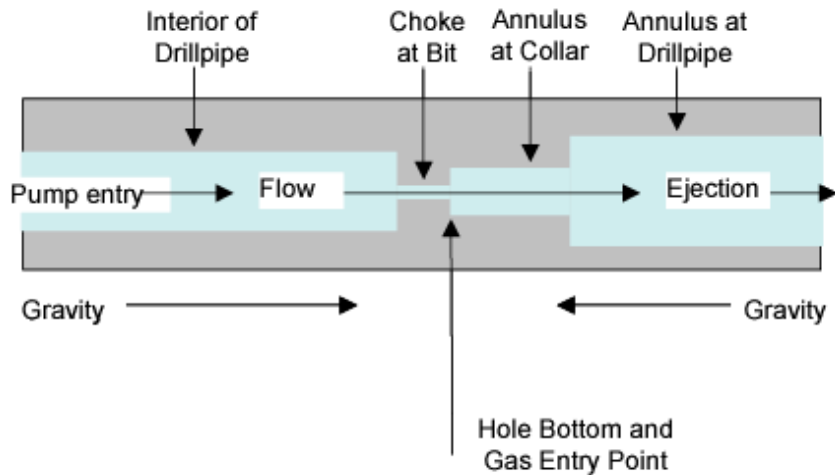
2 *Flow in the well is modeled as one-dimensional pipe flow with cross-sectional areas*  
 3 *corresponding to the appropriate flow area at a given position in the well, as shown in Figure*  
 4 *PA-17 and Figure PA-18. In concept, this model is similar to that proposed by Podio and*  
 5 *Yang (1986) and now in use in the oil and gas industry. Drilling mud is added at the wellbore*  
 6 *entrance by the pump. Flow through the drill bit is treated as a choke with cross-sectional*  
 7 *area appropriate for the bit nozzle area. At the annulus output to the surface, mixture ejection*  
 8 *is to a constant atmospheric pressure. The gravitational body force acts in its appropriate*  
 9 *direction based on position before or after the bit.*

10 *Prior to drill bit penetration into the repository, gas from the repository can flow through*  
 11 *drilling-damaged salt into the well. After penetration, the cavity at the bottom of the wellbore*  
 12 *couples the wellbore flow and the repository flow models; gas and waste material can exit the*  
 13 *repository domain into the cavity. The cavity radius increases as waste materials are moved*  
 14 *into the wellbore.*

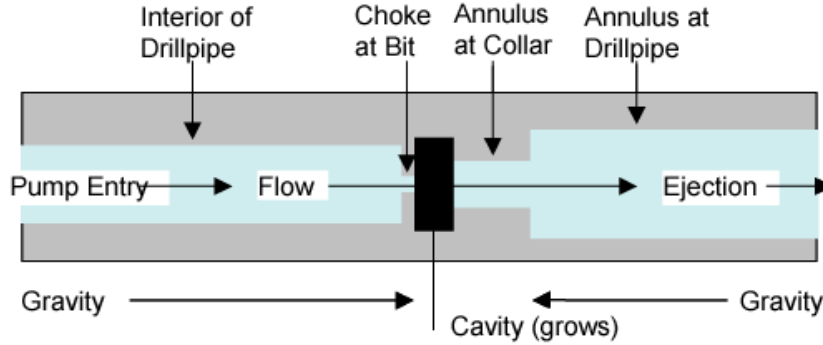
15 *The system of equations representing flow in the wellbore includes: four equations for mass*  
 16 *conservation, one for each phase (salt, waste, mud and gas); one equation for conservation of*  
 17 *total momentum; two equations relating gas and mud density to pressure; the definition of*  
 18 *density for the fluid mixture; and one constraint imposed by the fixed volume of the wellbore.*  
 19 *The conservation of mass and momentum are described by:*

20 
$$\frac{\partial}{\partial t}(\rho_q V_q) + \frac{\partial}{\partial z}(\rho_q V_q u) = S_q \tag{125a}$$

21 
$$\frac{\partial}{\partial t}(\rho V u) + \frac{\partial}{\partial z}(\rho V u^2) = -V \left( \frac{\partial P}{\partial z} - \rho g + F \right) + S_{mom}, \tag{125b}$$



22 ***Figure PA-17. Effective Wellbore Flow Geometry Before Bit Penetration.***  
 23



1  
2 **Figure PA-18. Effective Wellbore Flow Geometry After Bit Penetration.**

3 *where*

4  $q$  = phase (*w* for waste, *s* for salt, *m* for mud, and *g* for gas),

5  $V_q$  = volume ( $m^3$ ) of phase  $q$ ,

6  $V$  = total volume ( $m^3$ ),

7  $\rho_q$  = density ( $kg/m^3$ ) of phase  $q$ , constant for salt and waste (2180 and  
8 2650  $kg/m^3$ , respectively) and pressure-dependent for gas and mud (see  
9 Equation (126) and Equation (127)),

10  $\rho$  = density of fluid mixture ( $kg/m^3$ ) determined by Equation (128),

11  $u$  = velocity ( $m/s$ ) of fluid mixture in wellbore ,

12  $t$  = time ( $s$ ),

13  $z$  = distance ( $m$ ) from inlet at top of well ,

14  $S_q$  = rate of mass ( $kg/s$ ) of phase  $q$  entering and exiting wellbore domain at  
15 position  $z$  (Equation (138)),

16  $S_{mom}$  = rate of momentum ( $kg\ m / s^2$ ) entering and exiting wellbore domain at  
17 position  $z$  (Equation (141)),

18  $P$  = pressure ( $Pa$ ) at position  $z$  ,

19  $g$  = gravity constant ( $9.8067\ kg/m\ s^2$ ),

20  $F$  = friction loss using pipe flow model ( $kg/m^2\ s^2$ ) determined by Equation (130).

21 *Gas is treated as isothermal and ideal, so*

$$\frac{\rho}{\rho_{g,0}} = \frac{P}{P_{atm}}, \quad (126)$$

2 where  $\rho_{g,0}$  is the density of the gas at atmospheric pressure ( $8.24182 \times 10^{-2} \text{ kg/m}^3$  in the  
3 CRA-2004 PA).

4 The mud is assumed to be a compressible liquid, so

$$\rho_m = \rho_{m,0} [1 + c_m (P - P_{atm})], \quad (127)$$

6 where  $\rho_{m,0}$  is the density of the mud at atmospheric pressure ( $1210 \text{ kg/m}^3$  in the CRA-2004  
7 PA) and  $c_m$  is the compressibility of the mud ( $3.1 \times 10^{-10} \text{ Pa}^{-1}$  in the CRA-2004 PA).

8 The density of the fluid mixture is determined from the densities and volumes occupied by the  
9 phases:

$$\rho = \frac{\rho_g V_g + \rho_m V_m + \rho_s V_s + \rho_w V_w}{V}. \quad (128)$$

11 The volume of each phase is constrained by the fixed volume of the wellbore:

$$V = V_g + V_m + V_s + V_w. \quad (129)$$

13 The friction loss is a standard formulation for pipe flow (Fox and McDonald 1985), where the  
14 head loss per unit length is given as:

$$F = f \frac{\rho}{d_h} \frac{u^2}{2}. \quad (130)$$

16 The hydraulic diameter  $d_h$  is given by

$$d_h = \frac{4A}{\pi(D_i + D_o)}. \quad (131)$$

18 In the CRA-2004 PA,  $D_o = 0.31115 \text{ m}$  throughout the domain. From the bit to the top of the  
19 collar,  $D_i = 0.2032 \text{ m}$ ; above the collar,  $D_i = 0.1143 \text{ m}$ . The area  $A$  is calculated as the area of  
20 the annulus between the outer and inner radii. Thus,  $d_h = 0.108 \text{ m}$  from the bit to the top of  
21 the collar, and  $d_h = 0.197 \text{ m}$  above the collar.

22 The friction factor  $f$  is determined by method of Colebrook (Fox and MacDonald 1985). In  
23 the laminar regime ( $Re < 2100$ )

1 
$$f = \frac{64}{\text{Re}}, \tag{132}$$

2 *and in the turbulent regime ( $\text{Re} > 2100$ )*

3 
$$\frac{1}{\sqrt{f}} = 1.0 \log \left( \frac{\varepsilon/d_h}{3.7} + \frac{2.51}{\text{Re}\sqrt{f}} \right), \tag{133}$$

4 *where  $\text{Re} = \frac{u\rho d_h}{\eta}$  is the Reynolds number of the mixture, and  $\eta$  is the viscosity calculated by*  
 5 *Equation (134). As the wellbore mixture becomes particle-laden, the viscosity of the mixture is*  
 6 *determined from an empirical relationship developed for proppant slurry flows in channels for*  
 7 *the oil and gas industry (Barree and Conway 1995). Viscosity is computed by an approximate*  
 8 *slurry formula based on the volume fraction of waste solids:*

9 
$$\eta = \eta_0 \left( 1 - \frac{w}{w_{\max}} \right)^s, \tag{134}$$

10 *where  $\eta_0$  is a base mixture viscosity ( $9.17 \times 10^{-3}$  Pa sec in the CRA-2004 PA),  $w = V_w / V$  is*  
 11 *the current volume fraction of waste solids,  $w_{\max}$  is an empirically determined maximal*  
 12 *volume fraction above which flow is choked (0.615 in the CRA-2004 PA), and  $s$  is an*  
 13 *empirically determined constant ( $-1.5$  in the CRA-2004 PA) (Hansen et al. 2003).*

14 **PA.-4.6.2.1.1 Wellbore initial conditions**

15 *Initial conditions in the wellbore approximate mixture flow conditions just prior to penetration*  
 16 *into the waste. The wellbore is assumed to contain only mud and salt. Initial conditions for*  
 17 *the pressure, fluid density, volume fractions of mud and salt, and the mixture velocity are set*  
 18 *by the following algorithm.*

19 *Step 1. Set pressure in the wellbore to hydrostatic:  $P(z) = P_{\text{atm}} + \rho_{m,0}gz$ .*

20 *Step 2. Set mud density using Equation (127).*

21 *Step 3. Set mixture velocity:  $u(z) = \frac{R_m}{A(z)}$ , where  $R_m$  is the volume flow rate of the*  
 22 *pump ( $0.0202 \text{ m}^3/\text{s}$  in the CRA-2004 PA), and  $A(z)$  is the cross-sectional area of the*  
 23 *wellbore.*

1 *Step 4. Set volume of salt in each cell:  $V_{s,i} = R_{drill} A_{bit} \frac{\Delta z_i}{u_i}$ , where  $R_{drill}$  is the rate of*  
 2 *drilling (0.004445 m/s in the CRA-2004 PA),  $A_{bit} = \frac{\pi d_{bit}^2}{4}$  is the area of the bottom of*  
 3 *the wellbore and  $d_{bit}$  is the diameter of the bit (0.31115 m in the CRA-2004 PA).*

4 *Step 5. Set volume fraction of mud in each cell:  $V_{m,i} = V_i - V_{s,i}$ .*

5 *Step 6. Recalculate mixture density using Equation (128), assuming no waste or gas in*  
 6 *the wellbore.*

7 *The initial conditions set by this algorithm approximate a solution to the wellbore flow*  
 8 *(Equation (125)) for constant flow of mud and salt in the well. The approximation rapidly*  
 9 *converges to a solution for wellbore flow if steady-state conditions are maintained (WIPP PA*  
 10 *2003f).*

11 *PA-4.6.2.1.2 Wellbore boundary conditions*

12 *For simplicity, the CRA-2004 PA does not model flow of mud down the pipe to the bit. Mass*  
 13 *can enter the wellbore below the drill bit, and can exit at the wellbore outlet. Below the bit,*  
 14 *mud, salt, gas, and waste can enter the wellbore. The CRA-2004 PA assumes a constant*  
 15 *volume of mud flow down the drilling pipe; therefore, the source term for mud,  $S_{m,in}$  is set by*  
 16 *the volume flow rate of the pump  $R_m$  (0.0202 m<sup>3</sup>/s in the CRA-2004 PA) and the density of the*  
 17 *mud at the bottom of the wellbore:*

18 
$$S_{m,in} = \rho_m R_m \cdot \tag{135}$$

19 *Until the drill bit penetrates the repository, salt enters the wellbore at a constant rate:*

20 
$$S_{s,in} = \rho_s R_{drill} A_{bit} \cdot \tag{136}$$

21 *Additional mass enters the wellbore by gas flow from the repository ( $S_{gas,in}$ ) or by drilling or*  
 22 *spalling of waste material ( $S_{w,in}$ ); these mass sources are discussed in Section PA-4.6.2.3. The*  
 23 *outlet of the wellbore is set to atmospheric pressure. Mass exiting the wellbore is determined*  
 24 *from the mixture velocity, the area of the outlet  $A_{out}$  (0.066 m<sup>2</sup> in the CRA-2004 PA), and the*  
 25 *density and volume fraction of each phase at the outlet of the wellbore:*

26 
$$S_{q,out} = \rho u_{out} A_{out} \frac{V_q}{V} \cdot \tag{137}$$

27 *Finally, the net change in mass for phase q is*

28 
$$S_q = S_{q,in} - S_{q,out} \cdot \tag{138}$$

1 
$$S_{mom,in} = \frac{\rho_{0,m}}{A_p} R_{mudpump} \cdot \quad (139)$$

2 *The outlet of the wellbore is set to atmospheric pressure. Momentum exiting the wellbore is*  
 3 *determined from the fluid velocity and the area of the outlet  $A_{out}$  (0.066 m<sup>2</sup> in the CRA-2004*  
 4 *PA):*

5 
$$S_{mom,out} = -\rho A_{out} u_{out}^2 \cdot \quad (140)$$

6 *No momentum is added by mass flow into the wellbore from the repository, thus:*

7 
$$S_{mom} = S_{mom,in} - S_{mom,out} \cdot \quad (141)$$

8 **PA-4.6.2.2 Repository Flow Model**

9 *The repository is modeled as a radially-symmetric domain. A spherical coordinate system is*  
 10 *used for this presentation and for most DRSPALL calculations in the CRA-2004 PA. In a few*  
 11 *circumstances, cylindrical coordinates are used in CRA-2004 PA calculations, where spall*  
 12 *volumes are large enough that spherical coordinates are not representative of the physical*  
 13 *process (Lord et al. 2003). Cylindrical coordinates are also available; the Design Document*  
 14 *for DRSPALL (WIPP PA 2003g) provides details on the implementation of the repository flow*  
 15 *model in cylindrical coordinates.*

16 *Flow in the repository is transient, compressible, viscous, and single phase (gas) flow in a*  
 17 *porous medium. Gas is treated as isothermal and ideal. The equations governing flow in the*  
 18 *repository are the equation of state for gas, conservation of mass, and Darcy's law with the*  
 19 *Forchheimer correction (Aronson 1986; Whitaker 1996):*

20 
$$\frac{\rho_g}{\rho_{g,0}} = \frac{P}{P_{atm}}, \quad (142a)$$

21 
$$\phi \frac{\partial \rho_g}{\partial t} + \nabla \cdot (\rho_g u) = 0, \quad (142b)$$

22 
$$\nabla P = -\frac{\eta_g}{k} (1 + F) u, \quad (142c)$$

23 *where*

24  $P = \text{pressure in pore space (Pa)},$

25  $\rho_g = \text{density of gas (kg/m}^3\text{)},$

26  $u = \text{velocity of gas in pore space (m/s)},$

- 1  $\phi =$  porosity of the solid (unitless),
- 2  $\eta_g =$  gas viscosity ( $8.934 \times 10^{-6}$  Pa s),
- 3  $k =$  permeability of waste solid ( $m^2$ ),
- 4  $F =$  Forchheimer coefficient (unitless).

5 *The Forchheimer correction is included to account for inertia in the flowing gas, which*  
 6 *becomes important at high gas velocities (Ruth and Ma 1992). When the Forchheimer*  
 7 *coefficient is zero, Equation (142c) reduces to Darcy’s Law. A derivation of Equation (142c)*  
 8 *from the Navier-Stokes equations is given by Whitaker (1996); the derivation suggests that F*  
 9 *is a linear function of gas velocity for a wide range of Reynolds numbers.*

10 *In the CRA-2004 PA, the Forchheimer coefficient takes the form*

11 
$$F = \beta_{nd} \rho u, \tag{143}$$

12 *where  $\beta_{nd}$  is the non-Darcy coefficient, which depends on material properties such as the*  
 13 *tortuosity and area of internal flow channels, and is empirically determined (Belhaj et al.*  
 14 *2003). The CRA-2004 PA uses a value from a study by Li et al. (2001) that measured high-*  
 15 *velocity nitrogen flow through porous sandstone wafers, giving the result*

16 
$$\beta_{nd} = \frac{1.15 \times 10^{-6}}{k \phi}. \tag{144}$$

17 *Equation (142) combines into a single equation for pressure in the porous solid:*

18 
$$\frac{\partial P}{\partial t} = \frac{k'}{2\phi\eta_g} \nabla^2 P^2 + \frac{1}{2\phi\eta_g} \nabla P^2 \cdot \nabla k', \tag{145}$$

19 *where*

20 
$$k' = \frac{k}{1 + F} = \frac{k}{1 + \beta_{nd} \rho u}, \tag{146}$$

21 *and the operator in a radially-symmetric coordinate system is given by*

22 
$$\nabla^2 = \frac{1}{r^{n-1}} \frac{\partial}{\partial r} \left( r^{n-1} \frac{\partial}{\partial r} \right), \tag{147}$$

23 *where  $n = 2$  and  $n = 3$  for cylindrical and spherical coordinates, respectively.*

24 *In the CRA-2004 PA, the permeability of the waste solid is a subjectively uncertain parameter*  
 25 *that is constant for waste material that has not failed and fluidized. In a region of waste that*

1 *has failed, the permeability increases as the waste fluidizes by a factor of  $1 + F_f$  where  $F_f$  is*  
 2 *the fraction of failed material that has fluidized and is based on the fluidization relaxation*  
 3 *time. This approximately accounts for the bulking of material as it fluidizes.*

4 *Initial pressure in the repository is set to a constant value  $P_{ff}$ . A no-flow boundary condition*  
 5 *is imposed at the outer boundary ( $r = R$ ):*

6 
$$\nabla P(R) = 0. \tag{148}$$

7 *At the inner boundary ( $r = r_{cav}$ ), the pressure is specified as  $P(r_{cav}, t) = P_{cav}(t)$ , where*  
 8  *$P_{cav}(t)$  is defined in the next section. The cavity radius  $r_{cav}$  increases as drilling progresses*  
 9 *and as waste material fails and moves into the wellbore; calculation of  $r_{cav}$  is described in*  
 10 *Section PA-4.6.2.3.3.*

11 **PA-4.6.2.3 Wellbore to Repository Coupling**

12 *Prior to penetration, a cylinder of altered-permeability salt material with diameter equal to the*  
 13 *drill bit is assumed to connect the bottom of the wellbore to the repository. At the junction of*  
 14 *the repository and this cylinder of salt, a small, artificial cavity is used to determine the*  
 15 *boundary pressure for repository flow. After penetration, the cavity merges with the bottom of*  
 16 *the wellbore to connect the wellbore to the repository.*

17 **PA-4.6.2.3.1 Flow Prior to Penetration**

18 *The cylinder of salt connecting the wellbore to the repository is referred to as the Drilling*  
 19 *Damaged Zone (DDZ) in Figure PA-15. The permeability of the DDZ,  $k_{DDZ}$ , is  $1 \times 10^{-14}$  ( $m^2$ )*  
 20 *in the CRA-2004 PA. The spall model starts with the bit 0.15 m above the repository; the bit*  
 21 *advances at a rate of  $R_{drill} = 0.004445$  (m/s).*

22 *To couple the repository to the DDZ, the model uses an artificial pseudo-cavity in the small*  
 23 *hemispherical region of the repository below the wellbore, with the same surface area as the*  
 24 *bottom of the wellbore (Figure PA-18). The pseudo-cavity is a numerical device that smoothes*  
 25 *the discontinuities in pressure and flow that would otherwise occur upon bit penetration of the*  
 26 *repository. The pseudo-cavity contains only gas and is initially at repository pressure. The*  
 27 *mass of gas in the cavity  $m_{cav}$  is given by:*

28 
$$\frac{dm_{cav}}{dt} = S_{rep} - S_{g,in}, \tag{149}$$

29 *where*

30  $S_{rep}$  = *gas flow from repository into pseudo-cavity (kg/s); see Equation (150),*

31  $S_{g,in}$  = *gas flow from pseudo-cavity through DDZ into wellbore (kg/s); see Equation*  
 32 *(151).*

1 *Flow from the repository into the pseudo-cavity is given by*

$$2 \quad S_{rep} = \rho_{g,rep} u_{rep} \phi A_{cav}, \quad (150)$$

3 *where*

$$4 \quad \rho_{g,rep} = \text{gas density in repository at cavity surface (kg/m}^3\text{)} = \rho_g(r_{cav}),$$

$$5 \quad u_{rep} = \text{gas velocity (m/s) in repository at cavity surface} = u(r_{cav}),$$

$$6 \quad \phi = \text{porosity of waste (unitless),}$$

$$7 \quad A_{cav} = \text{surface area of hemispherical part of the cavity (m}^2\text{),}$$

$$8 \quad = \frac{\pi}{4} d_{bit}^2, \text{ where } d_{bit} \text{ is the diameter of the bit (m).}$$

9 *Flow out of the pseudo-cavity through the DDZ and into the wellbore is modeled as steady-*  
 10 *state using Darcy's Law:*

$$11 \quad S_{g,in} = \frac{k_{DDZ} \pi \left( \frac{d_{bit}}{2} \right)^2}{2 \eta_g R_0 T L} (P_{cav}^2 - P_{BH}^2), \quad (151)$$

12 *where*

$$13 \quad \eta_g = \text{gas viscosity (} 8.934 \times 10^{-6} \text{ Pa s),}$$

$$14 \quad R_0 = \text{ideal gas constant for hydrogen (4116 J / kg }^\circ\text{K),}$$

$$15 \quad T = \text{repository temperature (constant at } 300 \text{ }^\circ\text{K),}$$

$$16 \quad L = \text{length (m) of DDZ (from bottom of borehole to top of repository)}$$

$$17 \quad P_{cav} = \text{pressure in pseudo-cavity (Pa),}$$

$$18 \quad P_{BH} = \text{pressure at bottom of wellbore (Pa).}$$

19 *A justification for the use of this steady-state equation is provided in the Design Document for*  
 20 *DRSPALL (WIPP PA 2003g). The pseudo-cavity is initially filled with gas at a pressure of  $P_{ff}$*   
 21 *The boundary pressure on the well side ( $P_{BH}$ ) is the pressure immediately below the bit,*  
 22 *determined by Equation (125). The pressure in the pseudo-cavity ( $P_{cav}$ ) is determined by the*  
 23 *ideal gas law:*

1 
$$P_{cav} = \frac{m_{cav}R_0T}{V_{cav}}, \quad (152)$$

2 *where the volume of the cavity  $V_{cav}$  is given by*

3 
$$V_{cav} = \left( \frac{\pi}{24\sqrt{2}} \right) d_{bit}^3. \quad (153)$$

4 *In the CRA-2004 PA the drilling rate is constant at 0.004445 (m/s) thus  $L = L_i - 0.004445t$*   
 5 *until  $L = 0$ , at which time the bit penetrates the waste. The term  $L_i$  is the distance from the bit*  
 6 *to the waste at the start of calculation (0.15 m in the CRA-2004 PA).*

7 **PA-4.6.2.3.2 Flow After Penetration**

8 *After penetration of the waste, the bottom of the wellbore is modeled as a hemispherical cavity*  
 9 *in the repository, the radius of which grows as drilling progresses and as material fails and*  
 10 *moves into the cavity. Gas, drilling mud, and waste are assumed to thoroughly mix in this*  
 11 *cavity; the resulting mixture flows around the drill collars and then up the annulus between*  
 12 *the wellbore and the drill string. Gas flow from the repository into the cavity is given by*  
 13 *Equation (150); however,  $A_{cav}$  is now dependent on the increasing radius of the cavity (see*  
 14 *Section PA-4.6.2.3.3). Mudflow into the cavity from the wellbore is given by Equation (135).*  
 15 *Waste flow into the cavity is possible if the waste fails and fluidizes; these mechanisms are*  
 16 *discussed in Sections PA-4.6.2.3.4 and PA-4.6.2.3.5. Pressure in the cavity is equal to the*  
 17 *pressure at the bottom of the wellbore and is computed by Equation (152).*

18 **PA-4.6.2.3.3 Cavity Volume After Penetration**

19 *The cylindrical cavity of increasing depth created by drilling is mapped to a hemispherical*  
 20 *volume at the bottom of the wellbore to form the cavity. This mapping maintains equal*  
 21 *surface areas in order to preserve the gas flux from the repository to the wellbore. The cavity*  
 22 *radius from drilling is thus*

23 
$$r_{drill} = \sqrt{\frac{d_{bit}^2 + 4d_{bit}\Delta H}{8}}, \quad (154)$$

24 *where  $\Delta H$  is the depth of the drilled cylinder. In the CRA-2004 PA, the drilling rate is*  
 25 *constant at 0.004445 (m/s) thus  $\Delta H = 0.004445t$  until  $\Delta H = H$ , the height of compacted*  
 26 *waste (m). Since the initial height of the repository is 3.96 m,  $H$  is computed from the porosity*  
 27  *$\phi$  by  $H = 3.96 \times \frac{1 - \phi_0}{1 - \phi}$ , where  $\phi$  is the initial porosity of a waste-filled room.*

28 *The cavity radius  $r_{cav}$  is increased by the radius of failed and fluidized material  $r_{fluid}$  which is*  
 29 *the depth to which fluidization has occurred beyond the drilled radius. That is,*

$$r_{cav} = r_{drill} + r_{fluid} \quad (155)$$

#### PA-4.6.2.3.4 Waste Failure

Gas flow from the waste creates a pressure gradient within the waste, which induces elastic stresses in addition to the far-field confining stress. These stresses may lead to tensile failure of the waste material, assumed to be prerequisite to spallings releases. While the fluid calculations using Equation (142) are fully transient, the elastic stress calculations are assumed to be quasi-static (i.e., sound-speed phenomena in the solid are ignored). Elastic effective stresses are (Timoshenko and Goodier 1970):

$$\sigma_r(r) = \sigma_{sr}(r) + \sigma_{ff} \left( 1 - \left( \frac{r_{cav}}{r} \right)^3 \right) + P(r_{cav}) \left( \frac{r_{cav}}{r} \right)^3 - \beta P(r), \quad (156)$$

$$\sigma_\theta(r) = \sigma_{s\theta}(r) + \sigma_{ff} \left[ 1 + \frac{1}{2} \left( \frac{r_{cav}}{r} \right)^2 \right] - \frac{P(r_{cav})}{2} \left( \frac{r_{cav}}{r} \right)^3 - \beta P(r), \quad (157)$$

where  $\beta$  is Biot's constant (1.0 in the CRA-2004 PA) and  $\sigma_{ff}$  is the confining far-field stress (assumed constant at 14.9 MPa in the CRA-2004 PA).

The flow-related radial and tangential stresses ( $\sigma_{sr}$  and  $\sigma_{s\theta}$ , respectively) are computed by equations analogous to differential thermal expansion (Timoshenko and Goodier 1970):

$$\sigma_{sr}(r) = 2\beta \left( \frac{1-2\nu}{1-\nu} \right) \frac{1}{r^3} \int_{r_{cav}}^r (P(s) - P_{ff}) s^2 ds, \quad (158)$$

$$\sigma_{s\theta}(r) = -\beta \left( \frac{1-2\nu}{1-\nu} \right) \left( \frac{1}{r^3} \int_{r_{cav}}^r (P(s) - P_{ff}) s^2 ds - (P(r) - P_{ff}) \right), \quad (159)$$

where  $P_{ff}$  is the initial repository pressure and  $\nu$  is Poisson's ratio (0.38 in the CRA-2004 PA).

Since stresses are calculated as quasi-static, an initial stress reduction caused by an instantaneous pressure drop at the cavity face propagates instantaneously through the waste. The result of calculating Equation (156) can be an instantaneous early-time tensile failure of the entire repository if the boundary pressure is allowed to change suddenly. This is non-physical and merely a result of the quasi-static stress assumption combined with the true transient pore pressure and flow-related stress equations. To prevent this non-physical behavior, tensile failure propagation is limited by a tensile failure velocity (1000 m/s in the CRA-2004 PA; see Hansen et al. 1997). This limit has no quantitative effect on results other than to prevent non-physical tensile failure.

1 *At the cavity face, Equation (156) and Equation (158) evaluate to zero, consistent with the*  
 2 *quasi-static stress assumption. This implies that the waste immediately at the cavity face*  
 3 *cannot experience tensile failure; however, tensile failure may occur at some distance into the*  
 4 *waste material. Consequently, the radial effective stress  $\sigma_r$  is averaged from the cavity*  
 5 *boundary into the waste over a characteristic length  $L_t$  (0.02 m in the CRA-2004 PA). If this*  
 6 *average radial stress  $\bar{\sigma}_r$  is tensile and its magnitude exceeds the material tensile strength*  
 7 *( $|\bar{\sigma}_r| > TENSSTR$ ), the waste is no longer capable of supporting radial stress and fails,*  
 8 *permitting fluidization. The waste tensile strength is an uncertain parameter in the analysis*  
 9 *(see TENSSTR in Table PA-14).*

10 *Equation (157) and (159) evaluate shear stresses in the waste. The CRA-2004 PA does not use*  
 11 *the shear stresses in the waste in the calculation of waste failure for spall releases. These*  
 12 *stresses are included in this discussion for completeness.*

13 *PA-4.6.2.3.5 Waste Fluidization*

14 *Failed waste material is assumed to be disaggregated, but not in motion; it remains as a*  
 15 *porous, bedded material lining the cavity face, and is treated as a continuous part of the*  
 16 *repository from the perspective of the porous flow calculations. The bedded material may be*  
 17 *mobilized and may enter the wellbore if the gas velocity in the failed material (see Equation*  
 18 *(142c) exceeds a minimum fluidization velocity,  $U_f$ . The minimum fluidization velocity is*  
 19 *determined by solving the following quadratic equation (Cherimisinoff and Cherimisinoff*  
 20 *1984; Ergun 1952):*

21 
$$\frac{1.75 \left( \frac{d_p U_f \rho_g}{\eta_g} \right)^2}{a \phi^3} + 150 \left( \frac{1 - \phi}{a^2 \phi^3} \right) \left( \frac{d_p U_f \rho_g}{\eta_g} \right) = \frac{d_p^3 \rho_g (\rho_w - \rho_g) g}{\eta_g^2}, \quad (160)$$

22 *where*

23  $a$  = particle shape factor (unitless),

24  $d_p$  = particle diameter (m).

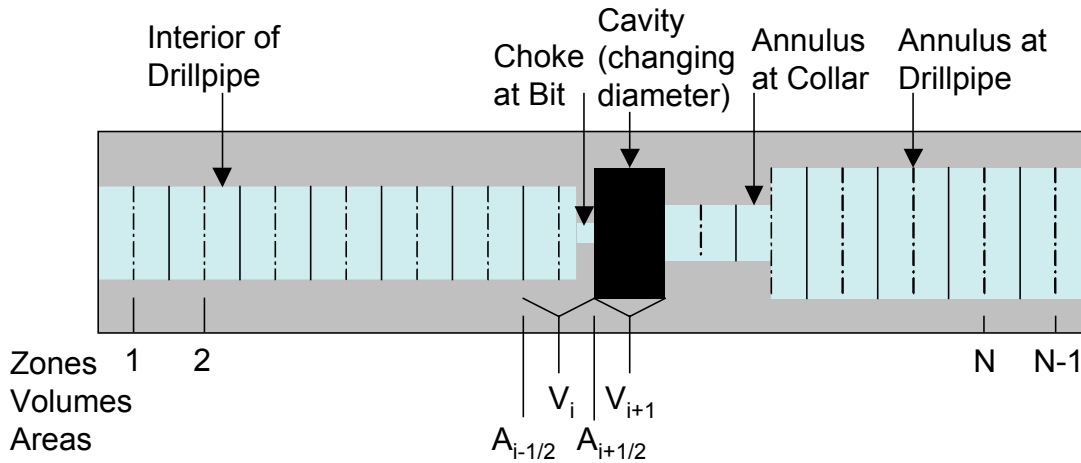
25 *Fluidization occurs in the failed material to the depth at which gas velocity does not exceed the*  
 26 *fluidization velocity; this depth is denoted by  $r_{fluid}$  and is used to determine cavity radius*  
 27 *(Section PA-4.6.2.3.3). If fluidization occurs, the gas and waste particles mix into the cavity at*  
 28 *the bottom of the wellbore. To account for the fact that this mixing cannot be instantaneous,*  
 29 *which would be non-physical (much as allowing instantaneous tensile failure propagation*  
 30 *would be non-physical), a small artificial relaxation time, equal to the cavity radius  $r_{cav}$*   
 31 *divided by the superficial gas velocity  $u(r_{cav})$ , is imposed upon the mixing phenomenon. The*  
 32 *fluidized material is released into the cavity uniformly over the relaxation time.*

1 **PA-4.6.3 Numerical Model**

2 *The numerical model implements the conceptual and mathematical models described above.*  
 3 *Both the wellbore and the repository domain calculations use time-marching finite*  
 4 *differences. These are part of a single computational loop and therefore use the same time*  
 5 *step. The differencing schemes for the wellbore and repository calculations are similar, but*  
 6 *not identical.*

7 **PA-4.6.3.1 Numerical Method – Wellbore**

8 *The wellbore is zoned for finite differencing as shown in Figure PA-19. This shows zones,*  
 9 *zone indices, grid boundaries, volumes, and interface areas. The method is Eulerian; i.e.,*  
 10 *zone boundaries are fixed, and fluid flows across the interfaces by advection. Quantities are*  
 11 *zone-centered and integration is explicit in time.*



12  
13 **Figure PA-19. Finite Difference Zoning for Wellbore.**

14 *To reduce computation time, an iterative scheme is employed to update the wellbore flow*  
 15 *solution. The finite difference scheme first solves Equation (125) for the mass of each phase*  
 16 *in each grid cell and the momentum in each grid cell.*

17 *The updated solution to Equation (125) is then used to compute the volume of each phase, the*  
 18 *pressure, and the mixture velocity in each grid cell.*

19 *All of the materials (mud, salt, gas, and waste) are assumed to move together as a mixture.*  
 20 *Since fluid moves through the cell boundaries, the calculation requires values for the flow*  
 21 *through cell boundaries during a timestep. These values are obtained by averaging the fluid*  
 22 *velocities at the zone centers, given by:*

23 
$$u_{i+1/2} = \frac{1}{2}(u_{i+1}^{n-1} + u_i^{n-1}). \quad (161)$$

24 *The mass transport equation, prior to any volume change, becomes*

$$V_i \rho_i^* = V_i \rho_i^{n-1} - \Delta t \left( A_{i+1/2} \rho_{i+1/2}^{n-1} u_{i+1/2} - A_{i-1/2} \rho_{i-1/2}^{n-1} u_{i-1/2} \right) + \Delta t S_{m,i} \quad (162)$$

Here, the source terms ( $S_{m,i}$ ) are set to correspond to material entering or exiting at the pump, cavity, and surface. The “upwind” zone centered densities are used for the interfaces values,

$$\rho_{i+1/2}^{n-1} \text{ and } \rho_{i-1/2}^{n-1}.$$

Finally any changed volumes are incorporated and numerical mass diffusion is added for stability:

$$V_i \rho_i^n = V_i \rho_i^* + \Delta z_i \sum_{q=w,m,s,g} \zeta_q D_{i,q}, \quad (163)$$

where

$$D_{i,q} = \left[ A_{i+1/2} \left( (\rho f_q)_{i+1}^{n-1} - (\rho f_q)_i^{n-1} \right) - A_{i-1/2} \left( (\rho f_q)_i^{n-1} - (\rho f_q)_{i-1}^{n-1} \right) \right]$$

and  $\zeta_q$  is the diffusion coefficient for phase  $q$ . The density  $\rho f_q$  for the phase  $q$  being diffused is calculated from the mixture density,  $\rho$ , and the mass fraction,  $f_q$  of the phase  $q$  in the referenced cell ( $f_q = \rho V_{q,i} / \rho V_i$ ). The numerical diffusion coefficient  $\zeta_q$  is chosen empirically for stability. Separate diffusion coefficients could be used for the different materials (mud, gas, etc.). However, sufficient stability is obtained by only diffusing mud and salt using the same coefficient ( $\zeta_m = \zeta_s = 0.0001$  and  $\zeta_w = \zeta_g = 0$  in the CRA-2004 PA).

Momentum is differenced as:

$$V_i (\rho u)_i^* = V_i (\rho u)_i^{n-1} - \Delta t \left( A_{i+1/2} (\rho u)_{i+1/2}^{n-1} u_{i+1/2} - A_{i-1/2} (\rho u)_{i-1/2}^{n-1} u_{i-1/2} \right) - V_i \Delta t \left( \frac{P_{i+1}^{n-1} - P_{i-1}^{n-1}}{2\Delta z} - \rho_i^{n-1} g + F_i^{n-1} \right) + \Delta t S_{mom,i}, \quad (164)$$

where the dissipation term  $F_i^{n-1}$  is obtained from Equation (130) and is constrained by:

$$|F_i^{n-1}| \leq \left| \frac{P_{i+1}^{n-1} - P_{i-1}^{n-1}}{2\Delta z} - \rho_i^{n-1} g \right|, \quad (165)$$

1 *and the sign of  $F_i^{n-1}$  is chosen to oppose flow. Finally, numerical momentum diffusion is*  
 2 *added without distinguishing between phases in the mixture ( $\rho$  is the mixture density).*

$$3 \quad V_i (\rho u)_i^n = V_i (\rho u)_i^* - \zeta_p \Delta x_i \left[ A_{i+1/2} \left( (\rho u)_{i+1}^{n-1} - (\rho u)_i^{n-1} \right) - A_{i-1/2} \left( (\rho u)_i^{n-1} - (\rho u)_{i-1}^{n-1} \right) \right]. \quad (166)$$

4 *In the CRA-2004 PA,  $\zeta_p = 0.01$ .*

5 *Equation (127), Equation (128), and Equation (129) comprise a simultaneous system of*  
 6 *equations for the volumes of gas and mud, and the pressure in the wellbore. The volumes of*  
 7 *salt and waste will be known, since they are considered incompressible. Equation (127) and*  
 8 *Equation (128) combine into a quadratic equation for gas volume*

$$9 \quad aV_g^2 + bV_g - c = 0, \quad (167)$$

10 *where*

$$\begin{aligned} a &= 1 - c_m P_{atm}, \\ b &= c_m P_{atm} V_{g,0} - aV^* + V_{m,0}, \\ c &= V^* c_m P_{atm} V_{g,0}, \end{aligned}$$

11

$$\begin{aligned} V_{g,0} &= m_g / \rho_{g,0}, \\ V_{m,0} &= m_m / \rho_{m,0}, \end{aligned}$$

12 *and*

13

$$V^* = V_m + V_g = V - V_s - V_w$$

14 *The volume of the mud phase follows from Equation (127) and the pressure from Equation*  
 15 *(126). Once mixture density in each cell ( $\rho_i$ ) is updated by Equation (128), mixture velocity in*  
 16 *each cell ( $u_i$ ) is computed by*

17

$$u_i = \frac{(\rho u)_i}{\rho_i},$$

18 *where the quantity  $\rho u$  is determined by Equation (166).*

19 **PA-4.6.3.2 Numerical Method – Repository**

20 *The time integration method for the repository flow is implicit, with spatial derivatives*  
 21 *determined after the time increment. This method requires the inversion of a matrix for the*  
 22 *entire repository, which is usually straightforward. The implicit scheme is unconditionally*  
 23 *stable. However, it is still necessary to use small time steps to ensure gradient accuracy.*

1 *The numerical method follows Press et al. (1989). For simplicity, the equations are presented*  
 2 *for constant zone size, although DRSPALL implements difference equations that allow for a*  
 3 *variable zone size. Near the cavity, a small, constant zone size is used, and then zones are*  
 4 *allowed to grow geometrically as the outer boundary is approached. This procedure greatly*  
 5 *increases computational efficiency without sacrificing accuracy in the region of interest.*

6 *For an isothermal ideal gas, the pseudopressure is defined as*

$$7 \quad \psi = \frac{P^2}{\eta} \quad \text{or} \quad P = \sqrt{\eta\psi}. \quad (168)$$

8 *Using Equation (168), Equation (145) is expanded to*

$$9 \quad \frac{\partial \psi}{\partial t} = D(\psi) \left[ \frac{\partial^2 \psi}{\partial r^2} + \frac{(m-1)}{r} \frac{\partial \psi}{\partial r} + \frac{1}{k'} \frac{\partial k'}{\partial r} \frac{\partial \psi}{\partial r} \right], \quad (169)$$

10 *where  $D(\psi) = \frac{k'}{\phi} \sqrt{\frac{\psi}{\eta}} = \frac{k'P}{\phi\eta}$ ; Equation (169) is then converted to a difference equation by*

11 *treating  $D(\psi)$  as constant over a zone, using its zone-centered value at the current time  $D_j^n$ :*

$$12 \quad \frac{\psi_j^{n+1} - \psi_j^n}{\Delta t} = \frac{D_j^n}{\Delta r} \left[ \frac{\psi_{j+1}^{n+1} - 2\psi_j^{n+1} + \psi_{j-1}^{n+1}}{\Delta r} + \frac{(m-1)(\psi_{j+1}^{n+1} - \psi_{j-1}^{n+1})}{2r_j} \right. \\ \left. + \frac{(k_{j+1}^{n+1} - k_{j-1}^{n+1})(\psi_{j+1}^{n+1} - \psi_{j-1}^{n+1})}{4k' \Delta r} \right]. \quad (170)$$

13 *Collecting similar terms in  $\psi$  leads to a tridiagonal system:*

$$14 \quad -\alpha_1 \psi_{j-1}^{n+1} + (1 + 2\alpha) \psi_j^{n+1} - \alpha_2 \psi_{j+1}^{n+1} = \psi_j^n \quad j = 1, 2, \dots, \quad (171)$$

15 *where*

$$16 \quad \alpha = \frac{D_j^n \Delta t}{(\Delta r)^2},$$

$$17 \quad \alpha_1 = \left( \frac{D_j^n}{\Delta r} \right) \left( \frac{1}{\Delta r} - \frac{(m-1)}{2r_j} - \frac{k_{i+1}^{n+1} - k_{i-1}^{n+1}}{4k' \Delta r} \right) \Delta t,$$

$$\alpha_2 = \left( \frac{D_j^n}{\Delta r} \right) \left( \frac{1}{\Delta r} + \frac{(m-1)}{2r_j} + \frac{k_{i+1}^{n+1} - k_{i-1}^{n+1}}{4k' \Delta r} \right) \Delta t.$$

Equation (171) may be solved by simplified LU decomposition as presented in Press et al. (1989).

The boundary condition at the inner radius is implemented by noting that for  $i = 1$  (the first intact or non-fluidized cell),  $\psi_{i-1}$  is the cavity pseudopressure, which is known, and therefore can be moved to the right hand side of Equation (171):

$$(1 + 2\alpha) \psi_1^{n+1} - \alpha_2 \psi_2^{n+1} = \psi_1^n + \alpha_1 \psi_{cav}^{n+1}. \tag{172}$$

The far field boundary condition is a zero gradient, which is implemented by setting  $\psi_{j+1}^{n+1} = \psi_j^{n+1}$  in Equation (172), recognizing that  $1 + 2\alpha = 1 + \alpha_1 + \alpha_2$  and rearranging, which gives

$$-\alpha_1 \psi_{j-1}^{n+1} + (1 + \alpha_1) \psi_j^{n+1} = \psi_j^n, \tag{173}$$

where  $j$  is the index of the last computational cell.

**PA-4.6.3.3 Numerical Method – Wellbore to Repository Coupling**

The term  $u_{rep}$ , appearing in Equation (150), is the gas velocity in the repository at the waste-cavity interface and is determined from the pressure gradient inside the waste. The CRA-2004 PA uses the pressure ( $P_1$ ) at the center of the first numerical zone in the waste to determine  $u_{rep}$ :

$$u_{rep} = \frac{k(P_1 - P_{cav})}{\Delta r \eta_g \phi}. \tag{174}$$

**PA-4.6.4 Implementation**

During development of the spallings model, a total of five parameters were determined to be both uncertain and potentially significant to model results (Hansen et al. 2003; Lord and Rudeen 2003). All five parameters relate to the repository conditions or the state of the waste at the time of intrusion. Table PA-14 lists the uncertain parameters in the DRSPALL calculations.

The computational requirements of DRSPALL prohibit calculation of spall volumes for all possible combinations of initial conditions and parameter values. Since repository pressure is a time-dependent value computed by the BRAGFLO model (see Section PA-4.2), DRSPALL calculations were performed for a small number of pressures. Sensitivity studies showed that spall does not occur at pressures below 10 MPa; this value was used as the lower bound on

1

**Table PA-14. Uncertain Parameters in the DRSPALL Calculations**

<i>Parameter</i>	<i>Variable</i>	<i>Implementation</i>
<i>Repository Pressure</i>	<i>REIPRES</i>	<i>Initial repository pressure (Pa); spall calculated for values of 10, 12, 14, and 14.8 MPa. Defines initial repository pressure in Equation (145) (see Section PA-4.6.2.2) and Pff in Equation (158).</i>
<i>Repository Permeability</i>	<i>REIPERM</i>	<i>Permeability (m<sup>2</sup>) of waste, implemented by parameter SPALLMOD/REIPERM. Loguniform distribution from <math>2.4 \times 10^{-14}</math> to <math>2.4 \times 10^{-12}</math>. Defines <math>k</math> in Equation (142c).</i>
<i>Repository Porosity</i>	<i>REIPOR</i>	<i>Porosity (dimensionless) of waste, implemented by parameter SPALLMOD/REIPOR. Uniform distribution from 0.35 to 0.66. Defines <math>\phi</math> in Equation (142b).</i>
<i>Particle Diameter</i>	<i>PARTDIAM</i>	<i>Particle diameter of waste (m) after tensile failure, implemented by parameter SPALLMOD/PARTDIAM. Loguniform distribution from 0.001 to 0.1 (m). Defines <math>d_p</math> in Equation (160).</i>
<i>Tensile Strength</i>	<i>TENSLSTR</i>	<i>Tensile strength of waste (Pa), implemented by parameter SPALLMOD/TENSLSTR. Uniform distribution from 0.12 MPa to 0.17 MPa. Defines <math>\bar{\sigma}_p</math> in Section PA-4.6.2.3.5.</i>

2 *pressure. In DRSPALL, the repository pressure cannot exceed the far-field confining stress*  
3 *(14.9 MPa in the CRA-2004 PA); consequently, 14.8 MPa was used as the upper bound on*  
4 *pressure. Computations were also performed for intermediate pressures of 12 and 14 MPa.*

5 *The remaining four parameters listed in Table PA-14 were treated as subjectively uncertain.*  
6 *The uncertainty represented by these parameters pertains to the future state of the waste,*  
7 *which is modeled in PA as a homogeneous material with uncertain properties. In order to*  
8 *ensure that sampled values are independent and that the extremes of each parameter's range*  
9 *are represented in the results, the CRA-2004 PA uses Latin hypercube sampling to generate a*  
10 *sample of 50 elements. The LHS generated for DRSPALL calculations is independent of the*  
11 *LHS generated for the general PA calculations. Spall volumes are computed for each*  
12 *combination of initial pressure and sample element, for a total of  $4 \times 50 = 200$  model runs.*  
13 *Although repository porosity could be treated as an initial condition (using the time-dependent*  
14 *value computed by BRAGFLO), to reduce the number of computational cases, and to ensure*  
15 *that extreme porosity values were represented, repository porosity was included as a sampled*  
16 *parameter. The LHS for DRSPALL and the results of the DRSPALL calculations are*  
17 *presented in Lord et al. (2003).*

18 *The spallings submodel of the code CUTTINGS\_S uses the DRSPALL results to compute the*  
19 *spall volume for a given initial pressure  $P$ . An uncertain parameter SPALLMOD/RNDSPALL*  
20 *is included in the LHS for performance assessment (see Section PA-5.2) and is sampled from*  
21 *a uniform distribution on  $[0,1]$ . This parameter selects a sample element from the LHS for*  
22 *DRSPALL. The DRSPALL results for the selected sample element are used to construct the*  
23 *spall volume. If  $P < 10$  MPa or  $P > 14.8$  MPa, the spall volume is the value computed for*  
24 *REIPRESS = 10 MPa or REIPRESS = 14.8 MPa, respectively. If  $P$  falls between 10 and*

1 *14.8 MPa, the spall volume is constructed by linear interpolation between the DRSPALL*  
 2 *results for pressures which bracket P.*

3 *PA-4.6.5 Additional Information*

4 *Additional information on DRSPALL and its use in the CRA-2004 PA to determine spillings*  
 5 *releases can be found in the User's Manual for DRSPALL (WIPP PA 2003h) and in the*  
 6 *analysis package for spillings releases (Lord et al. 2003). Additional information on the*  
 7 *construction of spall volumes by the code CUTTINGS\_S can be found in the CUTTINGS\_S*  
 8 *Design Document (WIPP PA 2003i).*

9 *PA-4.7 Direct Brine Release to Surface: BRAGFLO*

10 *This section describes the model for direct brine release (DBR) volumes, which are volumes of*  
 11 *brine released to the surface at the time of a drilling intrusion. DBR volumes are calculated*  
 12 *by the code BRAGFLO, the same code used to compute two-phase flow in and around the*  
 13 *repository (see Section PA-4.2).*

14 *PA-4.7.1 Overview of Conceptual Model*

15 *DBRs could occur if the pressure in the repository at the time of a drilling intrusion exceeds 8*  
 16 *MPa, which is the pressure exerted by a column of brine-saturated drilling fluid at the depth*  
 17 *of the repository (Stoelzel and O'Brien 1996). For repository pressures less than 8 MPa, no*  
 18 *DBRs are assumed to occur. However, even if the repository pressure exceeds 8 MPa at the*  
 19 *time of a drilling intrusion, a DBR is not assured, as there might not be sufficient mobile brine*  
 20 *in the repository to result in movement towards the borehole.*

21 *DBRs are estimated for the following cases: (1) an initial intrusion into the repository into*  
 22 *either a lower (down-dip), middle, or upper (up-dip) panel, (2) an intrusion into a waste panel*  
 23 *that has been preceded by an E1 intrusion into either the same waste panel, an adjacent panel,*  
 24 *or a non-adjacent panel, and (3) an intrusion into a waste panel that has been preceded by an*  
 25 *E2 intrusion into either the same waste panel, an adjacent panel, or a non-adjacent panel (see*  
 26 *Section PA-6.7). To determine releases for the above cases, the DBR calculations use a*  
 27 *computational grid that explicitly includes all 10 waste panels (Figure PA-20).*

28 *The DBRs are assumed to take place over a relatively short period of time (i.e., 3 to 11 days)*  
 29 *following the drilling intrusion. The initial value conditions for determining DBR volumes*  
 30 *are obtained by mapping solutions of Equation (25) obtained from BRAGFLO with the*  
 31 *computational grid in Figure PA-8 onto the grid in Figure PA-20.*

32 *In concept, the DBR for a drilling intrusion has the form*

$$33 \quad DBR = \int_0^{t_e} rDBR(t) dt, \quad (175)$$

34 *where*

35 *DBR = direct brine release volume (m<sup>3</sup>) for drilling intrusion,*

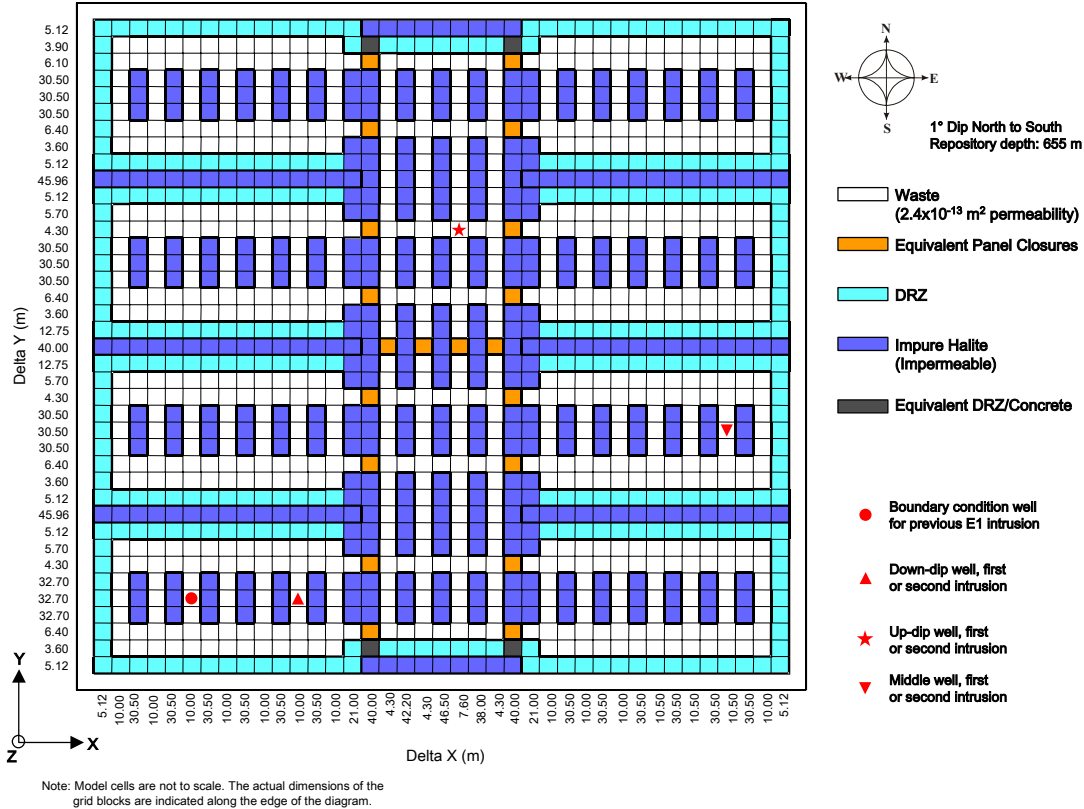


Figure PA-20. DBR Logical Mesh.

$rDBR(t)$  = rate ( $m^3$ ) at time  $t$  at which brine flows up intruding borehole,

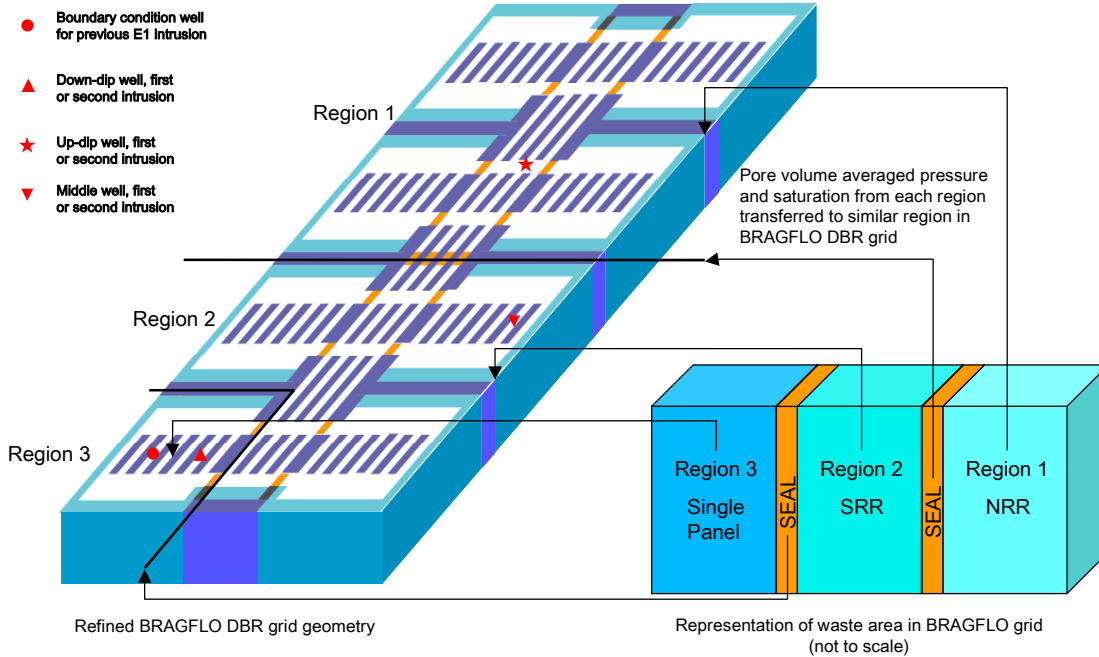
$t$  = elapsed time (s) since drilling intrusion,

$t_e$  = time (s) at which direct brine release ends.

The definition of  $rDBR(t)$  is discussed in the following sections and is based on the two-phase flow relationships in Equation (25) and use of the Poettmann-Carpenter correlation (Poettmann and Carpenter 1952) to determine a boundary pressure at the connection between the intruding borehole and the repository. The time  $t_e$  is based on current drilling practices in the Delaware Basin (Section PA-4.7.8).

PA-4.7.2 Linkage to Two-Phase Flow Calculation

The mesh in Figure PA-20 was linked to the mesh in Figure PA-8 by subdividing the waste disposal area in the mesh in Figure PA-8 into three regions (Figure PA-21). Region 1 represents the northern rest of repository North RoR area in Figure PA-8. Region 2 represents the southern rest of repository South RoR area in Figure PA-8. Region 3 represents the farthest down-dip repository area Waste Panel in Figure PA-8 that contained waste and thus corresponds to the single down-dip waste panel. The linkage between the solutions to



1  
2 **Figure PA-21. Assignment of Initial Conditions for DBR Calculation at Each Intrusion Time.**

3 **Equation (25) and the DBR calculations was made by assigning quantities calculated by**  
4 **BRAGFLO for each region in Figure PA-8 to the corresponding waste region in Figure**  
5 **PA-20.**

6 **The height of the grid in Figure PA-20 was assigned a value that corresponded to the crushed**  
7 **height  $h$  (m) of the waste as predicted by the solution of Equation (25). Specifically,**

8

$$h = h_i \frac{1 - \phi_i}{1 - \phi}, \quad (176)$$

9 **where  $h_i$  and  $\phi_i$  are the initial height (m) and porosity of the waste and  $\phi$  is the volume-**  
10 **averaged porosity of the waste at the particular time under consideration (Section PA-4.2.3).**  
11 **The areas designated equivalent panel closures, DRZ, and impure halite in Figure PA-20 were**  
12 **assigned the same pressures and saturations as the corresponding grid blocks in the 10,000**  
13 **year BRAGFLO calculations. The area designated equivalent DRZ/concrete (Figure PA-20)**  
14 **was assigned the same pressures and saturations as the DRZ. These areas were assigned**  
15 **porosities that resulted in a conservation of the initial pore volumes used for these areas in the**  
16 **solution of Equation (25) on the grid in Figure PA-8. Specifically, the pore volumes**  
17 **associated with the panel closures, DRZ, and impure halite do not change with time, with this**  
18 **constancy implemented by the definitions of  $\phi(x, y, 0)$  in Table PA-15.**

19 **The initial brine pressure  $p_b(x, y, 0)$  and gas saturation  $S_g(x, y, 0)$  in the grid in Figure**  
20 **PA-20 are assigned by:**

$$p_b(x, y, \theta) = \int_R \tilde{p}_b(\tilde{x}, \tilde{y}, t_{int}) dV / \int_R dV, \quad (177)$$

$$S_g(x, y, \theta) = \int_R \tilde{S}_g(\tilde{x}, \tilde{y}, t_{int}) dV / \int_R dV, \quad (178)$$

where  $(x, y)$  designates a point in the grid in Figure PA-20,  $\tilde{p}_b$  and  $\tilde{S}_g$  denote solutions to Equation (25),  $\tilde{x}$  and  $\tilde{y}$  denote the variables of integration,  $t_{int}$  is the time at which the drilling intrusion occurs, and  $R$  corresponds to the region in the computational grid for BRAGFLO (Figure PA-8) that is mapped into the region in the computational grid for BRAGFLO for DBR (Figure PA-20) that contains the point  $(x, y)$  (Figure PA-21). Note that  $t_{int}$  defines a time in the solution of Equation (25);  $t = 0$  defines the start time for the DBR calculation and corresponds to  $t_{int}$  in the solution of Equation (25).

The initial porosity  $\phi(x, y, 0)$  in the grid in Figure PA-20 is set by the equations listed in Table PA-15. In Table PA-15,  $h_i$  is initial height of waste panels (3.96 m),  $\phi_{WP,i}$  is initial porosity of waste panels (0.848),  $h(t_{int})$  is height of repository at time of intrusion (typically 1 to 1.5 m; corresponds to  $h$  in Equation (25)),  $h_{DRZ,i}$  is initial height for DRZ (43.60 m) that results in DRZ in Figure PA-20 having the same pore volume as the initial pore volume of the DRZ in Figure PA-8,  $A_{DRZ}$  is area associated with DRZ in Figure PA-20, and  $\phi_{DRZ,i}$  is initial porosity of DRZ (see Table PA-2). The quantity  $h_{DRZ,i} \times A_{DRZ} \times \phi_{DRZ,i}$  is equal to pore volume of DRZ above and below the waste filled regions in Figure PA-8. In Table PA-15, the term  $\phi_C$  is the porosity of the panel closure concrete material (CONC\_PCS; see Table PA-2),  $d_1$  is the length of the drift/explosion wall portion of the panel closure (32.1 m; see Figure PA-13), and  $d_2$  is the length of the concrete portion of the panel closure (7.9 m; see Figure PA-13). The porosity of the panel closure and the equivalent DRZ/concrete materials are defined as the volume-weighted mean porosity of the component materials; this definition results in the same brine volume within the pore space in each set of panel closures in Figure PA-8 and Figure PA-20. In Table PA-15,  $h_{H,i}$  is initial height of undisturbed halite in Figure PA-20, which is arbitrarily taken to be 8.98 m. However, this value is unimportant because of the extremely low permeability of the undisturbed halite ( $\sim 3.16 \times 10^{-23} \text{ m}^2$ ); any brine in the halite could not flow into the waste over the short time period of the DBR calculation, so no effort was made to preserve halite pore volume when mapping from the computational grid in Figure PA-8 to the computational grid in Figure PA-20. The quantity  $\phi_{H,i}$  is initial porosity of halite (HALPOR, see Table PA-17).

### PA-4.7.3 Conceptual Representation for Flow Rate $r_{DBR}(t)$

The driving force that would give rise to the DBR is a difference between waste panel pressure,  $p_w$  (Pa), and the flowing bottomhole pressure in the borehole,  $p_{wf}$  (Pa) at the time of the intrusion. The flowing bottomhole pressure  $p_{wf}$ , defined as the dynamic pressure at the

1

**Table PA-15. Initial Porosity in the DBR Calculation**

<b>Grid region</b>	<b>Initial Porosity <math>\phi(x, y, \theta)</math></b>
<i>Waste</i>	$1 - h_i \frac{1 - \phi_{WP,i}}{h(t_{int})}$
<i>Panel Closures</i>	$\frac{\phi_C d_2 + d_1 \left[ 1 - h_i \left( 1 - \phi_{WP,i} \right) / h(t_{int}) \right]}{d_1 + d_2}$
<i>DRZ</i>	$\frac{h_{DRZ,i} \phi_{DRZ,i}}{h(t_{int})}$
<i>Impure Halite</i>	$\frac{h_{H,i} \phi_{H,i}}{h(t_{int})}$
<i>Equivalent DRZ/Concrete</i>	$\frac{\phi_C d_1 + \phi_{DRZ,i} d_2}{d_1 + d_2}$

2 *inlet of the intruding borehole to the waste panel, is less than the static pressure  $p_w$  due to*  
 3 *elevation, friction and acceleration effects. The rate at which brine and gas are transported*  
 4 *up the intruding borehole is determined by the difference  $p_w - p_{wf}$  and a productivity index*  
 5  *$J_p$  for the intruded waste panel (Mattax and Dalton 1990, p. 79):*

6 
$$q_p(t) = J_p [p_w(t) - p_{wf}], \quad (179)$$

7 *where*

8  $q_p(t)$  = *flow rate ( $m^3/s$ ) at time  $t$  for phase  $p$  ( $p = b \sim$  brine,  $p = g \sim$  gas),*

9  $J_p$  = *productivity index ( $m^3/Pa \cdot s$ ) for phase  $p$*

10 *and  $p_w$  and  $p_{wf}$  are defined above. As indicated by the inclusion/exclusion of a dependence on*  
 11  *$t$ , the terms  $J_p$  and  $p_{wf}$  are constant during the determination of  $q_p(t)$  for a particular*  
 12 *drilling intrusion in the present analysis, and  $p_w(t)$  changes as a function of time. In*  
 13 *concept, the DBR is given by*

14 
$$DBR = \int_0^{t_e} rDBR(t) dt = \int_0^{t_e} J_b [p_w(t) - p_{wf}] dt, \quad (180)$$

15 *once  $J_p$ ,  $p_w$  and  $p_{wf}$  are determined. Section PA-4.7.4 discusses the determination of  $J_p$ ;*  
 16 *Section PA-4.7.5 presents the numerical determination of  $p_w$  and DBR; and the determination*

1 of  $p_{wf}$  is discussed in Section PA-4.7.6. The associated gas release is given by the  
 2 corresponding integral with  $J_g$  rather than  $J_b$ . In the computational implementation of the  
 3 analysis, DBR is determined as part of the numerical solution of the system of partial  
 4 differential equations that defines  $p_w$  (Section PA-4.7.5).

5 **PA-4.7.4 Determination of Productivity Index  $J_p$**

6 In a radial drainage area with uniform saturation, which is assumed to be valid throughout  
 7 the DBR, the following representation for  $J_p$  can be determined from Darcy's law (Mattax and  
 8 Dalton 1990, p. 79; Williamson and Chapplear 1981; Chapplear and Williamson 1981):

9 
$$J_p = \frac{2\pi k k_{rp} h}{\mu_p [\ln(r_e/r_w) + s + c]}, \quad (181)$$

10 where

11  $k$  = absolute permeability (assumed to be constant through time at  $2.4 \times 10^{-13}$   
 12  $m^2$ ),

13  $k_{rp}$  = relative permeability to phase  $p$  (calculated with modified Brooks-Corey  
 14 model in Equation (32) and brine and gas saturations,  $S_b$  and  $S_g$ , obtained by  
 15 mapping solutions of Equation (25) obtained with grid in Figure PA-8 onto  
 16 grid in Figure PA-20),

17  $h$  = crushed panel height (Equation (176)),

18  $\mu_p$  = viscosity of fluid phase (assumed to be constant through time with  
 19  $\mu_b = 1.8 \times 10^{-3}$  Pa·s, and  $\mu_g = 8.92 \times 10^{-6}$  Pa·s (Kaufmann 1960)),

20  $r_e$  = external drainage radius (for use with the rectangular grid-blocks in Figure  
 21 PA-20,  $r_e$  is taken to be the equivalent areal radius; see Equation (182)),

22  $r_w$  = wellbore radius (assumed to be constant through time at 0.1556 m (Table  
 23 14.7, Gatlin 1960)),

24  $c$  = -0.50 for pseudo steady-state flow,

25  $s$  = skin factor, which is used to incorporate flow stimulation caused by spallings  
 26 release (see Equation (183)).

27 In the present analysis,

28 
$$r_e = \sqrt{(\Delta x)(\Delta y) / \pi}, \quad (182)$$

1 *where  $\Delta x$  is the x-dimension (m) and  $\Delta y$  is the y-dimension (m) of the grid block containing*  
 2 *the down-dip well in Figure PA-20 ( $\Delta x = 10$  m and  $\Delta y = 32.7$  m).*

3 *The skin factor  $s$  is derived from the spillings release through the following petroleum*  
 4 *engineering well testing relationship (pp. 5-7, Lee 1982):*

$$5 \quad s = \left( \frac{k}{k_s} - 1 \right) \ln \left( \frac{r_s}{r_w} \right), \quad (183)$$

6 *where*

7  $k_s =$  *permeability (m<sup>2</sup>) of an open channel as a result of spillings releases*  
 8 *(assumed to be infinite),*

9  $r_s =$  *effective radius (m) of the wellbore with the spalled volume removed.*

10 *In the CCA PA, the effective radius  $r_s$  was obtained by converting the spalled volume release*  
 11  *$V_i$  into a cylinder of equal volume, then computing the radius of the cylinder. The area of the*  
 12 *cylinder  $A_i$  is*

$$13 \quad A_i = \frac{V_i}{h_i}. \quad (184)$$

14 *Then,*

$$15 \quad r_s = \sqrt{A_i / \pi} \quad (185)$$

16 *and substitution of  $r_s$  into Equation (183) with  $k_s = \infty$  yields*

$$17 \quad s = -\ln \left[ \frac{\sqrt{A_i / \pi}}{r_w} \right]. \quad (186)$$

18 *For the CRA-2004 PA, calculation of the skin factor was simplified by assuming that the*  
 19 *spalled volume,  $V_{\bar{p}}$ , would be equal to 4 m<sup>3</sup> for all intrusions. This assumption was made only*  
 20 *for the calculation of the skin factor to determine DBRs. This assumption is conservative*  
 21 *since it will overestimate the well productivity index and consequently overestimate DBRs for*  
 22 *all intrusions where the spalled volume is less than 4 m<sup>3</sup>.*

23 **PA-4.7.5 Determination of Waste Panel Pressure  $p_w(t)$  and Direct Brine Release**

24 *The repository pressure  $p_w(t)$  in Equation (180) after a drilling intrusion is determined with*  
 25 *the same system of nonlinear partial differential equations discussed in Section PA-4.2. These*  
 26 *equations are solved numerically by the code BRAGFLO used with the computational grid in*

1 *Figure PA-20 and assumptions (i.e., parameter values, initial value conditions, and boundary*  
 2 *value conditions) that are appropriate for representing brine flow to an intruding borehole*  
 3 *over a relatively short time period immediately after the intrusion (i.e., 3 – 11 days). Due to*  
 4 *the short time periods under consideration, the model for DBR does not include gas*  
 5 *generation due to either corrosion or microbial action and also does not include changes in*  
 6 *repository height due to creep closure. Furthermore, to stabilize the calculation and thus*  
 7 *allow longer time steps in the numerical solution, the capillary pressure was assigned a value*  
 8 *of 0 Pa in all modeled regions (Figure PA-20); in the analysis of the full system in Section*  
 9 *PA-4.2, capillary pressure had a value of 0 Pa in the waste regions and the DRZ but a nonzero*  
 10 *value in the panel closures (Table PA-3). Use of a capillary pressure of 0 Pa results in the*  
 11 *brine pressure  $p_b(x, y, t)$  and the gas pressure  $p_g(x, y, t)$  being equal, with the pressure*  
 12  *$p_w(t)$  in Equation (180) given by*

$$13 \quad p_w(t) = p_b(x, y, t). \quad (187)$$

14 *Although the determination of DBR can be conceptually represented by the integral in*  
 15 *Equation (175), in the numerical implementation of the analysis, DBR is determined within*  
 16 *the numerical solution of the system of partial differential equations that defines  $p_b(x, y, t)$ .*

17 *With the specific assumptions for DBR, Equation (25) becomes:*

$$18 \quad \text{Gas Conservation} \quad \nabla \cdot \left[ \frac{\alpha \rho_g K_g k_{rg}}{\mu_g} (\nabla p_g + \rho_g g \nabla h) \right] = \alpha \frac{\partial (\phi \rho_g S_g)}{\partial t}, \quad (188a)$$

$$19 \quad \text{Brine Conservation} \quad \nabla \cdot \left[ \frac{\alpha \rho_b K_b k_{rb}}{\mu_b} (\nabla p_b + \rho_b g \nabla h) \right] = \alpha \frac{\partial (\phi \rho_b S_b)}{\partial t}, \quad (188b)$$

$$20 \quad \text{Saturation Constraint} \quad S_g + S_b = 1, \quad (188c)$$

$$21 \quad \text{Capillary Pressure Constraint} \quad p_g - p_b = 0, \quad (188d)$$

$$22 \quad \text{Gas Density } \rho_g \text{ determined by Redlich-Kwong-Soave equation of state (Equation (45))} \quad (188e)$$

$$23 \quad \text{Brine Density} \quad \rho_b = \rho_0 \exp[\beta_b (p_b - p_{b0})], \quad (188f)$$

$$24 \quad \text{Formation Porosity} \quad \phi = \phi_0 \exp[\beta_f (p_b - p_{b0})], \quad (188g)$$

25 *with all symbols having the same definitions as in Equation (25).*

26 *The primary differences between the BRAGFLO calculations described in Section PA-4.2 and*  
 27 *the BRAGFLO calculations described in this section are in the computational meshes used*  
 28 *(Figure PA-20 and Figure PA-8), the initial values used (Table PA-2 and Section PA-4.7.2),*

1 *and the boundary conditions used (Table PA-16). In particular, brine and gas flow associated*  
 2 *with intruding boreholes in the DBR calculations are incorporated by the appropriate*  
 3 *assignment of boundary conditions. Specifically, brine flow up an intruding borehole is*  
 4 *incorporated into Equation (188) by using the Poettmann-Carpenter wellbore model to*  
 5 *determine the pressure at the outflow point in a waste panel (Figure PA-20), with this pressure*  
 6 *entering the calculation as a boundary value condition (Table PA-16). The details of this*  
 7 *determination are discussed in Section PA-4.7.6. Further, for calculations that assume a prior*  
 8 *E1 intrusion, the effects of this intrusion are also incorporated into the analysis by specifying*  
 9 *a pressure specified as a boundary condition (Table PA-16). The determination of this*  
 10 *pressure is discussed in Section PA-4.7.6.*

11 **Table PA-16. Boundary Conditions for  $p_b$  and  $S_g$  in DBR Calculations**

<i><math>(x, y)</math> on Upper (Northern) or Lower (Southern) Boundary in Figure PA-20, <math>0 \leq t</math></i>	
$\left. (\nabla p_g + \rho_g g \nabla h) \right _{(x,y,t)} \cdot j = 0 \text{ Pa/m}$	<i>no gas flow condition</i>
$\left. (\nabla p_b + \rho_b g \nabla h) \right _{(x,y,t)} \cdot j = 0 \text{ Pa/m}$	<i>no brine flow condition</i>
<i><math>(x, y)</math> on Right (Eastern) or Left (Western) Boundary in Figure PA-20, <math>0 \leq t</math></i>	
$\left. (\nabla p_g + \rho_g g \nabla h) \right _{(x,y,t)} \cdot i = 0 \text{ Pa/m}$	<i>no gas flow condition</i>
$\left. (\nabla p_b + \rho_b g \nabla h) \right _{(x,y,t)} \cdot i = 0 \text{ Pa/m}$	<i>no brine flow condition</i>
<i><math>(x, y)</math> at Location of Drilling Intrusion under Consideration (see indicated points in Figure PA-20), <math>0 \leq t</math></i>	
$p_b(x, y, t) = p_{wf}$ (see Section PA.4.7.6)	<i>constant pressure condition</i>
<i><math>(x, y)</math> at Location of Prior Drilling Intrusion into Pressurized Brine (see indicated point in Figure PA-20), <math>0 \leq t</math></i>	
$p_b(x, y, t) = p_{wE1}$ (see Section PA.4.7.7)	<i>constant pressure condition</i>

12 *For perspective, the following provides a quick comparison of the assumptions that underlie*  
 13 *the solution of Equation (25) on the mesh in Figure PA-8 (i.e., the BRAGFLO mesh) and the*  
 14 *solution of Equation (188) on the mesh in Figure PA-20 (i.e., the BRAGFLO mesh for DBR):*

- 15 *1. The BRAGFLO mesh for DBR is defined in the areal plane with the z-dimension*  
 16 *(height) one element thick; the BRAGFLO mesh is defined as a cross-section, with*  
 17 *multiple layers in height and the thickness (y-dimension) one element thick.*
- 18 *2. The BRAGFLO mesh for DBR uses constant thickness, while BRAGFLO uses*  
 19 *rectangular flaring to account for three-dimensional volumes in a two-dimensional*  
 20 *grid (Figure PA-9).*

- 1       3. *The BRAGFLO mesh for DBR represents flow only in the waste area. The BRAGFLO*  
 2       *model includes the surrounding geology as well as the entire WIPP excavation*  
 3       *(including operations, experimental, and shaft regions).*
- 4       4. *Local scale heterogeneities are included in the BRAGFLO mesh for DBR, including*  
 5       *the salt pillars, rooms, panel closures, and passageways that contain waste. These are*  
 6       *not fully represented in the BRAGFLO mesh.*
- 7       5. *The DRZ is included in both models, but exists above and below the excavated regions*  
 8       *in the BRAGFLO model, whereas the DRZ surrounds the waste rooms on the sides of*  
 9       *the BRAGFLO mesh for DBR.*
- 10      6. *Both models include a one-degree formation dip through the excavated regions*  
 11      *(Equation (27)).*

12 *PA-4.7.6    Boundary Value Pressure  $p_{wf}$*

13 *The boundary value pressure  $p_{wf}$  at the inlet of the intruding borehole is defined by a system*  
 14 *of equations of the following form:*

$$15 \quad \frac{dp}{dh} = G\left(q_b [p(0)], q_g [p(0)], p(h), h\right), \quad 0 \leq h \leq 655 \text{ m}, \quad (189a)$$

$$16 \quad p(655) = 1.013 \times 10^5 \text{ Pa}, \quad (189b)$$

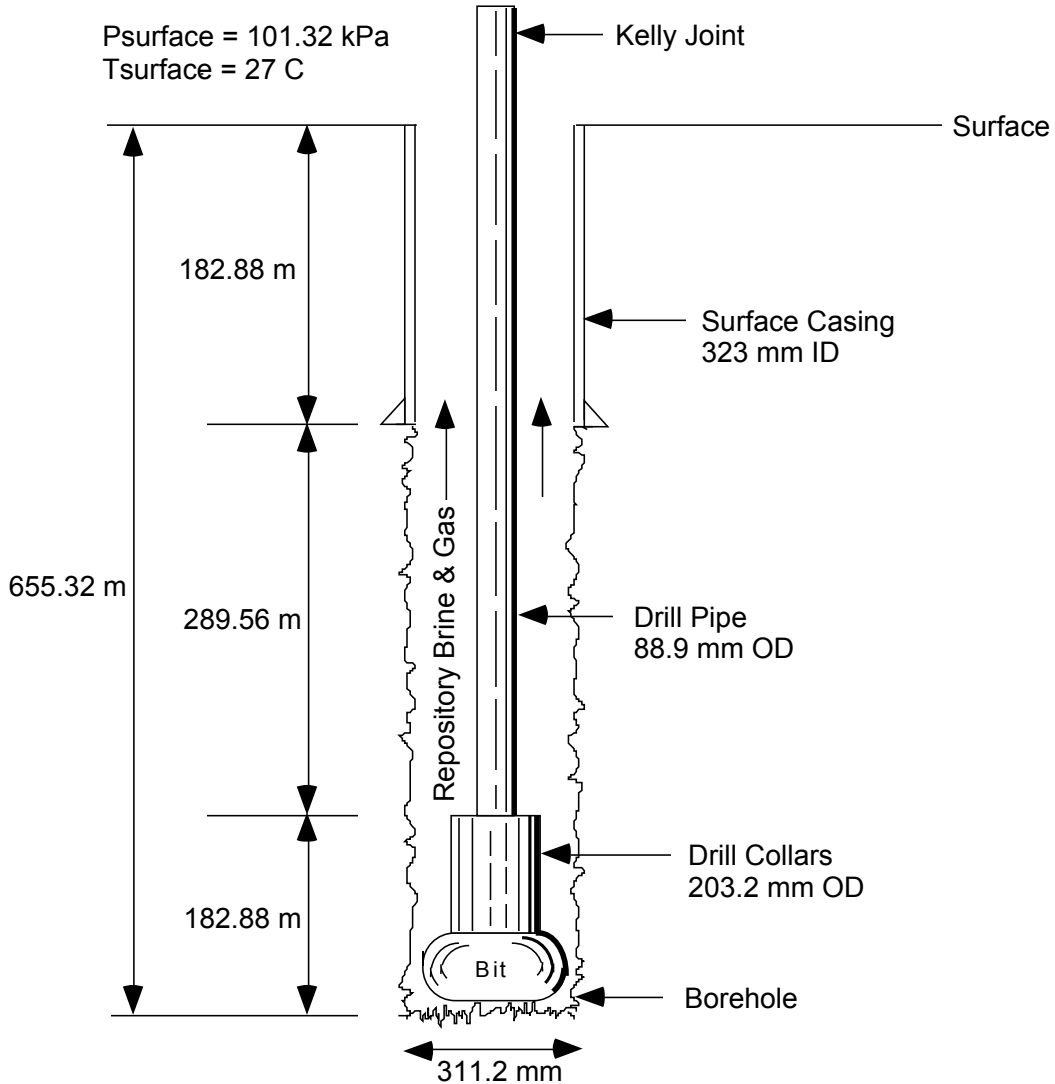
$$17 \quad q_b [p(0)] = J_b [p_w - p(0)], \quad (189c)$$

$$18 \quad q_g [p(0)] = J_g [p_w - p(0)], \quad (189d)$$

19 *where  $p(h)$  is pressure (Pa) at elevation  $h$  (m) in the borehole with  $h = 0$  m corresponding to*  
 20 *the entry point of the borehole into the waste panel and  $h = 655$  m corresponding to the land*  
 21 *surface (Figure PA-22),  $G$  is a function (Pa/m) characterizing the change of pressure with*  
 22 *elevation in the borehole,  $p(655)$  is an initial value condition requiring that pressure at the*  
 23 *land surface (i.e., the outlet point of the borehole) be equal to atmospheric pressure,*  
 24  *$q_b [p(0)]$  and  $q_g [p(0)]$  define brine and gas flow rates ( $\text{m}^3/\text{s}$ ) into the borehole,  $J_b$  and  $J_g$*   
 25 *are productivity indexes ( $\text{m}^3/\text{Pa s}$ ) (see Equation (181)), and  $p_w$  is the pressure (Pa) in the*  
 26 *repository at the time of the drilling intrusion.*

27 *The boundary value pressure  $p_{wf}$  is defined by*

$$28 \quad p_{wf} = p(0). \quad (190)$$



1  
2 **Figure PA-22. Borehole Representation Used for Poettmann-Carpenter Correlation.**

3 *Thus,  $p_{wf}$  is determined by the numerical solution of Equation (189a) for  $p(0)$  subject to the*  
4 *constraints in Equation (189b), Equation (189c) and Equation (189d).*

5 *The pressure  $p_w$  corresponds to the pressure  $p_w(0)$  in Equation (187) and is obtained from*  
6 *the solution of Equation (25) with the computational grid in Figure PA-8 (see Section*  
7 *PA-4.7.2). The production indexes  $J_b$  and  $J_g$  are defined in Equation (181). Thus, the only*  
8 *quantity remaining to be specified in Equation (189) is the function  $G$ .*

9 *Brine and gas flow up a borehole is governed by complex physics dependent on frictional*  
10 *effects and two-phase fluid properties. This phenomenon has been widely studied in the*  
11 *petroleum industry and many modeling procedures have been developed to predict flow rates*  
12 *and pressures in vertical two-phase pipe flow (i.e., to define  $G$  in Equation (189a)) (Brill and*  
13 *Beggs 1986). For this analysis, the Poettmann-Carpenter model (Poettmann and Carpenter*

1 *1952, Welchon et al. 1962) was used to define G because it accounts for multiphase frictional*  
 2 *effects based on empirical (i.e., field) data from flowing wells, is one of the few modeling*  
 3 *approaches that included annular flow data in its development, and is relatively easy to*  
 4 *implement. Specifically, the Poettmann-Carpenter model defines G by:*

$$5 \quad G(q_b [p(\theta)], q_g [p(\theta)], p(h), h) = gm(h) + f'(m(h), D(h), q_b [p(\theta)]) gm(h) F^2(h) / D^5(h), \quad (191)$$

6 *where*

7  $g =$  *acceleration due to gravity (9.8 m/s<sup>2</sup>),*

8  $m(h) =$  *density (kg/m<sup>3</sup>) of fluids (i.e., gas and brine) in wellbore at elevation h (Note:*  
 9 *m(h) is a function of q<sub>b</sub> [p(θ)] and q<sub>g</sub> [p(θ)]; see Equation (192), below),*

10  $f' \{m(h), D(h), q_b [p(\theta)]\} =$  *empirically defined scale factor (m/s<sup>2</sup>) (Note: f' is the scale*  
 11 *factor in the Poettmann-Carpenter model for fluid flow in a wellbore*  
 12 *[Poettmann and Carpenter 1952]; see discussion below),*

13  $F(h) =$  *flow rate (m<sup>3</sup>/s) of fluids (i.e., gas and brine) in wellbore at elevation h (Note:*  
 14 *F(h) is a function of q<sub>b</sub> [p(θ)] and q<sub>g</sub> [p(θ)]; see Equation (193), below),*

15  $D(h) =$  *effective diameter (m) of wellbore (see Equation (196), below).*

16 *The first term, gm(h), in Equation (191) results from the contribution of elevation to*  
 17 *pressure; the second term results from frictional effects (Poettmann and Carpenter 1952).*  
 18 *The fluid density m(h) at elevation h is given by*

$$19 \quad m(h) = \frac{q_b [p(\theta)] \rho_b [p(\theta)] + q_g [p(\theta)] \rho_g [p(\theta)]}{F(h)}, \quad (192)$$

20 *where*

$$21 \quad F(h) = q_b [p(\theta)] + \frac{z(h) p(h)}{p(\theta)} q_g [p(\theta)], \quad (193)$$

22 *and*

23  $\rho_b [p(\theta)] =$  *density (kg/m<sup>3</sup>) of brine at pressure p(θ) and temperature 300.1°K, which is*  
 24 *fixed at 1230 kg/m<sup>3</sup>,*

1  $\rho_g [p(0)] = \text{density (kg/m}^3\text{) of H}_2 \text{ at pressure } p(0) \text{ and temperature } 300.1^\circ\text{K (see}$   
 2  $\text{Equation (194), below),}$

3  $z(h) = z\text{-factor for compressibility of H}_2 \text{ at elevation } h \text{ (Note: } z(h) \text{ is a function of}$   
 4  $p(h); \text{ see Equation (195), below), and } q_b [p(0)] \text{ and } q_g [p(0)] \text{ are defined}$   
 5  $\text{in Equation (189).}$

6 *The gas density in Equation (192) is obtained from the universal gas law,  $PV = nRT$ , by*

$$7 \quad \rho_g [p(0)] = C_{m,kg} \frac{n}{V} = C_{m,kg} \frac{P}{RT}, \quad (194)$$

8 *where  $n$  is the amount of gas (mol) in a volume  $V$ ,  $C_{m,kg}$  is the conversion factor from moles*  
 9 *to kilograms for  $H_2$  (i.e.,  $2.02 \times 10^{-3}$  kg/mol),  $P = p(0)$ ,  $R = 8.3145$  kg  $m^2$ /mol $^\circ\text{K s}^2$ , and  $T =$*   
 10 *300.1 $^\circ\text{K}$ . The  $z$ -factor is given by*

$$11 \quad z(h) = 1 + (8.54 \times 10^{-8} \text{ Pa}^{-1}) p(h), \quad (195)$$

12 *and was obtained from calculations performed with the SUPERTRAPP program (Ely and*  
 13 *Huber 1992) for pure  $H_2$  and a temperature of 300.1 $^\circ\text{K}$  (Stoelzel and O'Brien 1996, Figure*  
 14 *4.7.4). The preceding approximation to  $z(h)$  was obtained by fitting a straight line between*  
 15 *the results for pressures of 0 psi and 3000 psi and a hydrogen mole fraction of 1 in Stoelzel*  
 16 *and O'Brien (1996, Figure 4.7.4); the actual calculations used the more complex, but*  
 17 *numerically similar, regression model given in Stoelzel and O'Brien (1996, Figure 4.7.4). The*  
 18 *numerator and denominator in Equation (192) involve rates, with the time units canceling to*  
 19 *give  $m(h)$  in units of kg/ $m^3$ .*

20 *The effective diameter  $D(h)$  in Equation (191) is defined with the hydraulic radius concept.*  
 21 *Specifically,*

$$22 \quad D^5(h) = [D_o(h) + D_i(h)]^2 [D_o(h) - D_i(h)]^3, \quad (196)$$

23 *where  $D_i(h)$  and  $D_o(h)$  are the inner and outer diameters (m) of the wellbore at elevation*  
 24  *$h(m)$  (see Figure PA-22). The factor  $f'$  in Equation (191) is a function of  $m(h)$ ,  $D(h)$  and*  
 25  *$q_b [p(0)]$ .*

26 *In the original development by Poettmann and Carpenter (1952, Figure 4),  $f'$  is defined in*  
 27 *terms of quantities commonly used to measure production from oil and gas wells. The result*  
 28 *is that  $f'$  is expressed in quantities that are unfamiliar outside of the oil and gas industry.*  
 29 *For clarity, Equation (191) and the quantities contained in it are expressed in SI units.*

1 *However, to allow use of the original correlations developed by Poettmann and Carpenter to*  
 2 *define  $f'$ , the calculations within the CCA PA (Stoelzel and O'Brien 1996) were performed in*  
 3 *the same oilfield units originally used by Poettmann and Carpenter (1952).*

4 *Subsequent to submittal of the CCA PA, it was discovered that the factor of  $2\pi$  was omitted*  
 5 *from Equation (181). This error was determined to be of no consequence to the conclusions*  
 6 *of the CCA PA (Hadgu et al. 1999) and has been corrected in the CRA-2004 PA. As a*  
 7 *consequence of the error correction, the regression models used to determine the boundary*  
 8 *pressure  $p_{wf}$  were recalculated (Hadgu et al. 1999). The corrected regression models are*  
 9 *reported in this appendix.*

10 *The following iterative procedure based on bisection method was used to approximate*  
 11 *solutions to Equation (189).*

12 *Step 1. Estimate  $p(0)$  using a bisection algorithm. (Initial guess for  $p(0)$  is the*  
 13 *midpoint  $\frac{1}{2} p_w$  of interval  $[0, p_w]$ , where  $p_w$  is the pressure in the repository at the*  
 14 *time of the drilling intrusion used in Equation (189)). Next guess for  $p(0)$  is at the*  
 15 *midpoint of either  $\left[0, \frac{1}{2} p_w\right]$  or  $\left[\frac{1}{2} p_w, p_w\right]$  depending on whether resultant*  
 16 *approximation to  $p(655)$  is above or below atmospheric pressure. Subsequent guesses*  
 17 *for  $p(0)$  are made in a similar manner.*

18 *Step 2. Use  $p(0)$ , known values for  $J_b$ ,  $J_g$  and  $p_w$ , and Equation (189) to determine*  
 19  *$q_b[p(0)]$  and  $q_g[p(0)]$ .*

20 *Step 3. Use the bisection method with  $\Delta h = 25 \text{ ft} = 7.62 \text{ m}$  and appropriate changes in*  
 21 *annular diameter (Figure PA-22) to determine  $p(655)$*   
 22 *(i.e.,  $p(h + \Delta h) = p(h) + G(q_b[p(0)], q_g[p(0)], p(h), h) \Delta h$ ).*

23 *Step 4. Stop if  $p(655)$  is within 0.07% of atmospheric pressure (i.e., if*  
 24  *$|1.013 \times 10^5 \text{ Pa} - p(655)| \leq 70 \text{ Pa}$ ). Otherwise, return to Step 1 and repeat process.*

25 *The preceding procedure is continued until the specified error tolerance (i.e., 0.07percent) has*  
 26 *been met. The computational design of the PA has the potential to require more than 23,000*  
 27 *separate DBR calculations (3 replicates  $\times$  5 scenarios  $\times$  3 drilling locations  $\times$  100 vectors  $\times$  5*  
 28 *to 6 intrusion times per scenario). In concept, each of these cases requires the solution of*  
 29 *Equation (189) with the iterative procedure just presented to obtain the boundary value*  
 30 *condition  $p_{wf} = p(0)$  (Table PA-16). To help hold computational costs down,  $p(0)$  was*  
 31 *calculated for approximately 2000 randomly generated vectors of the form*

1 
$$\mathbf{v} = [p_w, h, S_{br}, S_{gr}, S_b, A_i], \quad (197)$$

2 where  $p_w$  is the repository pressure (used in definition of  $q_b[p(0)]$  and  $q_g[p(0)]$  in  
 3 Equation (189)),  $h$  is the crushed height of the repository (used in definition of  $J_p$  in Equation  
 4 (181)),  $S_{br}$  and  $S_{gr}$  are the residual saturations for gas and brine in the repository (used in  
 5 definition of  $k_{rp}$  in Equation (181)),  $S_b$  is the saturation of brine in the repository (used in  
 6 definition of  $k_{rp}$  in Equation (181)), and  $A_i$  is the equivalent area of material removed by  
 7 spallings (used in definition of skin factor  $s$  in Equation (186)). The outcomes of these  
 8 calculations were divided into three cases:

- 9 1. mobile brine only (i.e.,  $k_{rg} = 0$  in Equation (188a))  
 10 2. brine-dominated flow (i.e.,  $k_{rb} > k_{rg}$ ), and  
 11 3. gas-dominated flow (i.e.,  $k_{rg} > k_{rb}$ ).

12 Then, regression procedures were used to fit algebraic models that can be used to  
 13 estimate  $p(0)$ . These regression models were then used to determine  $p(0)$ , and hence  $p_{wf}$ .  
 14 The resulting three regression models (or curve fit equations) for flowing bottomhole pressure  
 15 ( $p_{wf}$ ) are as follows.

- 16 1. For a system with only mobile brine (i.e.,  $k_{rg} = 0$ )

17 
$$p_{wf} = a + bx + cy + dx^2 + ey^2 + fxy + gx^3 + hy^3 + ixy^2 + jx^2y, \quad (198a)$$

18 where  $x = \log(J_b)$  and  $y = p_w$  (= repository pressure). The coefficients in Equation (198a)  
 19 were determined to be:

- 20  $a = 3.2279346 \times 10^{11}$ ,  
 21  $b = 9.4816648 \times 10^{10}$ ,  
 22  $c = -6.2002715 \times 10^3$ ,  
 23  $d = 9.2450601 \times 10^9$ ,  
 24  $e = 4.1464475 \times 10^{-6}$ ,  
 25  $f = -1.2886068 \times 10^3$ ,  
 26  $g = 2.9905582 \times 10^8$ ,  
 27  $h = 1.0857041 \times 10^{-14}$ ,  
 28  $i = 4.7119798 \times 10^{-7}$ ,  
 29  $j = -6.690712 \times 10^{-1}$ ,

30 with resulting coefficient of determination  $R^2 = 0.974$ .

- 31 2. For brine dominated flow ( $k_{rb} > k_{rg}$ ):

1 
$$P_{wf} = \frac{a + bx + cx^2 + dy}{1 + ex + fx^2 + gx^3 + hy}, \quad (198b)$$

2 where  $x = \log\left(\frac{k_{rg}}{k_{rb}}\right)$  and  $y = p_w$  (= repository pressure). The coefficients in Equation (198b)  
 3 were determined to be:

4  $a = 1.6065077 \times 10^6,$   
 5  $b = 2.6243397 \times 10^6,$   
 6  $c = 2.4768899 \times 10^6,$   
 7  $d = -5.3635476 \times 10^{-2},$   
 8  $e = 7.0815693 \times 10^{-1},$   
 9  $f = 3.8012696 \times 10^{-1},$   
 10  $g = 4.1916956 \times 10^{-3},$   
 11  $h = -2.4887085 \times 10^{-8},$

12 with resulting coefficient of determination  $R^2 = 0.997$ .

13 3. For gas dominated flow ( $k_{rg} > k_{rb}$ ):

14 
$$p_{wf} = a + b\frac{1}{x} + cy + d\frac{1}{x^2} + ey^2 + f\frac{x}{y} + g\frac{1}{x^3} + hy^3 + i\frac{y^2}{x} + j\frac{y}{x^2}, \quad (198c)$$

15 where  $x = \log(J_g)$  and  $y = p_w$  (= repository pressure). The coefficients in Equation (198c)  
 16 were determined to be:

17  $a = -1.0098405 \times 10^9,$   
 18  $b = -2.3044622 \times 10^{10},$   
 19  $c = 9.8039146,$   
 20  $d = -1.7426466 \times 10^{11},$   
 21  $e = 1.8309137 \times 10^{-7},$   
 22  $f = 1.7497064 \times 10^2,$   
 23  $g = -4.3698224 \times 10^{11},$   
 24  $h = -1.4891198 \times 10^{-16},$   
 25  $i = 1.3006196 \times 10^{-6},$   
 26  $j = 7.5744833 \times 10^2,$

27 with resulting coefficient of determination  $R^2 = 0.949$ .

1 *PA-4.7.7 Boundary Value Pressure  $p_{wE1}$*

2 *Some of the calculations for DBR are for a drilling intrusion that has been preceded by an E1*  
 3 *intrusion in either the same waste panel, an adjacent waste panel, or a nonadjacent waste*  
 4 *panel (Section PA-6.7.5). The effects of these prior E1 intrusions are incorporated into the*  
 5 *solution of Equation (188), and hence into the DBR, by the specification of a boundary*  
 6 *pressure  $p_{wE1}$  at the location of the E1 intrusion into the repository (Table PA-16).*

7 *Two cases are considered for the definition of  $p_{wE1}$ : (1) an open borehole between the brine*  
 8 *pocket and the repository, and (2) a borehole between the brine pocket and the repository filled*  
 9 *with material with properties similar to silty sand. The first case corresponds to the situation*  
 10 *in which the drilling intrusion under consideration has occurred within 200 years of a prior*  
 11 *drilling intrusion that penetrated the pressurized brine pocket, and the second case*  
 12 *corresponds to the situation in which the drilling intrusion under consideration has occurred*  
 13 *more than 200 years after a prior drilling intrusion that penetrated the pressurized brine*  
 14 *pocket.*

15 *PA-4.7.7.1 Solution for Open Borehole*

16 *In this case,  $p_{wE1}$  is set equal to the flowing well pressure  $p_{wfBP}$  of an open borehole between*  
 17 *the brine pocket and the repository and is given by:*

18 
$$Q = f_1(p_{BP}, p_{wfBP}), \quad (199a)$$

19 
$$Q = f_2(p_{wfBP}, p_{wfBI}), \quad (199b)$$

20 
$$Q = f_3(p_{wfBI}, p_{wfBO}), \quad (199c)$$

21 *where*

22  $p_B$  = *pressure (Pa) in brine pocket,*

23  $p_{wfBP}$  = *flowing well pressure (Pa) at outlet from brine pocket,*

24  $p_{wfBI}$  = *flowing well pressure (Pa) at inlet to repository from brine pocket,*

25  $p_{wfBO}$  = *flowing well pressure (Pa) at outlet from repository due to intruding borehole*  
 26 *(Note: The boreholes associated with  $p_{wfBI}$  and  $p_{wfBO}$  arise from different*  
 27 *drilling intrusions and hence are at different locations; see Figure PA-20),*

28  $Q$  = *brine flow rate ( $m^3/s$ ) from brine pocket to repository, through repository,*  
 29 *and then to surface,*

1 *and  $f_1, f_2$  and  $f_3$  are linear functions of their arguments. In the development,  $p_{BP}$  and  $p_{wfBO}$*   
 2 *are assumed to be known, with the result that Equation (199) constitutes a system of three*  
 3 *linear equations in three unknowns (i.e.,  $p_{wfBP}, p_{wfBI}, Q$ ) that can be solved to obtain  $p_{wfBI}$ .*  
 4 *In the determination of  $p_{wfBI} = p_{wEI}$  for use in a particular solution of Equation (188),  $p_{BP}$  is*  
 5 *the pressure in the brine pocket at the time of the intrusion obtained from the solution of*  
 6 *Equation (25) with BRAGFLO, and  $p_{wfBO}$  is the flowing well pressure obtained from*  
 7 *conditions at the time of the intrusion (from the solution of Equation (25)) and the solutions*  
 8 *of the Poettmann-Carpenter model embodied in Equation (198) (i.e., given pressure,  $k_{rg}$  and*  
 9  *$k_{rb}$  at the time of the intrusion from the solution of Equation (25) with BRAGFLO and  $J_b$*   
 10 *from both the solution of Equation (25) with BRAGFLO and the evaluation of the spillings*  
 11 *release (assumed to be a constant of  $4 \text{ m}^3$ ),  $p_{wfBO}$  is determined from the regression models*  
 12 *indicated in Equation (198).*

13 *The definition of Equation (199) is now discussed. Equation (199a) characterizes flow out of*  
 14 *the brine pocket into an open borehole and has the form (Williamson and Chappellear 1981,*  
 15 *Chappellear and Williamson 1981):*

$$16 \quad Q = \left( \frac{2\pi k_{BP} h_{BP}}{\mu [\ln(r_{eBP} / r_w) - 0.5]} \right) (p_{BP} - p_{wfBP}), \quad (200)$$

17 *where*

18  *$k_{BP}$  = brine pocket permeability ( $\text{m}^2$ ),*

19  *$h_{BP}$  = effective brine pocket height (m),*

20  *$r_{eBP}$  = effective brine pocket radius (m),*

21  *$r_w$  = wellbore radius (m),*

22  *$\mu$  = brine viscosity (Pa s).*

23 *In the present analysis,  $k_{BP}$  is an uncertain analysis input (see BHPRM in Table PA-17),*  
 24  *$h_{BP} = 125.83 \text{ m}$ ,  $r_{eBP} = 114 \text{ m}$  (Stoelzel and O'Brien 1996), which corresponds to the size of*  
 25 *the largest brine pocket that could fit under one waste panel,  $r_w = (8.921 \text{ in.}) / 2 = 0.1133 \text{ m}$ ,*  
 26 *which is the inside radius of a 9 5/8 in. outside diameter casing (Gatlin 1960, Table 14.7),  $\mu =$*   
 27  *$1.8 \times 10^{-3} \text{ Pa s}$ , and  $p_{BP}$  is determined from the solution of Equation (25) as previously*  
 28 *indicated.*

29 *Equation (199b) characterizes flow up an open borehole from the brine pocket to the*  
 30 *repository and is based on Poiseuille's Law (Prasuhn 1980, Eqs. 7-21, 7-22). Specifically,*  
 31 *Equation (199b) has the form*

$$Q = \left[ \frac{\pi D^4}{128 \mu (y_{BP} - y_{rep})} \right] \left[ (P_{wfBP} - P_{wfBI}) + g \rho (y_{rep} - y_{BP}) \right], \quad (201)$$

2 *where*

3  $D =$  *wellbore diameter (m),*

4  $y_{rep} =$  *elevation of repository (m) measured from surface,*

5  $y_{BP} =$  *elevation of brine pocket (m) measured from surface,*

6  $g =$  *acceleration due to gravity (9.8 m/s<sup>2</sup>),*

7  $\rho =$  *density of brine (kg/m<sup>3</sup>),*

8 *and the remaining symbols have already been defined.*

9 *In the present analysis,  $D = 2r_w = 0.2266$  m,  $\rho = 1230$  kg/m<sup>3</sup>, and  $y_{rep} - y_{BP} = 247$  m. With*  
 10 *the preceding values,*

$$128 \mu (y_{BP} - y_{rep}) / \pi D^4 = 6.87 \times 10^3 \text{ Pa s / m}^3, \quad (202)$$

$$g \rho (y_{rep} - y_{BP}) = 2.98 \times 10^6 \text{ Pa}. \quad (203)$$

13 *Thus,*

$$P_{wfBI} = P_{wfBP} - 2.98 \times 10^6 \text{ Pa}. \quad (204)$$

15 *when  $Q$  is small ( $\leq 0.1$  m<sup>3</sup>/s). When appropriate, this approximation can be used to simplify*  
 16 *the construction of solutions to Equation (199).*

17 *Equation (199c) characterizes flow through the repository from the lower borehole to the*  
 18 *bottom of the borehole associated with the drilling intrusion under consideration and has the*  
 19 *same form as Equation (200). Specifically,*

$$Q = \left( \frac{2 \pi k_{rep} h_{rep}}{\mu \left[ \ln (r_{e,rep} / r_w) - 0.5 \right]} \right) (P_{wfBI} - P_{wfBO}), \quad (205)$$

21 *where*

22  $k_{rep} =$  *repository permeability (m<sup>2</sup>),*

1  $h_{rep} =$  repository height (m),

2  $r_{e,rep} =$  effective repository radius (m),

3 and the remaining symbols have already been defined. In the present analysis,  
 4  $k_{rep} = 2.4 \times 10^{-13} \text{ m}^2$ ;  $h_{rep}$  at the time of the drilling intrusion under consideration is  
 5 obtained from the solution of Equation (25) (see Equation (176)); and  $r_{e,rep}$  is the same as the  
 6 radius  $r_e$  defined in Equation (182). As previously indicated,  $p_{wfBO}$  is obtained from the  
 7 solutions to the Poettmann-Carpenter model summarized in Equation (198).

8 Three equations (i.e., Equation (200), Equation (201) and Equation (205)) in three unknowns  
 9 (i.e.,  $p_{wfBP}$ ,  $p_{wfBI}$  and  $Q$ ) have now been developed. The solution for  $p_{wfBI}$  defines the initial  
 10 value  $p_{wE1}$  in Table PA-16. When the simplification in Equation (204) is used, the resultant  
 11 solution for  $p_{wfBI}$  is

12 
$$p_{wfBI} = \frac{p_{wfBO} + (p_{BP} - 2.98 \times 10^6) K_1}{1 + K_1}, \quad (206)$$

13 where

14 
$$K_1 = \frac{k_{BP} h_{BP} \left[ \ln \left( \frac{r_{e,rep}}{r_w} \right) - \frac{1}{2} \right]}{k_{rep} h_{rep} \left[ \ln \left( \frac{r_{eBP}}{r_w} \right) - \frac{1}{2} \right]}, \quad (207)$$

15 and  $-2.98 \times 10^6$  comes from Equation (203). The expression in Equation (207) was used to  
 16 define  $p_{wE1}$  in the CCA PA in the determination of DBRs for a drilling intrusion that occurred  
 17 within 200 years of a preceding E1 intrusion (see Table PA-5). The same approach was used  
 18 for the CRA-2004 PA.

19 **PA-4.7.7.2 Solution for Sand-Filled Borehole**

20 The determination of the pressure  $p_{wfBI}$  with the assumption that a borehole filled with  
 21 material with properties similar to silty sand connects the brine pocket and the repository is  
 22 now considered. The approach is similar to that used for the open borehole except that  
 23 Equation (199a) and Equation (199b) are replaced by a single equation based on Darcy's  
 24 Law. Specifically, flow from the brine pocket to the repository is represented by

25 
$$Q = \frac{k_{BH} A_{BH} \left[ (p_{wfBP} - p_{wfBI}) + g\rho \right]}{\mu (y_{BP} - y_{rep})}, \quad (208)$$

1 *where*

2  $k_{BH}$  = borehole permeability (m<sup>2</sup>),

3  $A_{BH}$  = borehole cross-sectional area (m<sup>2</sup>),

4 *and the remaining symbols have been defined previously. In the present analysis,  $k_{BH}$  is an*  
 5 *uncertain input (see BHPRM in Table PA-17) and  $A_{BH}$  is defined by the assumption that the*  
 6 *borehole diameter is the same as the drill bit diameter (i.e., 12.25 in. = 0.311 m).*

7 *The representation for flow from the brine pocket inlet point to the repository to the outlet*  
 8 *point associated with the drilling intrusion under consideration remains as defined in*  
 9 *Equation (205). Thus, two equations (i.e., Equation (208) and Equation (205)) and two*  
 10 *unknowns (i.e.,  $p_{wfBI}$  and  $Q$ ) are under consideration. Solution for  $p_{wfBI}$  and yields*

11 
$$p_{wfBI} = \frac{p_{wfBO} + K_2 p_{BP} - 2.98 \times 10^6 K_2}{1 + K_2} \quad (209)$$

12 *where*

13 
$$K_2 = \frac{\pi k_{BH} r_w^2 \left[ \ln \left( \frac{r_{eBP}}{r_w} \right) - \frac{1}{2} \right]}{2\pi h_{rep} k_{rep} (y_{BP} - y_{rep})} \quad (210)$$

14 *and  $-2.98 \times 10^6$  comes from Equation (203). The expression in Equation (209) was used to*  
 15 *define  $p_{wE1}$  in the determination of DBRs for a drilling intrusion that occurred more than 200*  
 16 *years after a preceding E1 intrusion (see Table PA-5).*

17 **PA-4.7.8 End of Direct Brine Release**

18 *The CRA-2004 PA has 23,400 cases that potentially required solution of Equation (188) to*  
 19 *obtain the DBR volume (See Section PA-6.7.5). However, the DBR was set to zero without*  
 20 *solution of Equation (188) when there was no possibility of a release (i.e., the intruded waste*  
 21 *panel at the time of the intrusion had either a pressure less than 8 MPa or a brine saturation*  
 22 *below the residual brine saturation  $S_{br}$ ).*

23 *For the remaining cases, Equation (188) was solved for a time period of 50 days, although the*  
 24 *value used for  $t_e$  was always less than 50 days. The minimum value used for  $t_e$  was three days,*  
 25 *which is an estimate of the time required to drill from the repository through the Castile*  
 26 *Formation and then cement the intermediate casing. If there is little or no gas flow associated*  
 27 *with brine inflow into the borehole during drilling in the Salado Formation, current industry*  
 28 *practice is to allow the brine to “seep” into the drilling mud and be discharged to the mud pits*  
 29 *until the salt section is cased.*

1 *If there is a significant amount of gas flow, then it is possible that the driller will lose control*  
 2 *of the well. In such cases, DBRs will take place until the gas flow is brought under control.*  
 3 *Two possibilities exist: (1) the driller will regain control of the well when the gas flow drops to*  
 4 *a manageable level, and (2) aggressive measures will be taken to shut off the gas flow before it*  
 5 *drops to a manageable level. In the CCA PA, the driller was assumed to be able to regain*  
 6 *control of the well when the gas flow dropped to a “cut-off” rate of  $1 \times 10^5$  standard cubic feet*  
 7 *per day (SCF/d in commonly used oil field units). Experience at the South Culebra Bluff Unit*  
 8 *#1, which blew out in January 1978, suggests that approximately 11 days may be needed to*  
 9 *bring a well under control before the gas flow drops to a manageable level (i.e.,  $1 \times 10^5$*   
 10 *SCF/d) (DOE 1996, Appendix MASS Attachment MASS 16-2). In particular, it took 11 days*  
 11 *to assemble the equipment and personnel needed to bring that well under control.*

12 *Given the preceding,  $t_e$  is defined by*

$$13 \quad t_e = \begin{cases} \max\{3 \text{ d}, t_f\} & \text{if } t_f \leq 11 \text{ d} \\ 11 \text{ d} & \text{if } t_f > 11 \text{ d} \end{cases} \quad (211)$$

14 *in the CRA-2004 PA, where  $t_f$  is the time at which the gas flow out of the well drops below*  
 15  *$1 \times 10^5$  SCF/d. As a reminder, gas flow out of the repository in the intruding borehole, and*  
 16 *hence  $t_e$ , is determined as part of the solution to Equation (188).*

17 **PA.-4.7.9 Numerical Solution**

18 *As previously indicated, the BRAGFLO program is used to solve Equation (188) with the*  
 19 *computational grid in Figure PA-20, the initial value conditions in Section PA-4.7.2, the*  
 20 *boundary value conditions in Table PA-16, and parameter values appropriate for modeling*  
 21 *DBRs. Thus, the numerical procedures in use for Equation (188) are the same as those*  
 22 *described in Section PA-4.2.10 for the solution of Equation (25).*

23 *In this solution, the boundary value conditions associated with drilling intrusions (i.e.,  $p_{wf}$*   
 24 *and  $p_{wE1}$  in Table PA-16) are implemented through the specification of fluid withdrawal*  
 25 *terms (i.e.,  $q_{wg}$  and  $q_{wb}$  in Equation (25)) rather than as defined boundary value conditions.*  
 26 *With this implementation, the representations in Equation (188a) and Equation (188b) for gas*  
 27 *and brine conservation become*

$$28 \quad \nabla \cdot \left[ \frac{\alpha \rho_g K_g k_{rg}}{\mu_g} (\nabla p_g + \rho_g g \nabla h) \right] + \alpha q_{wg} = \alpha \frac{\partial (\phi \rho_g S_g)}{\partial t} \quad (212a)$$

$$29 \quad \nabla \cdot \left[ \frac{\alpha \rho_b K_b k_{rb}}{\mu_b} (\nabla p_b + \rho_b g \nabla h) \right] + \alpha q_{wb} = \alpha \frac{\partial (\phi \rho_b S_b)}{\partial t}, \quad (212b)$$

30 *and the constraints in Equation (188) remain unchanged. As used in Equation (212),  $q_{wg}$  and*  
 31  *$q_{wb}$  are independent of the computational grid in use (Figure PA-20). In practice,  $q_{wg}$  and*

1  $q_{wb}$  are defined with a productivity index (see Equation (181)) that is a function of the specific  
 2 computational grid in use, with the result that these definitions are only meaningful in the  
 3 context of the computational grid that they are intended to be used with. This specificity  
 4 results because  $q_{wg}$  and  $q_{wb}$  as used in Equation (212) are defined on a much smaller scale  
 5 than can typically be implemented with a reasonable-sized computational grid. As a result, the  
 6 values used for  $q_{wg}$  and  $q_{wb}$  in the numerical solution of Equation (212) must incorporate the  
 7 actual size of the grid in use.

8 In the solution of Equation (212) with the computational grid in Figure PA-20,  $q_{wg}$  is used to  
 9 incorporate gas flow out of the repository and  $q_{wb}$  is used to incorporate both brine inflow to  
 10 the repository from a pressurized brine pocket and brine flow out of the repository. For gas  
 11 flow out of the repository,

$$12 \quad q_{wg}(x, y, t) = \frac{kk_{rg}(x, y, t)[p_g(x, y, t) - p_{wf}]}{\mu_g[\ln(r_e / r_w) + s + c]}, \quad (213)$$

13 if  $(x, y)$  is at the center of the grid cell containing the drilling intrusion (Figure PA-20) and  
 14  $q_{wg}(x, y, t) = 0$  (kg/m<sup>3</sup>)/s otherwise, where  $k$ ,  $k_{rg}$ ,  $\mu_g$ ,  $r_e$ ,  $r_w$ ,  $s$  and  $c$  are defined in  
 15 conjunction with Equation (181),  $p_g$  is gas pressure, and  $p_{wf}$  is the flowing well pressure at the  
 16 outlet borehole (i.e., the boundary value condition in Table PA-16). The factor  $h$  in Equation  
 17 (181) is the crushed height of the repository as indicated in Equation (176) and defines the  
 18 factor  $\alpha$  in Equation (212). In the numerical solution,  $q_{wg}(x, y, t)$  defines  $q_{wgi,j}^{n+1}$  in  
 19 Equation (79), with  $q_{wgi,j}^{n+1}$  having a nonzero value only when  $i, j$  correspond to the grid cell  
 20 containing the borehole through which gas outflow is taking place (i.e., the grid cells  
 21 containing the down-dip and up-dip wells in Figure PA-20).

22 For brine flow,

$$23 \quad q_{wb}(x, y, t) = \frac{kk_{rb}(x, y, t)[p_b(x, y, t) - p_{wf}]}{\mu_b[\ln(r_e / r_w) + s + c]}, \quad (214)$$

24 if  $(x, y)$  is at the center of the grid cell containing the drilling intrusion through which brine  
 25 outflow from the repository is taking place (Figure PA-20);

$$26 \quad q_{wb}(x, y, t) = \frac{kk_{rb}(x, y, t)[p_{wE1} - p_b(x, y, t)]}{\mu_b[\ln(r_e / r_w) + c]}, \quad (215)$$

27 if  $(x, y)$  is at the center of the grid cell containing a prior drilling intrusion into a pressurized  
 28 brine pocket (Figure PA-20), where  $p_{wE1}$  is the boundary value condition defined in Table  
 29 PA-16; and  $q_{wb}(x, y, t) = 0$  otherwise. In the numerical solution of Equation (212a),

1  $q_{wg}(x, y, t)$  defines  $q_{wbi,j}^{n+1}$  in a discretization for Equation (212b) that is equivalent to the  
 2 discretization for Equation (212a) shown in Equation (79), with  $q_{wbi,j}^{n+1}$  having a nonzero  
 3 value only when  $i, j$  correspond to the grid cell containing the borehole through which brine  
 4 outflow is taking place (i.e., the grid cells containing the down-dip and up-dip wells in Figure  
 5 PA-20, in which case, Equation (214) defines  $q_{wbi,j}^{n+1}$  or to the grid cell containing the  
 6 borehole through which brine inflow to the repository from a pressurized brine pocket is  
 7 taking place (i.e., the grid cell containing the E1 intrusion in Figure PA-20; in which case,  
 8 Equation (215) defines  $q_{wbi,j}^{n+1}$ .

9 **PA-4.7.10 Additional Information**

10 Additional information on BRAGFLO and its use in the CRA-2004 PA to determine DBRs  
 11 can be found in the analysis package for DBR (Stein 2003) and in the BRAGFLO User's  
 12 Manual (WIPP PA 2003c).

13 **PA-4.8 Brine Flow in Culebra: MODFLOW**

14 This section describes the model for the calculation of brine flow in the Culebra.

15 **PA-4.8.1 Mathematical Description**

16 Groundwater flow in the Culebra Dolomite is represented by the partial differential equation

17 
$$S \left( \frac{\partial h}{\partial t} \right) = \nabla \cdot (bK \nabla h) - Q, \tag{216}$$

18 where

19  $S$  = medium storativity (dimensionless),

20  $h$  = hydraulic head (m),

21  $t$  = time (s),

22  $b$  = aquifer thickness (m),

23  $K$  = hydraulic conductivity tensor (m/s),

24  $Q$  = source/sink term expressed as the volumetric flux per unit area  
 25  $((m^3/m^2)/s = m/s)$ .

26 Further, the Culebra is assumed to be isotropic, and as a result,  $K$  is defined by

27 
$$K(x, y) = k(x, y) \begin{bmatrix} 1 & 0 \\ 0 & 1 \end{bmatrix}, \tag{217}$$

1 *where  $k(x, y)$  is the hydraulic conductivity (m/s) at the point  $(x, y)$ . The following*  
 2 *simplifying assumptions are also made: fluid flow in the Culebra is at steady state (i.e.,*  
 3  *$\partial h/\partial t = 0$ ), and source and sink effects arising from borehole intrusions and infiltration are*  
 4 *negligible (i.e.,  $Q = 0$ ). Given these assumptions, Equation (216) simplifies to*

$$5 \quad \nabla \cdot (bK\nabla h) = 0, \quad (218)$$

6 *which is the equation actually solved to obtain fluid flow (i.e.,  $K\nabla h$ ) in the Culebra. In the*  
 7 *CRA-2004 PA,  $b = 7.75$  m, and  $k(x, y)$  in Equation (217) is a function of an imprecisely*  
 8 *known transmissivity field, as discussed in Section PA-4.8.2.*

### 9 *PA-4.8.2 Implementation*

10 *The first step in the analysis of fluid flow in the Culebra is to generate transmissivity fields*  
 11  *$t(x, y)$  ( $m^2/s$ ) for the Culebra and to characterize the uncertainty in these fields. This was*  
 12 *accomplished by generating a large number of plausible transmissivity fields. A description of*  
 13 *the method used to construct these transmissivity fields is included in Attachment TFIELD.*  
 14 *Below, a brief outline of the method is presented.*

15 *The transmissivity fields used for the CRA-2004 PA are based on several types of information,*  
 16 *including a regression model developed on WIPP-site geologic data, measured head levels in*  
 17 *the Culebra for the year 2000, and well drawdown test results. The following steps led to the*  
 18 *final transmissivity fields used in this analysis:*

19 *Geologic data including: (1) depth to the top of the Culebra, (2) reduction in thickness of the*  
 20 *upper Salado Formation by dissolution, and (3) the spatial distribution of halite in the Rustler*  
 21 *Formation below and above the Culebra were used to define a geologic regression model that*  
 22 *relates transmissivity at any location to a set of geologically defined parameters.*

23 *Base transmissivity fields are defined for a modeling domain measuring 22.4 km east-west by*  
 24 *30.7 km north-south using a method of stochastic simulation. The base transmissivity fields*  
 25 *were constructed from information on the depth to the Culebra, indicator functions defining*  
 26 *the location of Salado dissolution, halite occurrence, and high transmissivity zones.*

27 *Seed transmissivity fields are defined by conditioning base transmissivity fields to measured*  
 28 *values of transmissivity. This conditioning is performed with a Gaussian geostatistical*  
 29 *simulation algorithm.*

30 *The seed transmissivity fields are calibrated to transient water level data from the year 2000 in*  
 31 *37 wells across the region using parameter estimation program PEST (Doherty 2002). The*  
 32 *PEST program iteratively changes the seed transmissivity field values to minimize an objective*  
 33 *function, using MODFLOW to rerun the flow solution between each iteration. The objective*  
 34 *function minimized by PEST is a combination of the weighted sum of the squared residuals*  
 35 *between the measured and modeled head data and a second weighted sum of the squared*  
 36 *differences in the estimated transmissivity between pairs of pilot points. The second weighted*

1 *sum is designed to keep the transmissivity field as homogeneous as possible and to provide*  
 2 *numerical stability when estimating more parameters than there are data.*

3 *The calibrated transmissivity fields produced by PEST and MODFLOW are screened*  
 4 *according to specific acceptance criteria. Calibrated transmissivity fields that meet the*  
 5 *acceptance criteria are modified for the partial and full mining scenarios. This modification*  
 6 *increases transmissivity by a random factor between 1 and 1000 in areas identified as*  
 7 *containing potash reserves, as described below. Steady-state flow simulations are then run*  
 8 *using the mining-modified transmissivity fields.*

9 *The transport code SECOTP2D uses a grid with uniform cells of 50 × 50 m. Thus as a final*  
 10 *step, MODFLOW runs with a 50 × 50 m grid to calculate the flow fields required for the*  
 11 *transport code. The hydraulic conductivities for the finer grid are obtained by dividing each*  
 12 *100 × 100 m cell into four 50 × 50 m cells. The conductivity assigned to each of the four cells*  
 13 *is equal to the conductivity of the larger cell (Leigh et al. 2003).*

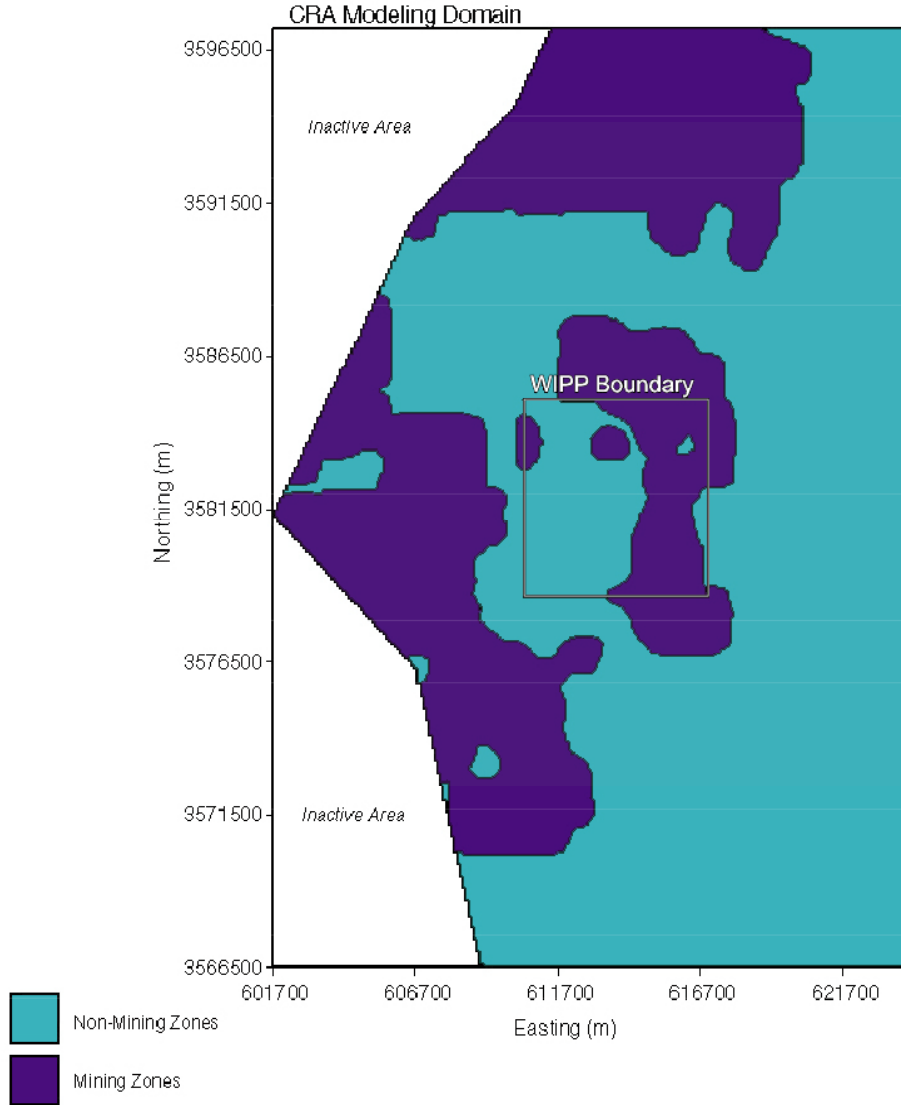
14 *The hydraulic conductivity  $k(x, y)$  in Equation (217) is defined in terms of the transmissivity*  
 15 *fields  $t(x, y)$  by*

$$16 \qquad k(x, y) = t(x, y) / b. \qquad (219)$$

17 *Fluid flow (i.e.,  $K\nabla h$ ) is determined by solving Equation (218) for two different cases: (1) a*  
 18 *partial mining case (mining of potash deposits outside the land withdrawal boundary), and (2)*  
 19 *a full mining case (mining of potash deposits inside and outside the land withdrawal*  
 20 *boundary) (Figure PA-23). As specified by guidance in 40 CFR Part 194 (p. 5229, EPA 1996),*  
 21 *potash mining increases the hydraulic conductivity in the Culebra in the vicinity of such*  
 22 *mining by an uncertain factor with a value between 1 and 1000. As specified in 40 CFR*  
 23 *§ 194.32 and described in Section PA-3.8, economic potash reserves outside the land*  
 24 *withdrawal boundary are assumed to have been fully mined by the end of the 100 year-period*  
 25 *of active institutional controls, after which the occurrence of potash mining within the land*  
 26 *withdrawal boundary follows a Poisson process with a rate constant of  $\lambda_m = 1 \times 10^{-4} \text{ yr}^{-1}$ .*

27 *In the partial mining case, the hydraulic conductivity  $k_{PM}(x, y)$  is defined by Equation (219)*  
 28 *inside the WIPP boundary and by  $k_{PM}(x, y) = k(x, y) \times MF$  outside the WIPP boundary,*  
 29 *where MF is determined by the uncertain parameter CTRANSFM (see Table PA-17). In the*  
 30 *full mining case, the hydraulic conductivity  $k_{FM}(x, y) = k(x, y) \times MF$  in all areas of the*  
 31 *modeling domain.*

32 *In turn,  $k_{PM}(x, y)$  and  $k_{FM}(x, y)$  result in the following definition for the hydraulic*  
 33 *conductivity tensor  $K$ :*



1  
2 **Figure PA-23. Areas of Potash Mining in the McNutt Potash Zone.**

3 
$$\mathbf{K}_i(x, y) = k_i(x, y) \begin{bmatrix} 1 & 0 \\ 0 & 1 \end{bmatrix}, \quad i = PM, FM . \quad (220)$$

4 *In the analysis, Equation (218) is solved with each of the preceding definitions of  $\mathbf{K}_i$  to obtain*  
 5 *characterizations of fluid flow in the Culebra for partially-mined conditions (i.e.,  $\mathbf{K}_{PM} \nabla h$ )*  
 6 *and fully-mined conditions (i.e.,  $\mathbf{K}_{FM} \nabla h$ ).*

7 *The determination of fluid flow in the Culebra through the solution of Equation (218) does*  
 8 *not incorporate the potential effects of climate change on fluid flow. Such effects are*  
 9 *incorporated into the analysis by an uncertain scale factor to introduce the potential effects of*

1 *climate change into the analysis (Corbet and Swift 1996a, 1996b). Specifically, the Darcy*  
 2 *fluid velocity  $\mathbf{v}_i(x, y)$  actually used in the radionuclide transport calculations is given by*

$$3 \quad \mathbf{v}_i(x, y) = [u_i(x, y), v_i(x, y)] = SFC [K_i(x, y) \nabla h_i(x, y)]^T, \quad (221)$$

4 *where  $u_i(x, y)$  and  $v_i(x, y)$  represent Darcy fluid velocities (m/s) at the point  $(x, y)$  in the  $x$*   
 5 *and  $y$  directions, respectively,  $\nabla h_i(x, y)$  is obtained from Equation (218) with  $K = K_i$ , and*  
 6 *SFC is a scale factor used to incorporate the uncertainty that results from possible climate*  
 7 *changes. The scale factor SFC is determined by the uncertain parameter CCLIMSF (see*  
 8 *Table PA-17).*

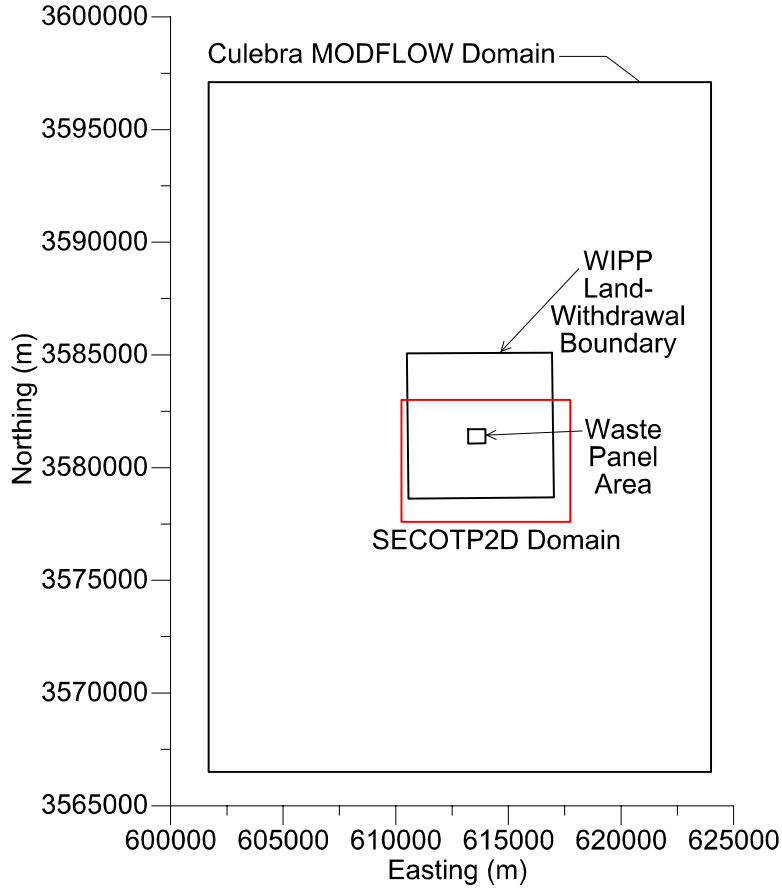
### 9 *PA-4.8.3 Computational Grids and Boundary Value Conditions*

10 *The representation for fluid flow in the Culebra in Equation (218) is evaluated on a numerical*  
 11 *grid 22.4 km east-west by 30.7 km north-south, aligned with the compass directions (Figure*  
 12 *PA-24). The modeling domain is discretized into 68,768 uniform 100-m  $\times$  100-m cells. The*  
 13 *northern model boundary is slightly north of the northern end of Nash Draw, 12 km north of*  
 14 *the northern WIPP site boundary, and about 1 km north of Mississippi Potash Incorporated's*  
 15 *east tailings pile. The eastern boundary lies in a low- $T$  region that contributes little flow to the*  
 16 *modeling domain. The southern boundary lies 12.2 km south of the southern WIPP site*  
 17 *boundary, 1.7 km south of WIPP's southernmost well (H-9), and far enough from the WIPP*  
 18 *site to have little effect on transport rates on the site. The western model boundary passes*  
 19 *through the IMC tailings pond (Laguna Uno; see Hunter (1985)) due west of the WIPP site in*  
 20 *Nash Draw.*

21 *Two types of boundary conditions are specified: constant-head and no-flow (Figure PA-25).*  
 22 *Constant-head conditions are assigned along the eastern boundary of the model domain, and*  
 23 *along the central and eastern portions of the northern and southern boundaries. Values of*  
 24 *these heads are obtained from the kriged initial head field. The western model boundary*  
 25 *passes through the IMC tailings pond (Laguna Uno) due west of the WIPP site in Nash Draw.*  
 26 *A no-flow boundary (a flow line) is specified in the model from this tailings pond up the axis*  
 27 *of Nash Draw to the northeast, reflecting the concept that groundwater flows down the axis of*  
 28 *Nash Draw, forming a groundwater divide. Similarly, another no-flow boundary is specified*  
 29 *from the tailings pond down the axis of the southeastern arm of Nash Draw to the southern*  
 30 *model boundary, coinciding with a flow line in the regional modeling of Corbet and Knupp*  
 31 *(1996). Thus, the northwestern and southwestern corners of the modeling domain are*  
 32 *specified as inactive cells in MODFLOW.*

### 33 *PA-4.8.4 Numerical Solution*

34 *The flow model in Equation (218) is evaluated with a second-order difference procedure*  
 35 *(McDonald and Harbaugh 1988, p. 126) on the computational grid described in Section*  
 36 *PA.4.8.3. Specifically, the discretized form of Equation (218) is*



1  
2 **Figure PA-24. Modeling Domain for Groundwater Flow (MODFLOW) and Transport**  
3 **(SECOTP2D) in the Culebra.**

4

$$0 = CR_{i,j-1/2} (h_{i,j-1} - h_{i,j}) + CR_{i,j+1/2} (h_{i,j+1} - h_{i,j})$$

5

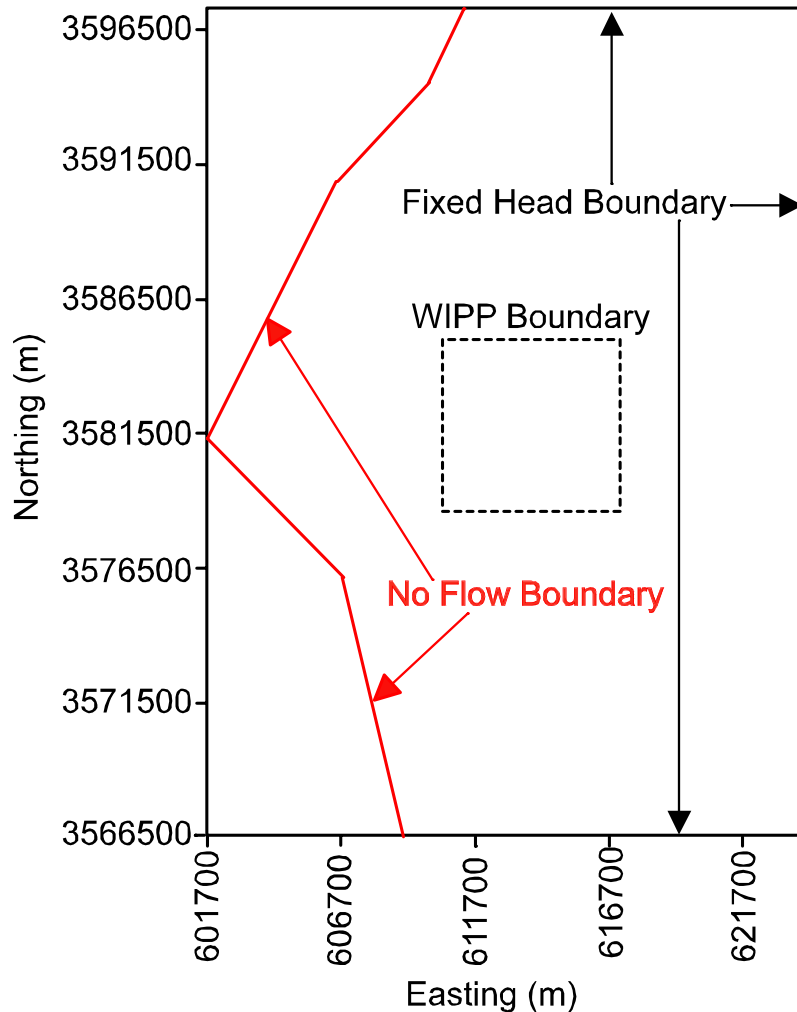
$$+ CC_{i-1/2,j} (h_{i-1,j} - h_{i,j}) + CC_{i+1/2,j} (h_{i+1,j} - h_{i,j}), \quad (222)$$

6 *where CR and CC are the row and column hydraulic conductances at the cell interface*  
7 *between node i, j and a neighboring node (m<sup>2</sup>/s). Since the grid is uniform, the hydraulic*  
8 *conductance is simply the harmonic mean of the hydraulic conductivity in the two*  
9 *neighboring cells multiplied by the aquifer thickness. For example, the hydraulic*  
10 *conductance between cells (i, j) and (i, j - 1) is given by CR<sub>i,j-1/2</sub> and the hydraulic*  
11 *conductance between cells (i, j) and (i + 1, j) is given by CC<sub>i+1/2,j</sub>:*

12

$$CR_{i,j-1/2} = \frac{2k_{i,j}k_{i,j-1}}{k_{i,j} + k_{i,j-1}} \times b \quad \text{and} \quad CC_{i+1/2,j} = \frac{2k_{i,j}k_{i+1,j}}{k_{i,j} + k_{i+1,j}} \times b,$$

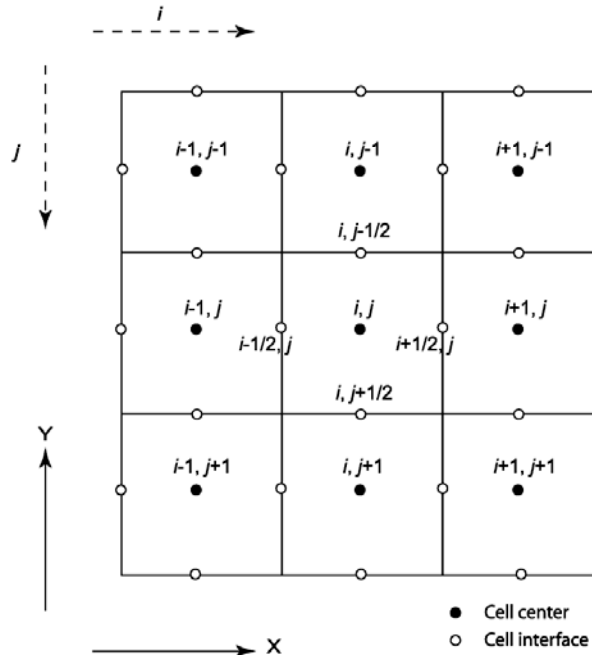
13 *where k<sub>i,j</sub> is the hydraulic conductivity in cell i, j (m/s) and b is the aquifer thickness (m).*



1

2 *Figure PA-25. Boundary Conditions Used for Simulations of Brine Flow in the Culebra.*

3 *Figure PA-26 illustrates the cell numbering convention used in the finite difference grid for*  
 4 *MODFLOW. The determination of  $h$  is then completed by the solution of the linear system of*  
 5 *equations in Equation (222) for the unknown heads  $h_{i,j}$ . The solution is accomplished using*  
 6 *the algebraic multigrid solver (AMG) (Ruge and Stuben 1987) that is part of the Link-AMG*  
 7 *(LMG) package within MODFLOW (Mehl and Hill 2001). The AMG method solves Equation*  
 8 *(222) with the successive over-relaxation (SOR) iterative method (Roache 1972) on different*  
 9 *grids that are coarser than the original grid. The coarser grid solutions provide the initial*  
 10 *condition to the next finer solution until a solution based on the original grid size is obtained.*  
 11 *The advantage of the AMG method is that the larger grid solutions reduce the large frequency*  
 12 *oscillations in the numerical solution much faster than if solved on a finer grid. The finer*  
 13 *grid solutions are then able to remove the small frequency oscillations to obtain the final*  
 14 *solution. While memory intensive, the AMG method produces solutions faster than ordinary*  
 15 *iterative methods (Mehl and Hill 2001). Brine fluxes at cell interfaces are calculated from the*  
 16 *values for  $h_{i,j}$  internally in MODFLOW.*



1  
2 **Figure PA-26. Finite Difference Grid Showing Cell Index Numbering Convention Used by**  
3 **MODFLOW.**

4 **PA-4.8.5 Additional Information**

5 *Additional information on MODFLOW and its use in the CRA-2004 PA to determine fluid*  
6 *flow in the Culebra can be found in the MODFLOW-2000 User's Manual (Harbaugh et al.*  
7 *2000) and in McKenna and Hart (2003) and Lowry (2003). The flow fields computed for the*  
8 *CRA-2004 PA are presented in Attachment TFIELD.*

9 **PA-4.9 Radionuclide Transport in Culebra: SECOTP2D**

10 *Radionuclide transport in the Culebra formation is computed using the SECOTP2D computer*  
11 *code. The mathematical equations solved by the code SECOTP2D and the numerical methods*  
12 *used are described in the following sections.*

13 **PA-4.9.1 Mathematical Description**

14 *Radionuclide transport in the Culebra Dolomite is described by a parallel plate dual porosity*  
15 *model (Meigs and McCord 1996). The parallel plate dual porosity conceptualization assumes*  
16 *that the numerous fractures within the formation are aligned in a parallel fashion and treats*  
17 *the fractured porous media as two overlapping continua: one representing the fractures and*  
18 *the other representing the surrounding porous rock matrix (See Figure PA-27). In this model,*  
19 *one system of partial differential equations (PDEs) is used to represent advective transport in*  
20 *fractures within the Culebra Dolomite and another PDE system is used to represent diffusive*  
21 *transport and sorption in the matrix that surrounds the fractures.*

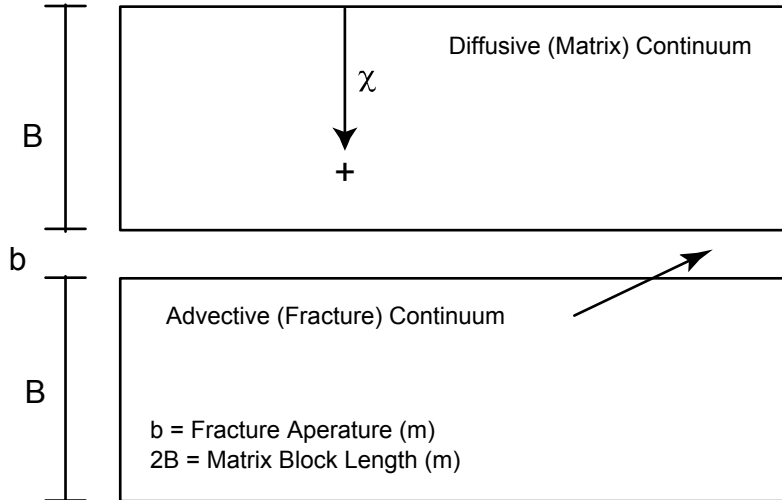


Figure PA-27. Parallel Plate Dual Porosity Conceptualization.

PA-4.9.1.1 Advective Transport in Fractures

The PDE system used to represent advective transport in fractures is given by (WIPP PA 1997b)

$$\nabla \cdot [\phi \mathbf{D}_k \nabla C_k - \mathbf{v} C_k] = \phi R_k \left( \frac{\partial C_k}{\partial t} \right) + \phi R_k \lambda_k C_k - \phi R_{k-1} \lambda_{k-1} C_{k-1} - Q_k - \Gamma_k, \quad (223)$$

for  $k = 1, 2, \dots, nR$ , where

$nR$  = number of radionuclides under consideration,

$C_k$  = concentration of radionuclide  $k$  in brine ( $\text{kg}/\text{m}^3$ ),

$\mathbf{D}_k$  = hydrodynamic dispersion tensor ( $\text{m}^2/\text{s}$ ),

$\mathbf{v}$  = Darcy velocity (i.e., specific discharge) of brine ( $\text{m}/\text{s} = (\text{m}^3/\text{m}^2)/\text{s}$ ),

$\phi$  = advective (i.e., fracture) porosity (dimensionless),

$R_k$  = advective retardation coefficient (dimensionless),

$\lambda_k$  = decay constant for radionuclide  $k$  ( $\text{s}^{-1}$ ),

$Q_k$  = injection rate of radionuclide  $k$  per unit bulk volume of formation ( $(\text{kg}/\text{s})/\text{m}^3$ )  
(Note:  $Q_k > 0$  corresponds to injection into the fractures),

1  $\Gamma_k$  = mass transfer rate of radionuclide  $k$  per unit bulk volume of formation due to  
 2 diffusion between fractures and surrounding matrix ((kg/s)/m<sup>3</sup>) (Note:  $\Gamma_k >$   
 3  $0$  corresponds to diffusion into fractures).

4 The Darcy velocity  $\mathbf{v}$  is obtained from the solution of Equation (218); specifically,  $\mathbf{v}$  is  
 5 defined by the relationship in Equation (221). The advective porosity  $\phi$ , defined as the ratio of  
 6 the interconnected fracture pore volume to the total volume, is determined by an uncertain  
 7 parameter (see CFRCPOR in Table PA-17).

8 The hydrodynamic dispersion tensor is defined by (WIPP PA 1997b; Bear 1972)

$$9 \quad \mathbf{D}_k = \frac{1}{\|\mathbf{v}\|\phi} \begin{bmatrix} u & -v \\ v & u \end{bmatrix} \begin{bmatrix} \alpha_L & 0 \\ 0 & \alpha_T \end{bmatrix} \begin{bmatrix} u & v \\ -v & u \end{bmatrix} + \tau D_k^* \begin{bmatrix} 1 & 0 \\ 0 & 1 \end{bmatrix}, \quad (224)$$

10 where  $\alpha_L$  and  $\alpha_T$  are the longitudinal and transverse dispersivities (m);  $u$  and  $v$  are the  $x$  and  
 11  $y$  components of  $\mathbf{v}$  (i.e.,  $\mathbf{v} = [u, v]$ );  $D_k^*$  is the free water molecular diffusion coefficient  
 12 ( $m^2 s^{-1}$ ) for radionuclide  $k$ ; and  $\tau$  is the advective tortuosity, defined as the ratio of the true  
 13 length of the flow path of a fluid particle to the straight-line distance between the starting and  
 14 finishing points of the particle's motion. As in the CCA PA (Helton et al. 1998), the  
 15 CRA-2004 PA uses  $\alpha_L = \alpha_T = 0$  m and  $\tau = 1$ . Thus, the definition of  $\mathbf{D}_k$  used in the  
 16 CRA-2004 PA reduces to

$$17 \quad \mathbf{D}_k = D_k^* \begin{bmatrix} 1 & 0 \\ 0 & 1 \end{bmatrix}. \quad (225)$$

18 The diffusion coefficient  $D_k^*$  equals  $3 \times 10^{-10} m^2/s$  for radionuclides in the +3 oxidation state  
 19 (i.e., Am(III), Pu(III)),  $1.53 \times 10^{-10} m^2/s$  for radionuclides in the +4 oxidation state (i.e.,  
 20 Pu(IV), Th(IV), U(IV)), and  $4.26 \times 10^{-10} m^2/s$  for radionuclides in the +6 oxidation state (i.e.,  
 21 U(VI)) (Attachment PAR, Table PAR-35). The existence of Pu in the +3 or +4 oxidation state  
 22 (i.e., as Pu(III) or Pu(IV)) and the existence of U in the +4 or +6 oxidation state (i.e., as U(IV)  
 23 or U(VI)) is determined by an uncertain parameter (see WOXSTAT in Table PA-17).

24 The advective retardation coefficient  $R_k$  is defined by

$$25 \quad R_k = 1 + (1 - \phi) \rho_A K_{Ak} / \phi, \quad (226)$$

26 where

27  $\rho_A$  = surface area density of fractures in Culebra ( $m^2/m^3 = 1/m$ ) (i.e., surface area  
 28 of fractures ( $m^2$ ) divided by volume of fractures ( $m^3$ )),

29  $K_{Ak}$  = surface area distribution coefficient ((kg/m<sup>2</sup>)/(kg/m<sup>3</sup>) = m) (i.e.,  
 30 concentration of radionuclide  $k$  sorbed on fracture surfaces (kg/m<sup>2</sup>) divided

1 *by concentration of radionuclide  $k$  dissolved in brine within fractures*  
 2 *( $\text{kg}/\text{m}^3$ ).*

3 *Following the logic of the CCA PA (Helton et al. 1998),  $K_{Ak} = 0$  and thus  $R_k = 1$  in the 2004*  
 4 *PA.*

5 *In concept, the term  $Q_k$  in Equation (223) provides the link between the releases to the*  
 6 *Culebra calculated with NUTS and PANEL (Section PA-6.7) and transport within the*  
 7 *Culebra. In the computational implementation of the CRA-2004 PA, radionuclide transport*  
 8 *calculations in the Culebra were performed for unit radionuclide releases to the Culebra and*  
 9 *then the outcomes of these calculations were used to construct the release to the accessible*  
 10 *environment associated with time-dependent releases into the Culebra derived from NUTS and*  
 11 *PANEL calculations (Section PA-6.8.7). The definition of  $Q_k$  is discussed in more detail in*  
 12 *Section PA-4.9.1.4.*

13 *The initial condition for Equation (223) is*

$$14 \quad C_k(x, y, 0) = 0 \text{ kg} / \text{m}^3. \quad (227)$$

15 *Furthermore, the boundary value conditions for Equation (223) are defined at individual*  
 16 *points on the boundary of the grid in Figure (PA-24) on the basis of whether the flow vector*  
 17  *$\mathbf{v} = [u, v]$  defines a flow entering the grid or leaving the grid. The following Neumann*  
 18 *boundary value condition is imposed at points  $(x, y)$  where flow leaves the grid:*

$$19 \quad \nabla C_k(x, y, t) \cdot \mathbf{n}(x, y) = 0 \text{ (kg/m}^3\text{)/m}, \quad (228)$$

20 *where  $\mathbf{n}(x, y)$  is an outward-pointing unit normal vector defined at  $(x, y)$ . The following*  
 21 *Dirichlet boundary value condition is imposed at points  $(x, y)$  where flow enters the grid:*

$$22 \quad C_k(x, y, t) = 0 \text{ kg/m}^3. \quad (229)$$

23 **PA-4.9.1.2 Diffusive Transport in the Matrix**

24 *The system of PDEs used to represent diffusive transport in the matrix surrounding the*  
 25 *fractures is given by (WIPP PA 1997b)*

$$26 \quad \frac{\partial}{\partial \chi} \left( \phi'_k D'_k \frac{\partial C'_k}{\partial \chi} \right) = \phi' R'_k \left( \frac{\partial C'_k}{\partial t} \right) + \phi' R'_k \lambda_k C'_k - \phi' R'_{k-1} \lambda_{k-1} C'_{k-1}, \quad (230)$$

27 *where  $\chi$  is the spatial coordinate in Figure PA-27,  $D'_k$  is the matrix diffusion coefficient*  
 28 *( $\text{m}^2/\text{s}$ ) for radionuclide  $k$  defined by  $D'_k = D_k^* \tau'$ , and  $\tau'$  is the matrix tortuosity. The*  
 29 *remaining terms have the same meaning as those in Equation (223) except that the prime*  
 30 *denotes properties of the matrix surrounding the fractures. A constant value ( $\tau' = 0.11$ ) for*

1 *the matrix (i.e., diffusive) tortuosity is used in the CRA-2004 PA (Meigs 1996). The matrix*  
 2 *(i.e., diffusive) porosity  $\phi'$  is an uncertain input to the analysis (see CMTRXPOR in Table*  
 3 *PA-17). The matrix retardation  $R'_k$  is defined by*

$$4 \qquad R'_k = 1 + (1 - \phi') \rho_s K_{dk} / \phi', \qquad (231)$$

5 *where  $\rho_s$  is the particle density (kg/m<sup>3</sup>) of the matrix and  $K_{dk}$  is the distribution coefficient*  
 6 *((Ci/kg)/(Ci/m<sup>3</sup>) = m<sup>3</sup>/kg) for radionuclide  $k$  in the matrix. The density  $\rho_s$  is assigned a value*  
 7 *of  $2.82 \times 10^3$  kg/m<sup>3</sup> (Martell 1996b). The distribution coefficients  $K_{dk}$  are uncertain inputs to*  
 8 *the analysis and dependent on the uncertain oxidation state of the relevant element (see*  
 9 *CMKDAM3, CMKDPU3, CMKDPU4, CMKDTH4, CMKDU4, CMKDU6, and WOXSTAT in*  
 10 *Table PA-17).*

11 *The initial and boundary value conditions used in the formulation of Equation (230) are*

$$12 \qquad C'_k(x, y, \chi, 0) = 0 \text{ kg/m}^3, \qquad (232)$$

$$13 \qquad \partial C'_k(x, y, 0, t) / \partial z = 0 \text{ kg/m}^2, \qquad (233)$$

$$14 \qquad C'_k(x, y, B, t) = C_k(x, y, t), \qquad (234)$$

15 *where  $(x, y)$  corresponds to a point in the domain on which Equation (223) is solved and  $B$  is*  
 16 *the matrix half block length (m) in Figure PA-27 (i.e.,  $2B$  is the thickness of the matrix*  
 17 *between two fractures). The initial condition in Equation (232) means that no radionuclide is*  
 18 *present in the matrix at the beginning of the calculation. The boundary value condition in*  
 19 *Equation (233) implies that no radionuclide movement can take place across the centerline of*  
 20 *a matrix block separating two fractures. The boundary value condition in Equation (234)*  
 21 *ensures that the dissolved radionuclide concentration in the matrix at the boundary with the*  
 22 *fracture is the same as the dissolved radionuclide concentration within the fracture. The*  
 23 *matrix half block length  $B$  is an uncertain input to the analysis (see CFR CSP in Table PA-17).*

24 **PA-4.9.1.3 Coupling Between Fracture and Matrix Equations**

25 *The linkage between Equation (223) and Equation (230) is accomplished through the term*  
 26  *$\Gamma_k$ , defining the rate at which radionuclide  $k$  diffuses across the boundary between a fracture*  
 27 *and the adjacent matrix (see Figure PA-27). Specifically,*

$$28 \qquad \Gamma_k = -\frac{2\phi}{b} \left( \phi' D'_k \frac{\partial C'_k}{\partial \chi} \Big|_{z=\chi} \right), \qquad (235)$$

29 *where  $b$  is the fracture aperture (m) defined by*

1 
$$b = \phi B(1 - \phi). \tag{236}$$

2 **PA-4.9.1.4 Source Term**

3 *As already indicated, Equation (223) and Equation (230) are solved for unit radionuclide*  
 4 *releases to the Culebra. Specifically, a release of 1 kg of each radionuclide under*  
 5 *consideration was assumed to take place over a time interval from 0 to 50 years, with this*  
 6 *release taking place into the computational cell WPAC, located at the center of the Waste*  
 7 *Panel Area in Figure PA-24, that has dimensions of 50 m × 50 m. The volume of this cell is*  
 8 *given by*

9 
$$V = (50m)(50m)(4m) = 1 \times 10^4 \text{ m}^3, \tag{237}$$

10 *where 4 m is the assumed thickness of the Culebra Dolomite (Meigs and McCord 1996). As a*  
 11 *result,  $Q_k(x, y, t)$  has the form*

12 
$$Q_k(x, y, t) = \frac{1 \text{ kg}}{(1 \times 10^4 \text{ m}^3)(50 \text{ yr})(3.16 \times 10^7 \text{ s/yr})} = 6.33 \times 10^{-14} \text{ kg/m}^3/\text{s} \tag{238}$$

13 *for  $0 \leq t \leq 50 \text{ yr}$  and  $(x, y)$  is in cell WPAC and  $Q_k(x, y, t) = 0$  (kg/m<sup>3</sup>/s) otherwise.*

14 **PA-4.9.1.5 Cumulative Releases**

15 *If  $\mathcal{B}$  denotes an arbitrary boundary (e.g., the land withdrawal boundary) in the domain of*  
 16 *Equation (223) (i.e., Figure PA-24), then the cumulative transport of  $C_k(t, \mathcal{B})$  of*  
 17 *radionuclide  $k$  from time 0 to time  $t$  across  $\mathcal{B}$  is given by*

18 
$$C_k(t, \mathcal{B}) = \int_0^t \left[ \int_{\mathcal{B}} \{ \mathbf{v}(x, y) C_k(x, y, \tau) - \phi \mathbf{D}_k(x, y, t) \nabla C_k(x, y, \tau) \} \cdot \mathbf{n}(x, y) ds \right] d\tau, \tag{239}$$

19 *where  $h$  is the thickness of the Culebra (4 m),  $\phi$  is the advective porosity in Equation (223),*  
 20  *$\mathbf{n}(x, y)$  is an outward pointing unit normal vector, and  $\int_{\mathcal{B}} ds$  denotes a line integral over  $\mathcal{B}$*

21 **PA-4.9.2 Numerical Solution**

22 *The numerical solution to the coupled PDE system represented by Equation (223), and*  
 23 *Equation (230) is computed using SECOTP2D, an implicit finite volume code for the*  
 24 *simulation of multispecies reactive transport. A high-level description of the numerical*  
 25 *procedures implemented in SECOTP2D follows, with more detail available in WIPP PA*  
 26 *(1997b).*